The molecular architecture of the meiotic chromosome axis as revealed by super-resolution microscopy

Dissertation zur Erlangung des naturwissenschaftlichen Doktorgrades der Julius-Maximilians-Universität Würzburg

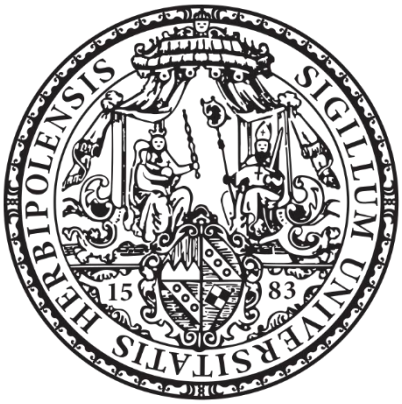

vorgelegt von
Katharina Schücker
aus Lengerich

Würzburg, 2017

Eingereicht am: _____

Mitglieder der Promotionskommission:

Vorsitzender: _____

Erstgutachter: Prof. Dr. Ricardo Benavente

Zweitgutachter: Prof. Dr. Markus Sauer

Tag des Promotionskolloquiums: _____

Doktorurkunde ausgehändigt am: _____

Content

List of figures

List of tables

Zusammenfassung

Innerhalb der Meiose sind Proteine der Chromosomenachse wichtig für das Monitoring der Chromatinstruktur und dessen Kondensation, sowie für die Paarung und Trennung der Chromosomen und für eine fehlerfreie Rekombination. Zu diesen Proteinen zählen HORMA-domain Proteine, Proteine des DNA-Reparatur-Systems und des synaptonemalen Komplexes, sowie Kohäsine und Kondesine. Um mehr über ihre Rolle in der Formgebung meiotischer Chromosomen zu erfahren, ist es unabdingbar ein genau definiertes Modell über ihre molekulare Architektur zu erstellen. Bis jetzt wurde ihre molekulare Organisation mit konventionellen Methoden wie dem konfokalen Laser-Scanning-Mikroskop (CLSM) und dem Transmissionselektronenmikroskop (TEM) untersucht. Beide Techniken sind jedoch entweder in ihrer Auflösung oder ihrer Lokalisationsgenauigkeit beschränkt, wodurch viele Daten zur molekularen Organisation der Chromosomenachse noch nicht erfasst werden konnten. Die vorliegende Arbeit untersucht mit isotropischer Auflösung die molekulare Struktur des synaptonemalen Komplexes (SC) der Maus und die Lokalisation seiner Proteine, sowie die Lokalisation von drei Kohäsinen, was neue Einsichten in deren Architektur und Topographie auf der nanomolekularen Ebene erbrachte. Dies gelang durch die Verwendung von Immunfluoreszenzmarkierungen in Kombination mit hochauflösender Mikroskopie, Linienprofilen und durchschnittlicher Positionsbestimmung. Es konnte gezeigt werden, dass der murine SC eine Weite von 221,6 nm ± 6,1 nm besitzt, inklusive einer 148,2 nm ± 2,6 nm weiten zentralen Region (CR). Innerhalb der CR konnte eine mehrschichtige Anordnung der Proteine des zentralen Elements (CE) bestätigt werden. Dies gelang indem ihre Strangdurchmesser und –abstände gemessen worden sind und zusätzlich potentielle Bindestellen von SYCP1 (synaptonemal complex protein 1) an den lateral Elementen des SCs (LEs) abgebildet werden konnten. Zusätzlich konnte gezeigt werden, dass die beiden LE Proteine, SYCP2 und SYCP3, kolokalisieren. Dabei zeigte SYCP2 keine präferentielle Lokalisation im inneren Bereich der LE.

Die Ergebnisse der vorliegenden Arbeit deuten auf eine organisierte Anordnung der murinen Kohäsin Komplexe (CCs) entlang der Chromosomenachse in Keimzellen hin und unterstützen die Hypothese, dass Kohäsine innerhalb der CR des SC eine Funktion unabhängig der von CCs haben.

Schlussendlich konnten neue Informationen zur molekularen Anordnung von zwei wichtigen Komponenten der murinen Chromosomenachse mit einer Präzision im

Nanometerbereich gewonnen werden und bisher nicht bekannte Details ihrer molekularen Architektur und Topographie aufgedeckt werden.

Summary

During meiosis proteins of the chromosome axis are important for monitoring chromatin structure and condensation, for pairing and segregation of chromosomes, as well as for accurate recombination. They include HORMA-domain proteins, proteins of the DNA repair system, synaptonemal complex (SC) proteins, condensins and cohesins. To understand more about their function in shaping the meiotic chromosome it is crucial to establish a defined model of their molecular architecture. Up to now their molecular organization was analysed using conventional methods, like confocal scanning microscopy (CLSM) and transmission electron microscopy (TEM). Unfortunately, these techniques are limited either by their resolution power or their localization accuracy. In conclusion, a lot of data on the molecular organization of chromosome axis proteins stays elusive. For this thesis the molecular structure of the murine synaptonemal complex (SC) and the localization of its proteins as well as of three cohesins was analysed with isotropic resolution, providing new insights into their architecture and topography on a nanoscale level. This was done using immunofluorescence labelling in combination with super-resolution microscopy, line profiles and average position determination. The results show that the murine SC has a width of 221.6 nm ± 6.1 nm including a central region (CR) of 148.2 nm ± 2.6 nm. In the CR a multi-layered organization of the central element (CE) proteins was verified by measuring their strand diameters and strand distances and additionally by imaging potential anchoring sites of SYCP1 (synaptonemal complex protein 1) to the lateral elements (LEs). We were able to show that the two LEs proteins SYCP2 and SYCP3 do co-localize alongside their axis and that there is no significant preferential localization towards the inner LE axis of SYCP2.

The presented results also predict an orderly organization of murine cohesin complexes (CCs) alongside the chromosome axis in germ cells and support the hypothesis that cohesins in the CR of the SC function independent of CCs.

In the end new information on the molecular organization of two main components of the murine chromosome axis were retrieved with nanometer precision and previously unknown details of their molecular architecture and topography were unravelled.

1. Introduction

1.1 Spermatogenesis of mice

Gametogenesis is the formation of gametes inside the gonads of sexually reproducing organisms. For males this process is called spermatogenesis and takes place inside the tubuli seminiferi contorti of male testes (Figure 1). The convoluted tubuli seminiferi contorti as well as the straight tubuli seminiferi recti are part of the seminiferous tubules, which lie embedded in the interstitium and are surrounded by mesenchymal cells. The interstitium consists of the contractile myoid cells, connective tissue, nerves, blood and lymphatic vessels, macrophages and steroid producing leydig cells. The tubuli seminiferi contorti consist of the seminiferous epithelium, which is made up of somatic sertoli cells and germ cells. Sertoli cells are polymorph cells, which stabilize the seminiferous epithelium, nourish the germ cells and monitor spermatogenesis. They also connect the interstitium with the seminiferous epithelium. The tubuli seminiferi recti do not contain any germ cells and connect the tubuli seminiferi contorti with the rete testis.

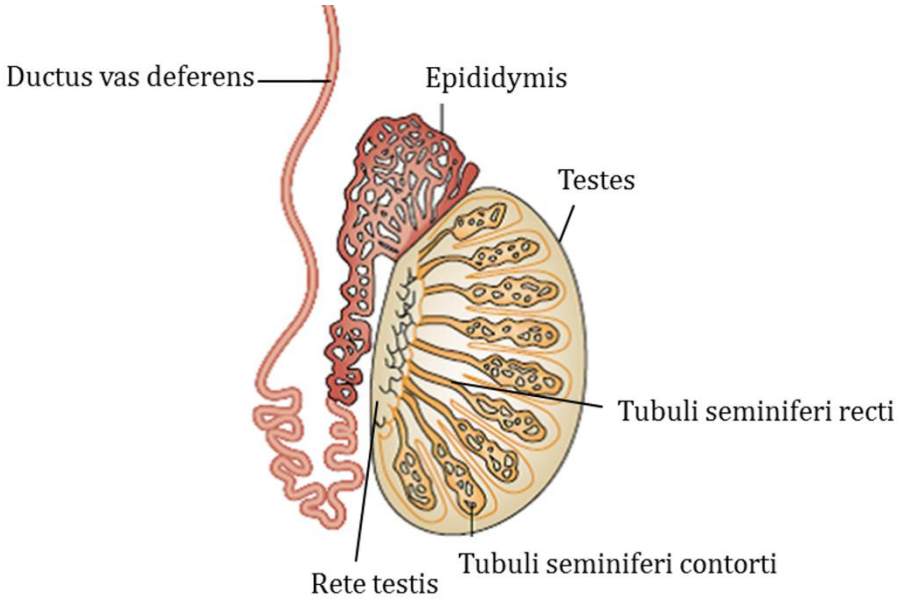

Figure 1: Cross-section of mammalian testes.
Spermatogenesis takes place inside the tubuli seminiferi contorti, which lie within the testes. Figure from Cooke and Sanders 2002.

Inside the tubuli seminiferi contorti the vectorial process of spermatogenesis starts at the tubus base and is directed towards the lumen (Figure 2). It is divided into the mitotic phase, the meiotic phase and the post-meiotic phase. The mitotic phase in males starts

with spermatogonia, which are embedded at the tubus base. They can either proliferate and produce more undifferentiated A_s (single)-spermatogonia stem cells or A_s-spermatogonia, which pass through several mitotic divisions and stay in contact with each other through cytoplasmic bridges due to unfinished cytokinesis (Oakberg, 1971). After the first mitotic division A_{pr} (paired) spermatogonia are produced. A_{pr} cells divide further into A_{al} (aligned) spermatogonia, consisting of 4, 8 or 16 cells (Huckins, 1971 a; Huckins, 1971 b). A_{al}-spermatogonia are the first differentiating germ cell. They differentiate into A_1-spermatogonia, which successively divide five times into A_2-, A_3, A_4, intermediate and B- spermatogonia (Huckins and Oakberg, 1978). B-spermatogonia are the last mitotically dividing male germ cells, which differentiate into primary spermatocytes. Primary spermatocytes then divide meiotically to form secondary spermatocytes, which subsequently divide meiotically into four spermatids. During the following post-meiotic process of spermiogenesis, spermatids differentiate into spermatozoa, which are released into the tubus lumen and afterwards transported into the epididymis (Figure 2) (de Rooij and Grootegoed, 1998; Oakberg, 1956 a).

Altogether spermatogenesis of male mice takes approximately 35 days and slightly varies between different strains (Oakberg, 1956 b).

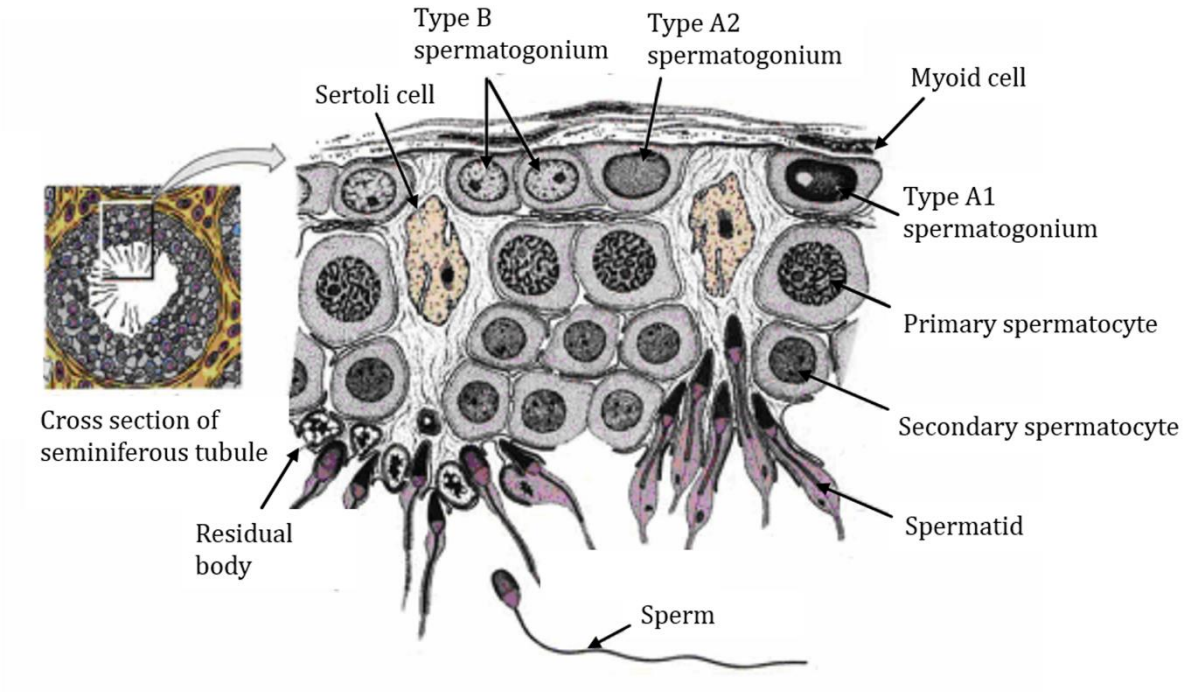

Figure 2: Overview of mammalian spermatogenesis.
The vectorial process of spermatogenesis takes place inside the tubuli seminiferi contorti of the testis. It is directed from the tubus base towards the lumen. Figure from Gilbert S.F. (2000): Developmental Biology, third edition.

1.2 Meiosis

Sexually reproducing diploid organisms halve their chromosome number during a specialized form of cell division, called meiosis. It leads to the formation of haploid gametes, which are used for reproduction. During the process of fertilization one male and one female gamete fuse into a diploid zygote, which then matures into a diploid organism. Mutations in meiosis specific genes can lead to various diseases concerning the reproductive system like aneuploidy, sterility and embryonic death. Since in male mice mutations usually lead to sterility, whereas females are still fertile, the meiotic control mechanisms clearly vary between the genders and seem to be more strictly regulated in males (Morelli and Cohen, 2005).

Another type of cell division is mitosis, which leads to the production of two diploid daughter cells originating from one diploid parent cell. It can be found in somatic cells. Meiosis differs from mitosis in several aspects. First, it only takes place in gonads (testis and ovary). Whereas mitosis leads to the formation of two genetic identical diploid cells, meiosis produces four haploid cells with different genotypes. This is achieved through recombination and random segregation of parental chromosomes. This way, meiosis provides genetic diversity to the genomic pool of a population.

Before cells enter meiosis they are in interphase which is divided into gap phase 1 (G_1-phase), synthesis phase (S-phase) and gap phase 2 (G_2-phase). During G_1-phase the cell grows and cellular components are duplicated. Subsequently the genetic material is replicated during S-phase. Each chromosome is then made up of two sister chromatids. During the following second gap phase the cell grows further, synthesizes proteins, checks for errors and repairs them before moving on to the meiotic phase (M-phase). During M-phase the cell separates twice during meiosis I and meiosis II, without an additional replication step. Meiosis I is a reducing division during which the homologue chromosome pairs are separated. It also includes recombination steps, which are important for the formation of unique haploid cells. Meiosis II on the other hand resembles mitosis and is an equatorial division during which the chromatids are randomly pulled to different cell poles, again contributing to genetic diversity. In the end of female gametogenesis one big ovum and three small polar bodies, which are going to be discarded, are formed. The ovum is the female gamete and provides mitochondria and other cell organelles as well as nutrients for the embryo. Male meiosis leads to the

formation of four sperm cells, each consisting of a tail for mobility and a head, which is mainly composed of the haploid cell nucleus and has little cytoplasm.

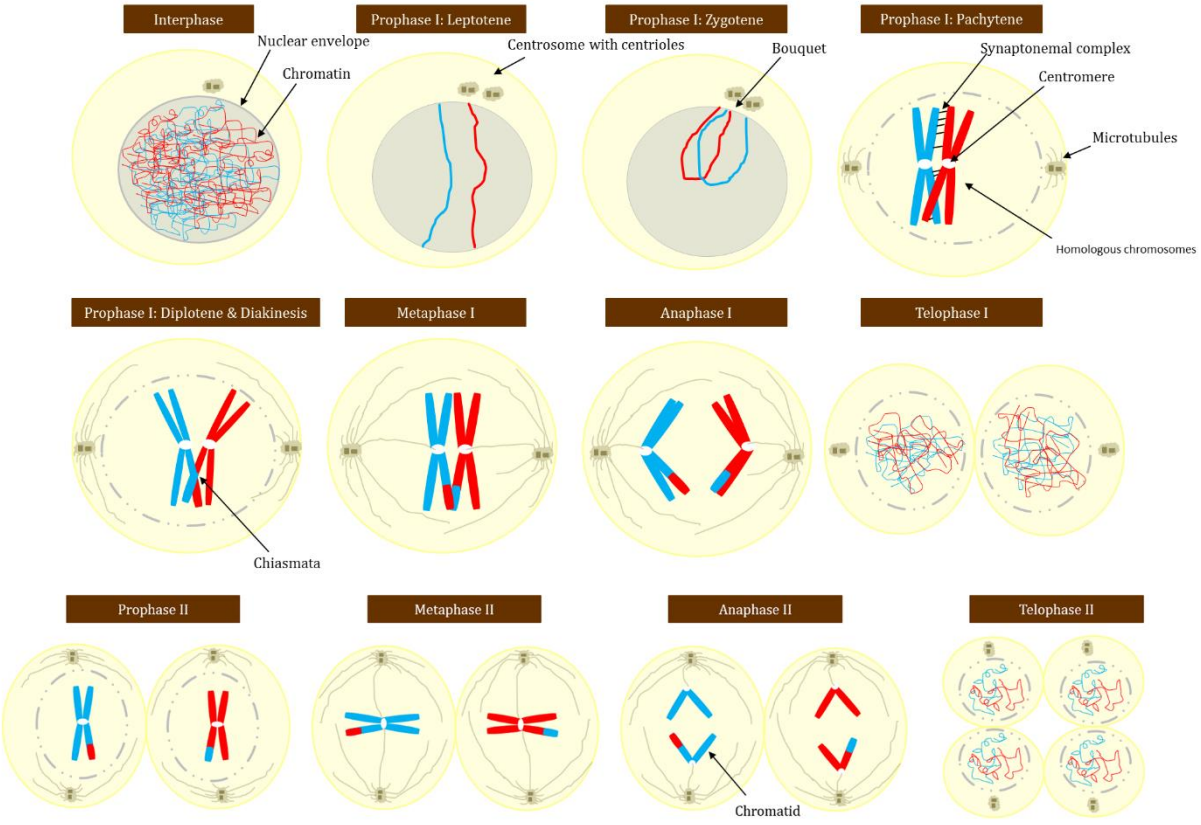

Figure 3: Overview of mammalian meiosis.
During meiosis the cell successively divides twice after one round of DNA replication, producing four genetically unique haploid gametes.

Meiosis I and II are each divided into prophase, metaphase, anaphase and telophase (Figure 3). The longest and most important phase is prophase I of meiosis I during which pairing and synapsis of homologous chromosomes take place and DNA segments between non-sister chromatids are exchanged. Prophase I is divided into leptotene, zygotene, pachytene, diplotene and diakinesis (Figure 3). Female oogonia start meiosis during the embryonic development and rest at the diplotene stage before birth, called the dictyotene stage. Beginning at puberty, female gametes (oocytes) successively start to continue with meiosis during ovulation. Male gametes (spermatocytes) start meiosis at puberty and do not arrest. Instead they develop gradually in the tubuli seminiferi contorti.

Each meiotic stage is characterized by certain structural and proteomic changes. In the beginning of prophase I chromatin is still organized into long thin chromatid filaments. During leptotene several specialized proteins start to mediate morphological changes and cohesins and condensins begin with the condensation of chromatin into a more compact form. This is important for subsequent recombination processes and the segregation of chromosomes. Additionally, proteins of the axial elements (AE) start to assemble along the chromosome axes (Eijpe et al., 2003). Kinetochores are formed on the centromeres of chromosomes. They are important anchoring sites for the spindle apparatus and important for correct segregation of homologues chromosomes. Also, the telomeres attach to the inner nuclear envelop via attachment plates (Liebe et al., 2004; Scherthan et al., 1996; von Wettstein, 1984).

During the following zygotene stage chromatin condenses further and the attached telomeres move towards the cell pole opposite of the centrosome where they meet, forming the bouquet structure (Figure 4). During this formation the chromosome axes extend into the interior of the nucleus (Scherthan et al., 1996; Zickler and Kleckner, 1998). The bouquet structure is an important feature of meiosis, which allows the homologue chromosomes to get into close vicinity of each other to pair, synapse and recombine (Page and Hawley, 2003). Additionally, the AEs become the lateral elements (LEs) of the SC, by getting connected in a zipper-like fashion by transversal filaments (TFs) (Fawcett, 1956; Moses, 1956). At the end of the zygotene stage the bouquet disassembles but the telomeres stay attached to the nuclear envelope (Scherthan et al., 1996; Zickler and Kleckner, 1998).

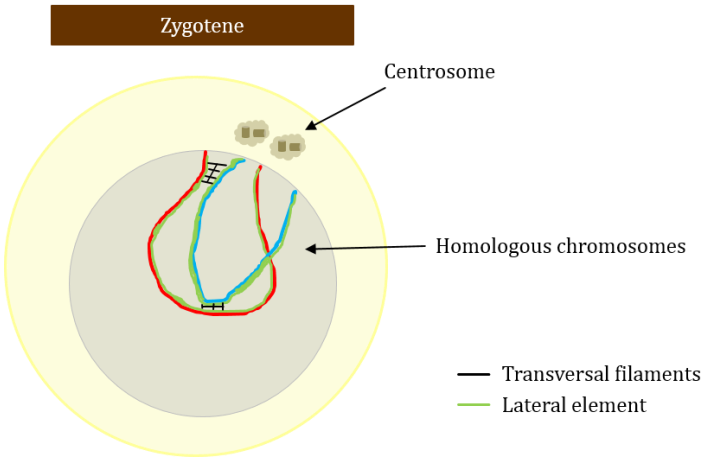

Figure 4: Bouquet formation of chromosomes during zygotene.
During zygotene of prophase I, telomeres polarize at one side of the nucleus opposite the centrosome and homologous chromosomes start to align and synapse.

During the pachytene stage of meiosis I all chromosomes are highly condensed and are visible in conventional light microscopes as thick threads (bivalents). All chromosomes are synapsed and the XY-body is visible. The XY-body is a heterochromatic structure of the X and Y chromosome, which is largely transcriptionally inactive. In the XY-body synapsis only takes place in pseudoautosomal regions (PAR), because of the lack of homologous regions (Handel, 2004; Solari, 1974).

After the long pachytene stage of prophase I diplotene follows. During diplotene the SC starts to disassemble and the homologues separate, with exception to regions where recombination took place. Here, the homologues stay connected by chiasmata (Creighton and McClintock, 1931; Henderson, 1970). This means that every homologues has to recombine at one locus minimum for correct segregation. The following diakinesis stage is the transition phase from prophase I to metaphase I. Here, the chromosomes condense even further and chiasmata and all four chromatids are visible as tetrads. Also the spindle apparatus is formed and the nuclear envelope disassembles.
In metaphase I the bivalents arrange themselves in the equatorial plane and microtubules of the spindle apparatus proliferate towards the chromosomes and bind their kinetochores. The mono-orientation of sister-kinetochores results in the separation of homologous chromosomes during anaphase I and their random segregation towards the two spindle poles (Page and Hawley, 2003). Sister chromatids stay attached by cohesins at the centromere region, whereas cohesins in the chromosomal axes region were cleaved by the protein separase preceding segregation. Also cytokinesis begins. The last phase of meiosis I is telophase I. Here, a nuclear envelope assembles around each chromosome set and cytokinesis forms the two originating daughter cells. The result of meiosis I are two haploid cells with two chromatids (1n 2c).
During the subsequent meiosis II, cells undergo a mitotic cell division, without a preliminary DNA replication. In conclusion, the two sister chromatids are separated during anaphase II, leading to four haploid cells with one chromatid (1n 1c). During meiosis II no recombination processes take place.

1.3 The synaptonemal complex

The synaptonemal complex (SC) is an evolutionary well conserved multiprotein complex, which plays an important role in mammalian meiosis. It is necessary for synapsis, recombination and correct segregation of homologue chromosomes during prophase I of meiosis I. Mutations of SC proteins lead to dysfunctional meiosis, aneuploidy, decreased fertility, sterility and embryonic death.

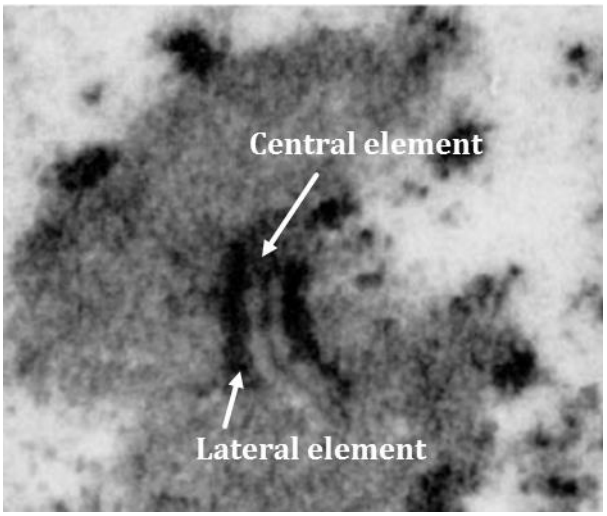

Figure 5: TEM image of the SC.
Transmission electron microscopy (TEM) image of the synaptonemal complex (SC) taken from pigeon spermatocytes. Figure from Fawcett 1956.

The SC was more or less simultaneously discovered for the first time in spermatocytes of pigeons, cats, humans and crayfishs in 1956 using electron microscopy (Figure 5) (Fawcett, 1956; Moses, 1956). EM imaging of the SC has shown that it has a ladder-like structure with two LEs forming the ladder pillars. In between them is the central region (CR), where transversal filaments (TFs) form the rung of the ladder and connect the two LEs (Figure 6). In the middle of the CR lies the central element (CE) (Figure 5, Figure 6). On each site of the LEs chromatin of the homologous chromosomes is bound, thereby connecting the two parental chromosomes (Figure 6).

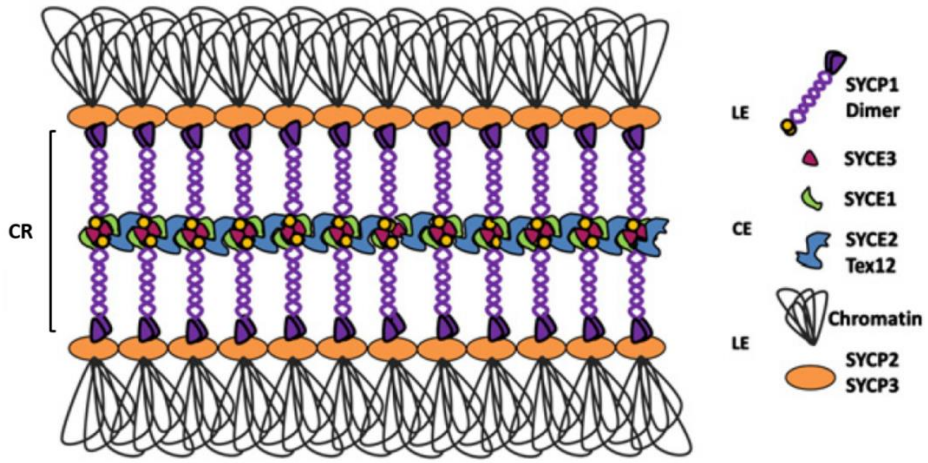

Figure 6: Model of the mammalian synaptonemal complex.
The mammalian synaptonemal complex (SC) has a ladder-like structure, with two lateral elements (LEs) consisting of SYCP3 and SYCP2 and a central region (CR) made up of SYCP1, TEX12 and SYCE1-3. Parental chromatin is bound to the LEs. Figure from Fraune et al. 2012.

The assembly of the SC starts early in prophase I, during leptotene, when synaptonemal complex protein 3 and 2 (SYCP2 and SYCP3) form the AEs alongside the chromosome axes. During zygotene, the TFs built a connection between the two AEs (Lammers et al., 1994; Meuwissen et al., 1997; Offenberg et al., 1998). This process is called synapsis. Thereby the AEs become LEs and the TFs bridge the CR between them (Figure 6). The TFs are formed by SYCP1, a homodimeric protein, the N-termini of which lie in the central element of the SC and whose C-termini are said to locate in the lateral elements (Liu et al., 1996; Meuwissen et al., 1992). In the CR the N-termini of opposing SYCP1 proteins do interact with each other (Liu et al., 1996). The CE is additionally made up of the synaptonemal complex central element proteins 1-3 (SYCE1, SYCE2 and SYCE3) and TEX12 (testis expressed 12). During diplotene the SC starts to disassemble again, beginning with the CR (Jordan et al., 2012; Parra et al., 2003).

1.3.1 Proteins of the murine synaptonemal complex

Proteins of the SC were first described in 1987 using immunocytochemical techniques as well as light microscopic and ultrastructural techniques (Heyting et al., 1987). In 1989 SCs were isolated from rat spermatocytes and the main SC proteins SYCP3, SYCP2 and SYCP1 were biochemically and morphologically analysed (Heyting et al., 1989). Further molecular analyses of those proteins were conducted by Meuwissen et al. (SYCP1), Offenberg et al. (SYCP2) and Lammers et al. (SYCP3) (Lammers et al., 1994; Meuwissen et al., 1997; Offenberg et al., 1998). A few years later the CE proteins were characterized by Costa et al. (SYCE1 and 2), Hamer et al. (TEX12) and Schramm et al. (SYCE3) (Costa et al., 2005; Hamer et al., 2006; Schramm et al., 2011). Today several SC proteins of different model organisms, including *M. musculus*, R. norvegicus, *C. elegans* and *D. melanogaster* are known and characterized.

SYCP3

SYCP3 is one of the best characterized SC proteins. It can be detected for the longest time during meiosis, starting in leptotene until metaphase I. During leptotene it is part of the AEs, which later on in prophase I become the LEs. In metaphase I it still locates axial to the chromosomes and to the centromere region but becomes absent afterwards (Dobson et al., 1994; Lammers et al., 1994; Page and Hawley, 2003).

The amino acid sequence of SYCP3 is generally preserved between mammals but there are species-specific differences (Botelho et al., 2001; Klink et al., 1997). Whereat in mouse and rat there are two isoforms of SYCP3 with a molecular mass of 30 and 33 kDA, other organisms like human and hamster only have one of 30 kDa (Botelho et al., 2001; Dobson et al., 1994; Heyting et al., 1987; Lammers et al., 1994; Miyamoto et al., 2003). In mice the protein is 254 amino acids long with an α-helical domain on its C-terminus, which is typical for the formation of coiled-coil structures (Alsheimer et al., 2010; Botelho et al., 2001; Lupas et al., 1991; Tarsounas et al., 1997). It is flanked by two non-helical domains, which contain the highly preserved motives CM1 (N-terminus) and CM2 (C-terminus). Those regions are important for the structural organization of the protein. SYCP3 can use the α-helical domain for interacting with itself in a homophilic protein-to-protein interaction (Tarsounas et al., 1997; Yuan et al., 1998). The low evolutionary preserved N-terminus of SYCP3 varies in size between different species and there is a potential nuclear localization signal (NLS) and a motif A, a typical structure for nucleotide binding proteins. Distributed over the whole SYCP3 protein there are many potential phosphorylation sites: One for a cATP or cGMP dependent kinase (Feramisco et al., 1980), five for casein kinase II (Pinna, 1990) and four for the protein kinase C (Kishimoto et al., 1985). The phosphorylation state of SYCP3 might play a role in its dynamics during meiosis (Tarsounas et al., 1999).

SYCP2

The other main protein component of the AEs/LEs is SYCP2. It can be detected as early as SYCP3 on the chromosome axis and starts to dissolve from them during diplotene. From the centromere region it dissolves later, after metaphase I. The murine SYCP2 is 1500 amino acids long and has a molecular mass of 190 kDa (Heyting et al., 1989; Wang et al., 2001). It contains two clusters of S/T-P motifs, which are potential target sites for the $p34^{cdc2}$ protein kinase (Offenberg et al., 1998). It also has eight potential target sites for a cAMP/cGMP dependent kinase (Offenberg et al., 1998).

SYCP1

In mice the homodimeric protein of the TFs, SYCP1, is a 993 amino acids long protein with a molecular weight of 125 kDa (Heyting et al., 1989; Meuwissen et al., 1992; Sage et al., 1995). Its molecules are organized in parallel homodimers with the same polarity.

Recruitment of SYCP1 to the SC begins during zygotene after the AEs have formed, (Dobson et al., 1994; Meuwissen et al., 1992). Its displacement starts during late pachytene and continues until the end of diplotene (Dobson et al., 1994; Meuwissen et al., 1992; Tarsounas et al., 1999). SYCP1 has a long central α-helical domain, which forms a coiled-coil structure and is surrounded by two globular ends (Dobson et al., 1994; Meuwissen et al., 1992) . In the central α-helical domain there is a DNA-binding motif in form of a leucine-zipper and also several potential target sites for cAMP/cGMP dependent protein kinases and one for a tyrosine kinase (Meuwissen et al., 1997). Its C-terminus has several DNA-binding motifs forming β-turns and potential target sites for the $p34^{cdc2}$ protein kinase and also a putative NLS (Meuwissen et al., 1997; Meuwissen et al., 1992). Overall there are 12 potential target sites for the protein kinase C distributed over the complete protein. Different phosphorylation states of the protein might be important for SC assembly and disassembly (Meuwissen et al., 1997).

CE proteins

In the CE of the murine SC four different proteins are located. SYCE1 (38 kDa) which is 329 amino acids long and has four potential coiled-coil domains (Costa et al., 2005), SYCE2 (19 kDa) which is 171 amino acids long and has one potential coiled-coil domain (Costa et al., 2005), SYCE3 (12 kDa) which is 88 amino acids long and one coiled-coil domain as well as two putative sites for phosphorylation (Schramm et al., 2011) and TEX12 (14 kDa) which is 123 amino acids long (Hamer et al., 2006).

1.3.2 Interplay of synaptonemal complex proteins

It is known that SYCP3 binds SYCP2 (Pelttari et al., 2001; Schalk et al., 1998). For this interaction the coiled-coil domain on the C-terminus of SYCP2 is essential (Offenberg et al., 1998; Yang et al., 2006). It is also said that SYCP2 connects SYCP1 with SYCP3 (Offenberg et al., 1998; Winkel et al., 2009). The N-terminus of SYCP1 seems to recruit more CE specific proteins, like SYCE1 and SYCE2, to the SC (Costa et al., 2005). It has been shown that SYCE1 interacts with itself, the N-terminus of SYCP1 and with SYCE2 and SYCE3 (Bolcun-Filas et al., 2007; Costa et al., 2005; Schramm et al., 2011).

SYCE2 interacts with itself, the N-terminus of SYCP1 and TEX12 (Bolcun-Filas et al., 2007; Costa et al., 2005). Together with TEX12 it forms a complex, which is important for the longitudinal polymerization of SYCP1 during synapsis. For SYCE1 and SYCE2

orthologous protein sequences have been found in several vertebrates (Costa et al., 2005). In contrast to all other CE proteins SYCE2 orthologous have also been found in non-vertebral animals (Costa et al., 2005).

SYCE3 binds SYCE1 and the N-terminus of SYCP1, forming the initiation complex for synapsis and then recruiting TEX12 and SYCE2 to the CE (Schramm et al., 2011). TEX12 was only confirmed to interact with SYCE2 (Hamer et al., 2006).

1.3.3 Evolutionary preservation of the synaptonemal complex

Even though the structure of the eukaryotic SC is evolutionary highly preserved, there are species specific differences in their protein compositions and primary amino acid sequences of the proteins caused by a dynamic evolutionary history of an ancient SC (Fraune et al., 2016; Page and Hawley, 2004). Just recently a single origin of the metazoan SC was verified by Fraune et al. (Fraune et al., 2016).

1.4 Murine cohesin complexes

During mitosis and meiosis specialized protein complexes called cohesin complexes (CCs) support sister chromatid cohesion by forming ring structures around the DNA strands (Gruber et al., 2003; Haering and Nasmyth, 2003; Hirano, 2002; Michaelis et al., 1997; Sumara et al., 2000). They are evolutionary conserved proteins and play an important role for the correct segregation of sister chromatids during meiosis and mitosis (Haering and Nasmyth, 2003; Nasmyth, 2001). CCs are V-shaped heterodimers of SMC1 and 3 (SMC= structural maintenance of chromosomes) which are bridged by an α-kleisin and a stromal antigen (STAG) (Gruber et al., 2003). So far six different CCs were characterized in vertebrates of which four seem to be meiosis-specific (Figure 7). The four meiosis specific CCs comprise four meiosis-specific cohesins namely REC8, RAD21L, SMC1ß and STAG3 (Jessberger, 2011; Lee and Hirano, 2011; Prieto et al., 2001; Uhlmann, 2011) (Figure 7 c-f).

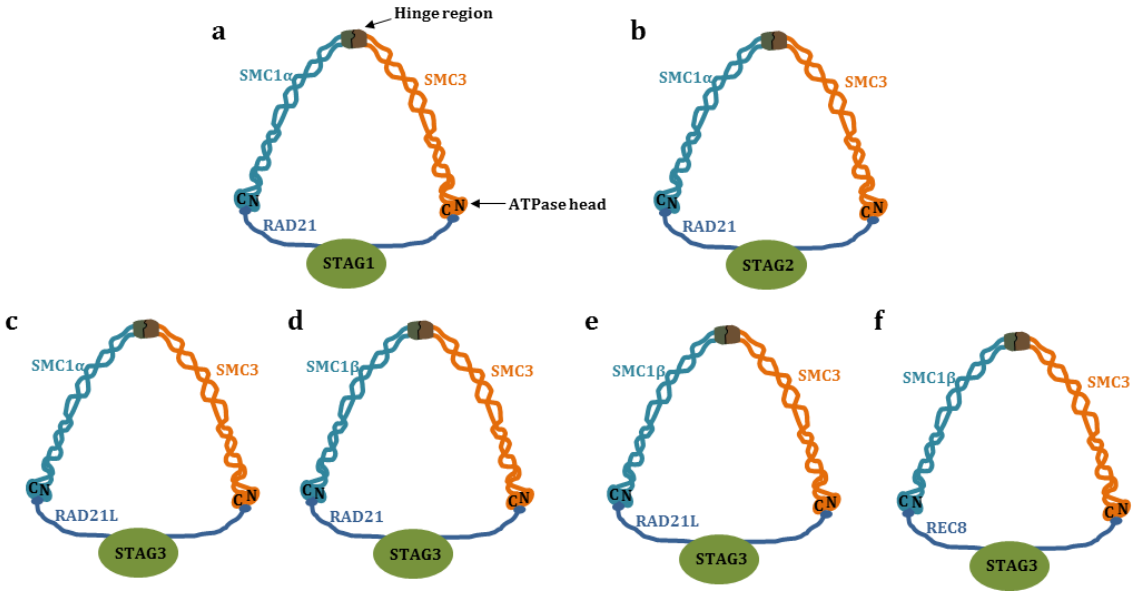

Figure 7: Mammalian cohesin complexes.
(a-b) Cohesin complexes which can be found in mitotic and meiotic cells. (c-f) Meiosis specific cohesin complexes.

1.4.1 Cohesin complexes during meiosis

During meiosis CCs play a role in AE assembly, synapsis, DSB repair, transcriptional control, chromosome axis-loop-structure formation, orientation of sister kinetochores, telomere integrity and telomere attachment to the nuclear envelope but their best known role is the regulation of sister chromatid cohesion during the two successive cell divisions (Adelfalk et al., 2009; Hopkins et al., 2014; Nasmyth, 2011). So far it is known that sister chromatid cohesion in vertebrate meiocytes is established during S-phase of interphase before cells enter meiosis. On chromosome arms it lasts until metaphase I/anaphase I transition but is maintained in the centromere region until the cell reaches metaphase II/ anaphase II transition. Conclusively, CCs maintain sister chromatid cohesion during meiosis I, while homologous chromosomes are pulled to opposite poles of the cell. Afterwards during the second division sister chromatids are separated. This led to the assumption that CCs play a regulatory role during those two separation events. This was confirmed by Buonomo et al. in 2000, who discovered that during anaphase I, cohesins in the arm regions are cleaved, whereas cohesins in the centromere region stay intact, ensuring sister chromatid cohesion (Buonomo et al., 2000). In more detail previous results showed that the cohesins Rec8, SMC1β, SMC3, STAG3 and Rad21L are present on chromosome arms until anaphase I and on centromeres until anaphase II, which point out their importance in maintaining sister chromatid cohesion (Buonomo et

al., 2000; Eijpe et al., 2003; Lee et al., 2003; McNicoll et al., 2013; Prieto et al., 2002; Revenkova et al., 2001). Additionally, Revenkova and Jessberger concluded in 2006 that the CC Rec8/STAG3/SMC1α/SMC3 is responsible for the cohesion of chromosome arms in prophase I. Two other CCs, namely Rec8/STAG3/SMC1β/SMC3 and Rad21/STAG3/SMC1β/SMC3, are not only holding chromosome arms together during the first meiotic division but additionally stabilize cohesion of the centromeric region (Revenkova and Jessberger, 2006). Just recently the group of Ward et al. concluded that CCs containing STAG3 and REC8 are the main complexes needed for centromeric cohesion (Ward et al., 2016).

This regulatory function of CCs might be controlled by the expression of different cohesin subunits during meiosis leading to the formation of different CCs, which verifies the hypothesis of sequential loading of various CCs to the chromosome axis (Valdeolmillos et al., 2007). The first cohesins that are present during meiosis are SMC1α, SMC3, RAD21L, RAD21, REC8, STAG1 and STAG2 (McNicoll et al., 2013). They are already expressed in pre-meiotic S-phase and somatic cohesins even before that (Eijpe et al., 2003; Lee and Hirano, 2011; McNicoll et al., 2013). In leptotene SMC1β and STAG3 appear simultaneously with SYCP3 and SYCP2 (Eijpe et al., 2003; Revenkova et al., 2001). In metaphase I cohesins dissociate from the chromosome axes except for Rad21L, Rec8, SMC1β, SMC3 and STAG3, which predominately stay in the centromeric region. SMC3, SMC1ß and REC8 stay in the centromeric region until metaphase II (Buonomo et al., 2000; Eijpe et al., 2003; Lee et al., 2003; McNicoll et al., 2013; Prieto et al., 2002; Revenkova et al., 2001). Rad21 already dissociates from the chromosomes after crossing-overs are established and SMC1α can be detected on the chromosome axes until late prophase I (Revenkova et al., 2001). Even though expression studies on cohesins throughout meiosis vary slightly, it is clear that the compositions of CCs vary between different meiotic phases (McDougall et al., 2005; McNicoll et al., 2013; Revenkova and Jessberger, 2006).

1.4.2 Spatiotemporal regulation of mammalian cohesin complex dynamics

It is known that CC dynamics are regulated by phosphorylation, acetylation and site specific proteolysis and that the regulatory mechanisms differ between mitosis and meiosis. Nonetheless the spatiotemporal regulation of cohesin loading onto the chromosomes, their maintenance and dissociation from the chromosomes in

mammalian meiocytes is still not very well understood. Even though the mechanism for mitotically dividing cells is much better understood, there are still some fundamental questions left unanswered for both types of cell division, like whether or not distinct CCs are exchanged by others during DNA replication or if cohesin subunits are replaced with or without dissociation of CCs from the chromosomes.

Spatiotemporal regulation in mammalian mitosis

During the murine mitotic cell cycle a complex called kollerin in combination with ATP hydrolysis by the nucleotide binding domains (NBDs) of the SMC-dimer are known to play a key role in loading cohesins onto chromatin during G1-phase of interphase (Nasmyth, 2011). Kollerin is described as a complex of nipped-B-like protein (NIPBL) and MAU2 chromatid cohesion factor homolog SCC4 (sister chromatid cohesion protein 4) (table 1). After loading cohesins onto the chromosomes, SMC3 acetylation by the cohesin acetlytransferases (CoAT) ESCO1 and ESCO2 leads to the recruitment of sororin to chromatin-bound CCs, which is responsible for maintaining sister chromatin cohesion by anatgonzing WAPL (Beckouet et al., 2010; Lafont et al., 2010; Nasmyth, 2011; Nishiyama et al., 2010; Rankin, 2005; Rankin et al., 2005). Sororin competes with WAPL for binding the α-kleisin binding sister chromatid cohesion protein PDS5 to form the releasing complex WAPL/PDS5 and therefore stabilizes chromatin-bound CCs.

Table 1: **Nomenclature of cohesin subunits and regulatory factors in different model organisms.** Table was taken from Nasmyth 2011.

	Saccharomyces cerevisiae	*Schizosaccharomyces pombe*	*Drosophila melanogaster*	*Homo sapiens*
Smc proteins	Smc1 Smc3	Psm1 Psm3	Smc1 Smc3	Smc1α, Smc1β Smc3
α-kleisins	Mcd1/Scc1, Rec8	Rad21, Rec8	Rad21, C(2)M	Rad21/Scc1, Rad21L, Rec8
α-kleisin binding subunits	Scc3 Pds5	Psc3, Rec11 Pds5	SA Pds5	SA1, SA2, STAG3, Pds5a, Pds5b/APRIN
Pds5 binding proteins	Rad61/Wapl ?	Wapl ?	Wapl Dalmatian	Wapl Sororin
Kollerin loading complex	Scc2 Scc4	Mis4 Ssl3	Nipped B Scc4	Scc2/Nipbl Scc4/Mau2
Cohesin acetyl transferases (CoAT)	Eco1	Eso1	Deco, San	Esco1, Esco2
Cohesin deacetylases (CoDAC)	Hos1	?	?	HDAC8

Proteins marked in blue are specific to meiotic cells. Orthologous proteins are on the same line as are alternative isoforms.

Beginning in prophase and following through metaphase a separase-independent pathway removes the majority of CCs from chromosome arms without α-kleisin cleavage (Sumara et al., 2002; Waizenegger et al., 2000). This pathway is not activated by deacetylation of SMC3, as one could have thought, but instead leads to the

deacetylation of SMC3 by cohesin deacetylases (CoDACs) after CCs are removed from chromosomes (Nasmyth, 2011). This prophase pathway is dependent on the polo-like kinase (PLK) in combination with Aurora B and seems to be directed by an interplay of phosphorylations of several cohesin subunits (STAG1-3, sororin, PDS5, WAPL, α-kleisins) and kollerin (Hauf et al., 2005). Especially the phosphorylation of sororin seems to play a key role since it leads to its inhibition and therefore enables WAPL to bind PDS5 and cause the dissociation of CCs (Nasmyth, 2011). The prophase pathway does not remove pericentric CCs. They are protected by a protein called shugosin 1 (SGO1), which recruits the protein phosphatase 2 A (PP2A) to the centromere region, forming the SGO1-PP2A complex (Kitajima et al., 2004; McGuinness et al., 2005; Riedel et al., 2006; Salic et al., 2004; Xu et al., 2009). SGO1-PP2A seems to inhibit the kinase activity of the polo-like kinase 1(PLK1), preventing phosphorylation of cohesin subunits including sororin.

After all bivalents are correctly aligned and oriented on the metaphase plate the spindle assembly checkpoint (SAC) activates a separase-dependent pathway, which until now was inhibited by securin and CDK1- cyclin B1 (McNicoll et al., 2013). This separase-dependent pathway removes centromeric CCs through the activity of the ubiquitin ligase APC/C (anaphase-promoting complex/cyclosome), which gets activated by the cell division cycle protein CDC20 (Figure 8). APC/C^{CDC20} removes the inhibitory chaperone securin from the enzyme separase and also degrades cyclin B, leading to a cleavage of α-kleisin subunits (Hauf et al., 2001; Uhlmann et al., 1999). Another paralog of shugoshin, SGO2, has been found to localise to the centromeric region of mitotic chromosomes, likewise. Gómez et al. proposed a model by which tension on the centromeres caused by the spindle apparatus leads to a redistribution of SGO2, unmasking CCs in the centromere region. CCs can now be released by WAPL/PDS5 or cleaved at their α-kleisin subunit by the active separase (Gomez et al., 2007). After centromeric CCs are removed sister chromatids can be segregated during anaphase. Interestingly, SGO2 is not necessary for sister chromatid cohesion in somatic cells (Llano et al., 2008).

CCs that were not cleaved at their α-kleisin subunit during the prophase pathway might be important for gene expression and chromatin restructuring during the subsequent interphase and maybe even reused in the next mitotic phase (McNicoll et al., 2013).

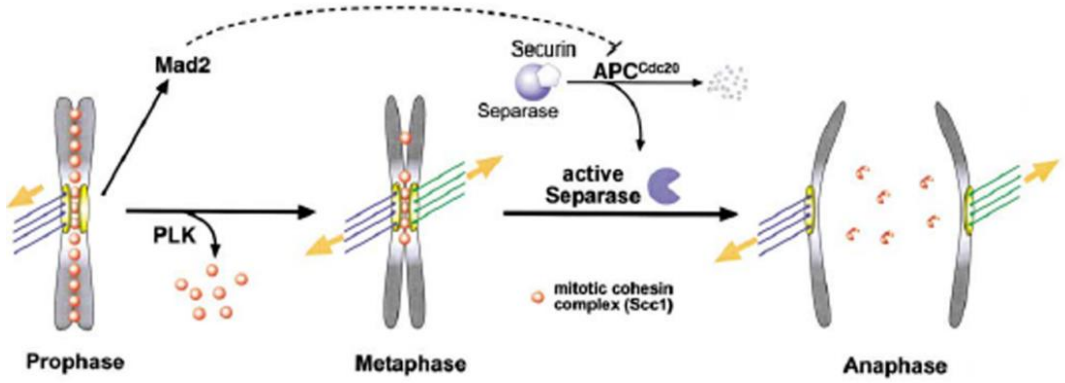

Figure 8: Spatiotemporal regulation of vertebrate chromosome segregation in mitosis.
From prophase to metaphase most cohesin complexes (CCs) of the chromosome arms are removed through a polo-like-kinase (PLK) dependent pathway. Once all chromosomes are bioriented in the metaphase plate, pericentric CCs are removed through cleavage of their α-kleisin subunit by the activated enzyme separase. MAD2, as part of the spindle assembly checkpoint (SAC), delays separase activity if not all chromosomes are bioriented. It inhibits the anaphase-promoting complex (APC), which is responsible for the activation of separase. Once all CCs are removed sister chromatids are pulled to opposite cell poles by the spindle apparatus. Figure from Petronczki et al. 2003.

Spatiotemporal regulation in mammalian meiosis

The basic principle of cohesin loading, maintenance and dissociation in mitosis also applies for meiosis. In murine meiocytes meiotic CCs are loaded onto chromatin entrapping the two sister chromatids during G1- and S-phase of interphase. Whereat cohesion is established by transforming temporary bound CCs into stably bound CCs during S-phase is not clear. Another question that remains is whether or not cohesins in murine meiocytes are also loaded onto chromatin after S-phase and if some already bound CCs are replaced by different CCs during meiosis and also during the replication of DNA in S-phase (McNicoll et al., 2013; Nasmyth, 2011; Revenkova and Jessberger, 2006). The exact role of CoATs and cohesin-associated factors (e.g. NIPBL, SCC4, sororin, WAPL and PDS5) in meiosis stays elusive. It is known, however, that in mice there are two isoforms of the cohesion regulating factor PDS5, namely PDS5A and PDS5B, of which PDS5B seems to be essential for spermatogenesis, while PDS5A is not (Zhang et al., 2009; Zhang et al., 2007). Information about a role of the binding partner sororin and WAPL in gametes is still deficient. Just recently Gómez et al. discovered that sororin seems to play a role in centromeric cohesion in collaboration with SGO2-PP2A (Gomez

et al., 2016). Up to now a possible role for WAPL in meiosis is suggested but not proven (Kuroda et al., 2005). Additionally it was confirmed that SGO2 is necessary for the protection of centromeric CCs from cleavage by separase during meiosis I as it does during mitosis (Gomez et al., 2007; Llano et al., 2008). Also centromeric tension leads to SGO2 redistribution, unmasking, again, CCs (Gomez et al., 2007; Kitajima et al., 2004). So far SGO1 was not described in mammalian meiocytes.

So far it is assumed that separase cleaves the CCs in the arm region preceding the first meiotic division and in the centromeric region preceding the second devision (Buonomo et al., 2000; Mark Petronczki, 2003). However, this mechanism was described in budding yeast and has not yet been proven to be true for mammals.

1.5 Significance of CCs and the SC for the chromosome axis

It is known that cohesins and SC proteins interact with each other and are essential for the formation of chromosome axis-loops, their pairing, recombination and subsequent segregation (Revenkova and Jessberger, 2006). The cohesin axis forms alongside the homologue chromosomes and in parallel to the AE axis of the SC (Figure 9). Just recently it was proven that the chromosome axis is multi-layered with one AE located to the outer part and two CC cores from the two sister chromatids located to the inner part (Figure 9) (Ortiz et al., 2016). The cohesin axis is important for loading and formation of the AEs as well as for synapsis. There is a high variety and redundancy of CCs in vertebrates and their significance in the processes of AE loading and formation as well as in synapsis vary (McNicoll et al., 2013; Revenkova and Jessberger, 2006). It is known that the axes of AEs and cohesins interact with each other (McNicoll et al., 2013). Thereby the AEs determine the length of the chromosome axis via chromosome compaction but it is still under discussion whether or not CCs act actively against the shortening of chromosome axes or passively. A role of cohesins in the determination of chromatin loop numbers and density on the chromosome axis by fixating the chromatin loop bases to the SC axes is assumed. This would limit the compaction caused by the AEs and reinforce a passive role of cohesins in the determination of chromosome axis lenght (McNicoll et al., 2013). Just recently evidence for an important role of RAD21L containing CCs in pericentric heterochromatin clustering was found by the group of Ward et al. as well as that CCs containing STAG3-REC8 or STAG3-RAD21L are required for chromosome axis formation (Ward et al., 2016).

Despite of all the newly retrieved information there are still many questions left unanswered on how SC proteins and cohesins in combination with other proteins of the chromosome axis codetermine the axis length.

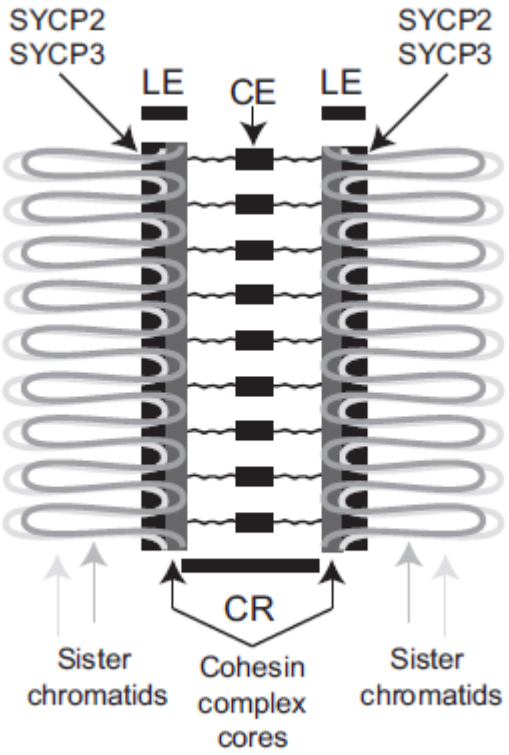

Figure 9: The chromosome axis. Model showing a multi-layered organization of the chromosome axis. Figure from Oritz et al. 2016.

1.6 The process of recombination during meiosis I

During prophase I of meiosis the process of DNA exchange between non-sister chromatids is recombination. It is a crucial process for creating genetic diversity and for correct chromosome segregation. During pachytene recombination occurs at distinct recombination nodules (Carpenter, 2003; Page and Hawley, 2003; Zickler and Kleckner, 1999). There are three different pathways of DNA repair and only reciprocal recombination caused by cross-over leads to chiasmata. Preceding the actual process of recombination, locations of possible DNA exchange are marked by the meiosis-specific topoisomerase II-like enzyme SPO11 which generates a few hundred Double Strand Breaks (DSB) throughout the genome (Figure 10) (Baarends and Grootegoed, 2003; Carpenter, 1975; Keeney et al., 1997; Moens et al., 2002). The formation of DSBs initiates a DNA damage response pathway, activating the kinases ATM (ataxia telangiectasia mutated) and ATR (ataxia telangiectasia and Rad3-related). ATM and ATR phosphorylate the histone variant H2AFX, forming γH2AX, which recruits repair

proteins to sites of DNA damage. In mice a complex of recombination specific proteins, RAD50, MRE11 and XRS2, removes SPO11 and leads to the degradation of the 5'-ends by exonucleases. This process is called "end-resection" and produces 3'-overhangings at the sites of DSBs (Figure 10). The 3'-overhangings are bound by RAD51 and DMC1, forming the early recombination nodules (ENs), which can be seen during leptotene as electron dense structures with a diameter of about 100 to 200 nm. ENs initiate the homology search in the genome and with the help of RAD54, RAD52, RAD55-57 and RPA homologous regions can be bound and the DNA helix can be unwound. During the following strand extension the 3'-strand infiltrates the homologue region and expands its binding site forming the characteristic D-loop formation (Figure 10). This partial region of homologue binding is called a heteroduplex. Specialized proteins (MSH2-MSH6, MLH1-MLH3, PMS2, BLM and TOPOIIIα) recognize this structure and start repairing the DNA damage via DNA synthesis and ligation. Transformed recombination nodules are formed (TNs). They can be detected on the AEs during the zygotene phase of meiosis I and there are about 200 in each murine spermatocyte. During pachytene TNs locate in the CR of the SC. Reparation of DSBs can lead to cross-over formations, non-cross-over formations and gene conversions. The two pathways leading to either of them are double strand break repair (DSBR) and synthesis dependent strand annealing (SDSA) in which SDSA does not lead to crossover events (Figure 10). SDSA either restores the damaged allele completely or gene conversion occurs. During DSBR the 3'-ends are prolonged and double holiday junctions (dHJ) are formed. By cutting the crossed DNA regions of dHJs in different ways, crossovers, non-crossovers and gene conversions are possible. Only about 25 of the TNs will lead to crossing-over events. They can be detected by locating the MLH1 protein, which is only present in late recombination nodules (RNs), which will lead to crossovers (Cohen et al., 2006).

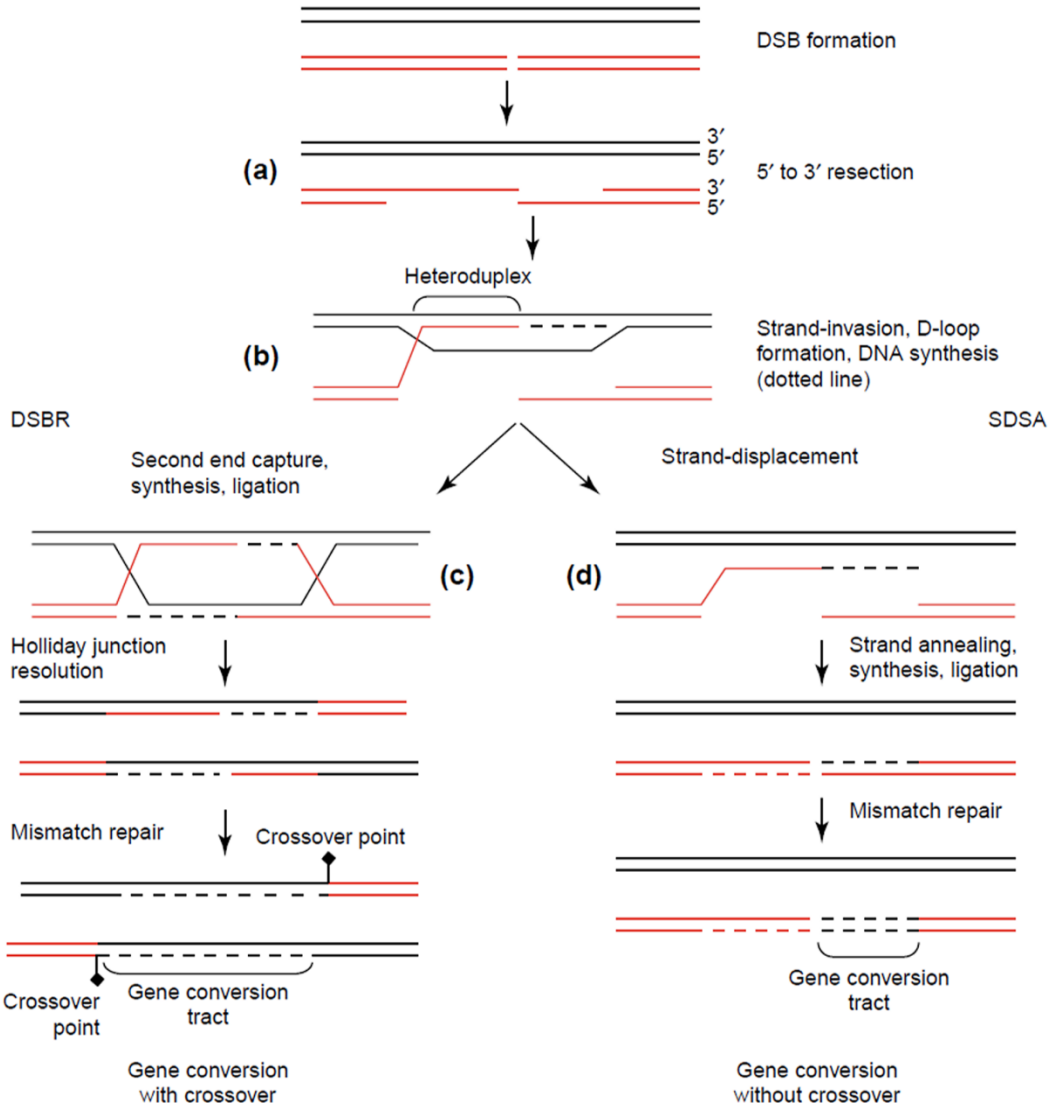

Figure 10: Reparation of double strand breaks.
The two reparation pathways of double strand breaks (DSBs) are shown. (a and b) DSB formation and strand invasion. (c) Double-strand-break-repair pathway. (d) Synthesis-dependent strand-annealing pathway. Figure from de Massy 2003.

1.7 Interplay between recombination, SC and CCs

The process of recombination is physically stabilized by the SC. Both processes, correct SC assembly and accurate recombination between homologues, are mutual dependent on each other. If one is flawed, so is the other (Bolcun-Filas et al., 2009; Hamer et al., 2008). However, the contribution of CCs in recombination is still not very well understood. It was shown, though, that SMC1ß is needed for successful recombination and formation of chiasmata (Hodges et al., 2005). It is also known that in somatic cells SMC1, SMC3 and α-kleisins are phosphorylated by the two kinases ATM and ATR at sites of DNA damage, which points to a role of cohesins in the DNA damage response

pathway. It is assumed that the phosphorylation of cohesins in the course of the DNA damage response pathway might bring sister chromatids into close proximity so that the DNA can be repaired and/or other proteins can be recruited (McNicoll et al., 2013).
It is still unknown if and how SC proteins and cohesins act together in the process of recombination.

1.8 Microscopic analysis of chromosome axis proteins

So far research of mammalian meiosis lacks functional cell culture systems. Therefore it highly depends on techniques outside of cell culture systems, like knock-out animal models and microscopic analyses. During this thesis advanced microscopic techniques were used to shed light onto murine SC and CC architecture and topography on the chromosome axis. Thereby the focus was placed on SIM and *d*STORM analyses, because of their increased resolution in combination with an easy sample preparation.

1.8.1 Confocal laser-scanning microscopic analyses

Confocal laser scanning microscopy (CLSM) is an optical imaging technique which uses lasers for analysing living and fixed biological specimens with high contrast and depth selectivity by stimulating fluorescence from fluorophores labelled to the sample and scanning it point-by-point. Confocal means that pinholes, specimen and objective lens are in the same focal plane. The pinholes help to focus the light onto the region of interest (ROI) rather than to illuminate the whole sample, which would cause photobleaching, lower processing speed and an increase in random-access memory (RAM) of the computer. You can acquire a series of images scanned point-by-point and section-by-section, which are then reconstructed into 2- or 3-D images on a computer. The clue of CLSM is that you can analyse thick specimens and produce an in-focus image of a chosen focal plane by optical sectioning. Blurring of the images is reduced by eliminating out-of-focus light with two pinhole apertures. The optical pathway is as follows: The emitted light of the microscope passes through the first pinhole aperture, situated in a conjugated plane, and is then reflected by a dichromatic mirror onto the chosen ROI of the sample. The movement of the beam is controlled by two high-speed oscillating mirrors situated behind the dichromatic mirror. They are driven by galvanometer motors. The emitted signal from the sample, called secondary

fluorescence, passes back through the mirror and is focused at the pinhole aperture in front of the detectors. The detectors are highly sensitive photomultiplier tubes (PMT), leading to an increase in the signal-to-noise ratio. Even the detection of one single photon is possible this way. The out-of-focus light rays are blocked by the detector pinhole. The PMT convert the light signal with their intensity into a corresponding analog electrical signal having a voltage. An analog-to-digital (A/D) converter transforms the analog signals into pixels of an image, which is pictured by a computer. The maximum resolution of a CLSM is limited to ~200 nm in the xy dimension and ~500 nm in the z dimension, because of the diffraction limit of light, described by Ernst Abbe.

$$\lambda/NA$$

NA= Numeric aperture of the objective= n* sin α

n= refraction index of the used immersion medium (air, water, oil, glycerol)

sin α= half the objective's opening angle

λ= wavelength of used light

In contrast to CLSM, conventional widefield light microscopy illuminates the whole surface of the specimen at once and cannot penetrate the sample to acquire images of different focal planes in thick samples. Autofluorescence and background noises are not blocked, reducing resolution and image contrast. Another advantage of CLSM is that sample preparation is easy and more cost-effective.

1.8.2 Super-resolution microscopic analyses

For analysing structures on a nanomolecular level, e.g. cell components, conventional microscopes do not provide sufficient resolution but are limited to the diffraction limit of the used light. Meaning that light, which enters an optical system like a microscope, is exposed to diffraction phenomenons leading to airy discs, which, according to the Rayleigh criterion, can only be distinguished if their brightness maxima are not closer than d= 1.22*λ*f/ D with λ= used wavelength, f= focal distance and D= diameter of the lense.

During the last couple of years several different super-resolution microscopic methods have been invented, like STED (Hell and Wichmann, 1994; Klar et al., 2000), PALM (Betzig et al., 2006), SIM (Gustafsson, 2000) and *d*STORM (Heilemann et al., 2008). All of which increase image resolution without changing optical components, but with exploiting physical and chemical properties of fluorescent dyes and the microscope system. During this work SIM (Structured Illumination Microscopy) and *d*STORM (*direct* stochastic optical reconstruction microscopy) have been used.

SIM uses patterned illumination to shrink the size of the PSFs. It provides the lowest resolution limit alongside the super-resolution microscopes with ~110 nm in xy- and ~ 300 nm in z- dimension, by superimposing the sample with a sinusoidal excitation pattern in different angles.

*d*STORM uses single molecule imaging by stochastically switching single fluorophores on and off. It belongs to the localization microscopic techniques like PALM and uses photostable organic fluorophores with high quantum efficiencies. In principal, single fluorophores are detected by separating signals of adjacent molecules in time and pin-pointing their position by fitting 2D Gaussian least squares to find their center. Therefore the stimulation probability of each fluorophore has to be low, meaning that the off state has to be longer than the on state. Ideally fluorophores emitting at the same time should have a distance exceeding the diffraction limit of light (> 200 nm). The switching ability of the fluorophores highly depends on the redox system of the surrounding buffer, the concentration of the reducing and the oxidizing agent (e.g. MEA and oxygen), the pH value and the laser intensity. This way thousands of photons are collected over time and the resolution is increased up to 20 nm on average in xy dimension and 40 nm in z dimension. The Nyquist-Shannon Theorem states that the labelling density has to be twice as high as the desired resolution (Patterson et al., 2010; Shannon, 1949). Conclusively, for a resolution of 20 nm there has to be a fluorophore every 10 nm. But still, the labelling density of concurrently active fluorophores should not exceed 1 fluorophore per μm^2 image, because the localization precision of most algorithms would decline, causing more artefacts in the image (Wolter et al., 2011).

In principal, the fluorophore is in its singlet ground state, before getting excited by the laser. The excited fluorophore can return to its singlet state by spontaneously emitting light. This phenomenon is called fluorescence. It can also be transferred into a triplet state by intersystem crossings (Feramisco et al., 1980). In its triplet state the

fluorophore can be reduced by thiol to its radical state, which is the stable off state of fluorophores. Some dyes can be reduced further, reaching their leucoform. The leucoform and the radical state are the two dark/off states of the fluorophores. They can be oxidized back to their singlet state by oxygen. Additionally, the radical form can be oxidized back to the ground state by radiation with light of 400 nm wavelength (van de Linde et al., 2011). Molecular oxygen can quench the fluorophore in its triplet state back to its ground state. It is therefore desirable to eliminate oxygen from the system to favor the reaction of the triplet state with thiol to reach the more desired radical form. Both reactions however, lead to photodamage by producing singlet oxygen and thiyl radicals.

$$\lambda/NA/\sqrt{n}$$

NA= numeric aperture of the objective

λ= wavelength of used light

n= number of detected photons

Summing up, now the resolution is not limited by the optical system anymore but by the total photon count from a single transmitter, its switching efficiency and the labelling density.

1.9 Aim of thesis: Elucidation of the organization of the meiotic chromosome axis

Often defects in the reproductive system, which is a major medical problem, lead to reproductive failure. To understand more about the cause for reproduction failure the system has to be understood. Therefore, it is of the utmost importance to understand the mechanisms behind the system. In the case of reproduction, the system is meiosis. Essential mechanisms for successful meiosis are among others synapsis of two homologue chromosomes provided by the SC and cohesion between homologues as well as sister chromatids provided by CCs. Understanding the complex relationships between these processes will help to comprehend medical problems in the reproduction system. In conclusion each process has to be described separately and links between them have to be found. In order to approach this challenging task the function of each protein

involved has to be unravelled and one essential aspect to understand the function of a protein is to know its structure and its topography.

So far, the molecular topography of proteins of the chromosome axis were analysed using conventional microscopy techniques like CLSM and transmission electron microscopy (TEM), which are limited either by resolution or signal density and accuracy. This thesis provides novel insights into the molecular structure of the chromosome axis with isotropic resolution and accuracy using the two super-resolution microscopes SIM and *d*STORM. In more detail proteins of the SC (SYCP3, SYCP2, SYCP1, SYCE1-3 and TEX12) and the cohesins STAG2, STAG3 and SMC3 were imaged during different meiotic stages. Ultimately, the topological relation of those proteins to one another and to each other were unravelled.

2. Material

2.1 Organisms

2.1.1 Mice strains

For all approaches wildtype male mice of the SYCE3 knock-out line, DA8 KO-B5 were used. This mouse strain was generated by Dr. Sabine Schramm during her PhD thesis 2006-2011 and is currently bred in the animal facility of the Biocenter, University of Würzburg. Additionally, male wildtype mice of the C57BL/6 mouse strain were kindly provided by the animal facility of the Biocenter, Würzburg.

2.1.2 Bacteria strains

For experiments conducted during this dissertation four different kind of bacteria were used:

Escherichia coli XL1-blue (Stratagen): This bacteria strain is used for cloning and amplification of plasmid DNA. Stock cultures of this bacteria strain do have a tetracycline resistance on their F plasmid but they dispose of it during the process of producing competent cells. They also are endonuclease deficient as well as recombination deficient, improving miniprep DNA quality and insert stability.

Escherichia coli Rosetta™ and **Escherichia coli Rosetta blue™** (Novagen): Both bacteria are expression strains used for producing recombinant proteins with elevated expression of eukaryotic proteins comprising codons rarely used in E.coli. They are recombination deficient and endonuclease deficient like E.coli XL1-blue. Additionally, they are lysogens of λDE3 that provides a T7 RNA polymerase gene and a chloramphenicol resistance. For control of T7 RNA polymerase expression both strains carry a pLysS plasmid. E.coli Rosetta™ and RosettaBlue™ are compatible with pET vectors, which have a T7 promotor for protein expression. RosettaBlue™ is also compatible with pQE vectors, because it additionally provides a T5 RNA polymerase. RosettaBlue™ bacteria are resistant against chloramphenicol and tetracycline.

StrataClone SoloPack Competent Cells (Stratagene): This is a bacteria strain that's part of the StrataClone Blunt PCR Cloning Kit of Stratagene. They are used for cloning PCR products into the StrataClone PCR cloning vector pSC-B-am/kan.

2.2 Molecular material

2.2.1 Enzymes

All used enzymes were purchased from Fermentas with the exception of the Tag-DNA Polymerase, which was self-manufactured in our laboratory by Silke Braune and Elisabeth Meyer-Natus.

2.2.2 Vectors

During this work three different vectors were used. For cloning the pSC-B-amp/kan vector (Figure 11) was used during all cloning experiments. It is part of the StrataClone Blunt PCR Cloning Kit of Stratagene. This vector has two blunt-ended topoisomerase I-charged arms and can be ligated with blunt PCR products. The equivalent bacteria strain, named StrataClone SoloPack Competent Cells, do express Cre recombinase, which then creates a circular DNA molecule containing a *lacZ'* α-complementation cassette for blue-white screening. The bacteria have to be grown on media containing ampicillin and/or kanamycin for selection of clones transformed with the plasmid.

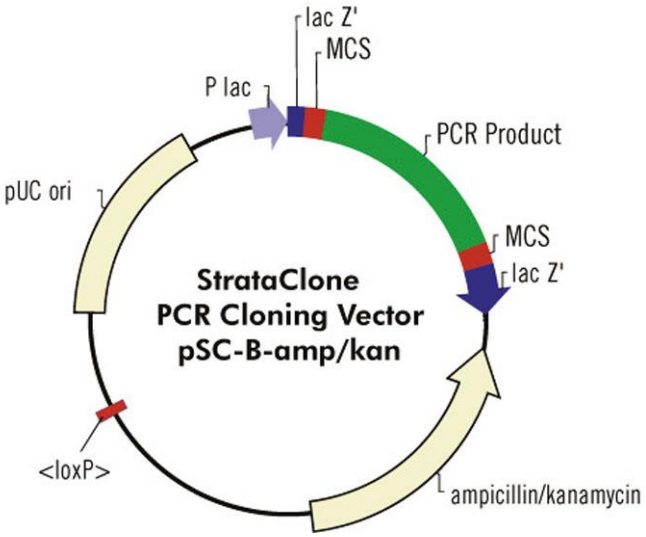

Figure 11: pSC-B-amp/kan vector by Stratagene.

The pQE-30 expression vector by Qiagen was used to generate recombinant proteins with an additional N-terminal RGS-His_6-tag (Figure 12). This has the disadvantage of purifying not only the recombined protein of interest but protein fragments as well. For selection of positive clones, media containing ampicillin was used.

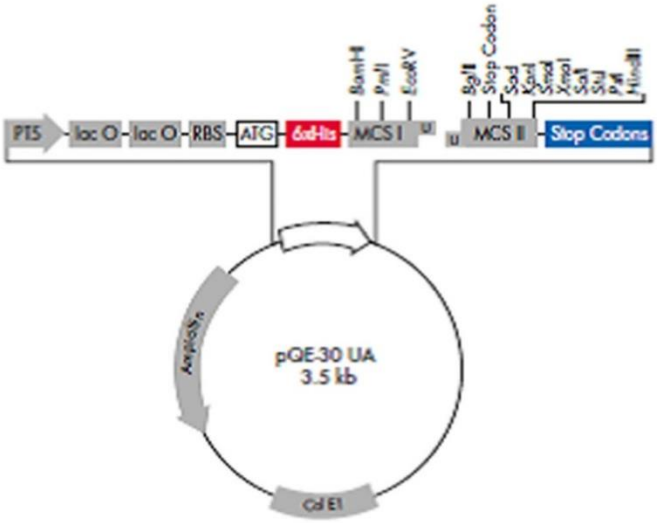

Figure 12: pQE-30 expression vector by Qiagen.

For the production of recombinant proteins with C-terminal His_6-tags the pET21a(+) vector by Novagen was used (Figure 13). On its N-terminus it has a T7·tag. Compatible bacteria have to be grown on media containing ampicillin.

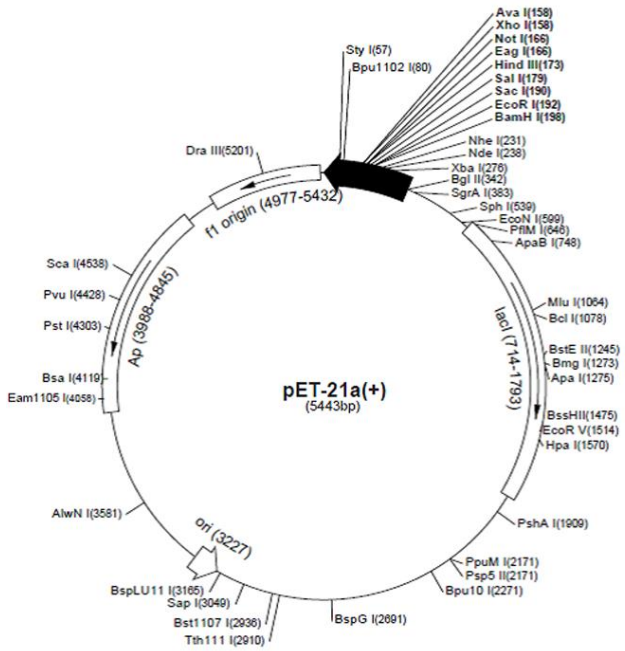

Figure 13: pET-21a(+) expression vector by Novagen.

2.2.3 Antibodies

All primary antibodies, if not stated otherwise, are polyclonal antibodies and were designed and purified in our laboratory. Injection of animals was carried out by BioScience, Göttingen. The rabbit anti-SYCP3 antibody was purchased from Novus Biologicals (NB300-232). The rabbit anti STAG3 antibody was provided by Prof. Rolf Jessberger, Institute of Physiological Chemistry, Dresden University of Technology (Biswas et al. 2016). The rabbit anti-SMC3 antibody, was purchased at Abcam® (ab-9263). The STAG2 antibody was provided by Dr. Alberto M. Pendas of the Centro de Investigacion del Cancer in Salamanca, Spain. The guinea pig anti-SYCE2 and partly the rabbit anti-SYCE1 antibody were provided by Professor Howard Cooke, MRC Human Genetics Unit MRC IGMM, University of Edinburgh. All primary and secondary antibodies used for this thesis are listed in table 2 and 3.

Table 2: List of primary antibodies used. Rb: Rabbit, Gp: Guinea pig, α: anti**.**

Label	Amino acid	Dilution CLSM	Dilution *d*STORM	Dilution SIM
Rb α SYCP1 N-terminus	1-124 rat	1:150	1:150	-
Rb α SYCP1 C-terminus	922-997 rat	1:150	1:150	-
Gp α SYCP1 N-terminus	110-468 rat	1:100	1:150	-
Gp α SYCP1 N-terminus	1-124 rat	1:100	1:150	-
Gp α SYCP2 C-terminus	1095-150 rat	1:100	1:150	1:100
Rb α SYCP2 C-terminus	1095-1505 rat	1:100	1:150	-
Gp α SYCP3 N-terminus	27-38 rat	1:150 1:200	1:200	-
Rb α SYCP3 C-terminus	human, bovine, porcine, rat	1:300	1:150	1:200
Rb α SYCE3	Full length mouse	1:150	1:150	-
Rb α SYCE1 N-terminus	316-329	1:150	1:150	1:150
Gp α SYCE1 N-terminus	316-329	1:150	1:150	1:150
Gp α TEX12	Full length rat	1:150	1:50	-
Gp α SYCE2	71-84 rat	1:50	1:100	1:150
Rb α STAG3	-	1:20-200	1:50-200	1:50
Rb α SMC3 C-terminus	mouse, human, Xenopus laevis	1:20-200	1:50-200	1:20
Rb α STAG2	mouse	-	-	1:20

Table 3: List of secondary antibodies. Rb: Rabbit, Gp: Guinea pig, α: anti.

Label	Enterprise	Catalog no.	Dilution *d*STORM/ SIM	Dilution CLSM
Goat α gp IgG (H+L) Alexa Fluor® 647 conjugated	Thermo Fisher Scientific	A-21450	1:200	1:200
F(ab′)2- goat α rb Alexa Fluor® 647conjugated	Thermo Fisher Scientific	A-21246	1:200	1:200
Rb α goat IgG (H+L) Alexa Fluor® 488 conjugated	Thermo Fisher Scientific	A-11078	1:200	1:200
Goat α mouse IgG (H+L) Superclonal™ Alexa Fluor® 488 conjugated	Thermo Fisher Scientific	A-28175	1:200	1:200
Goat α gp IgG(H+L) Alexa Fluor® 488 conjugated	Thermo Fisher Scientific	A-11073	1:200	1:200
Goat α mouse IgG (H+L) Alexa Fluor® 532 conjugated	Thermo Fisher Scientific	A-11002	1:200	1:200
Goat α rb IgG (H+L) Alexa Fluor® 532 conjugated	Thermo Fisher Scientific	A-11009	1:200	1:200
TexasRed goat α rb	DIANOVA	111-075-003	-	1:50
TexasRed goat α gp	DIANOVA	106-075-003	-	1:50

2.2.4 DNA and protein ladders

For estimating DNA product length the GeneRuler DNA Ladder Mix by Fermentas was used and for protein length determination the PageRuler Prestained protein ladder by Fermentas was used (Figure 14).

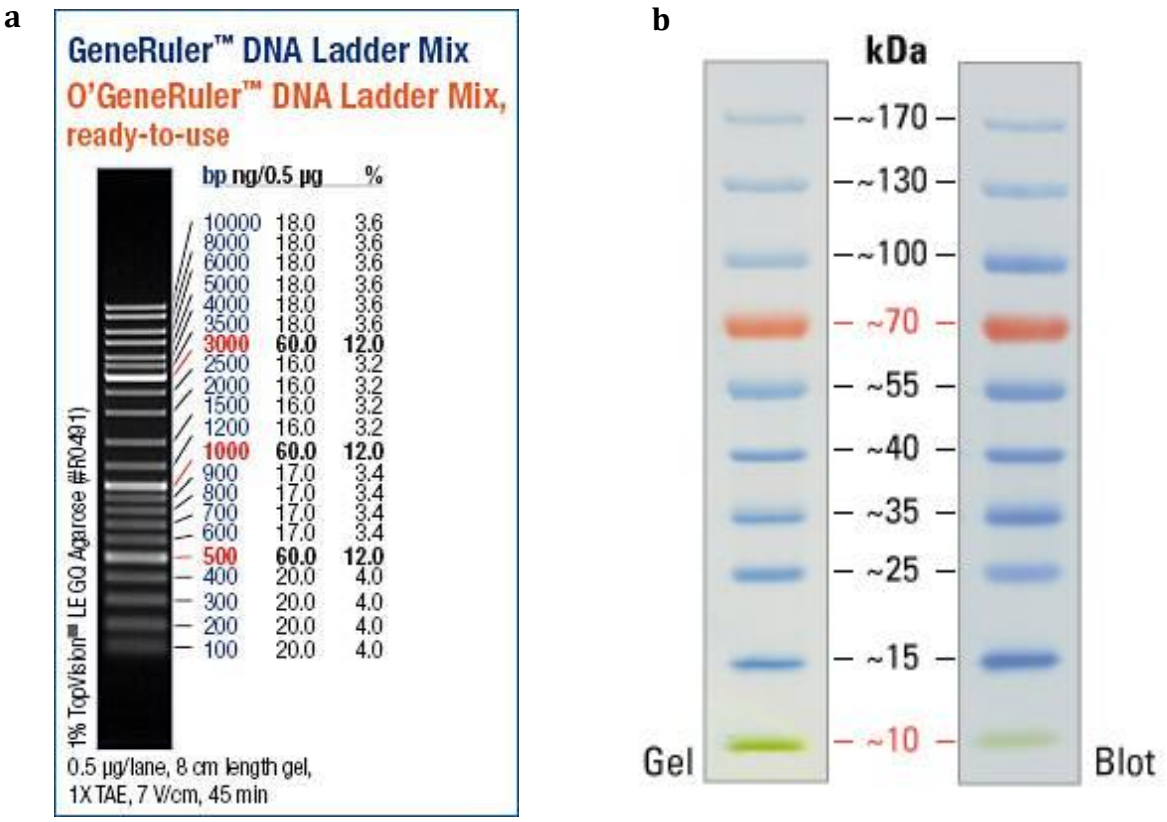

Figure 14: DNA and protein ladders.
(**a**) GeneRuler™ DNA Ladder Mix by Fermentas; (**b**) the PageRuler Prestained protein ladder by Fermentas.

2.2.5 Oligonucleotides

Table 4: List of oligonucleotides.

Label	Sequence	Annealing temperature [°C]	
		Taq	Phusion
M13_for	gtaaaacgacggccag	53/54	-
M13_rev	caggaaacagctatgac	53/54	-
pQE 3‘	aatccagatggagttctgagg	52	-
pQE 5‘	gagcggataacaatttcacac	52	-
T3	aattaaccctcactaaaggg	54	-
T7	gtaatacgactcactatagggc	54	-
SYCP1Nterm_BamHI_ mouse_for	ggatccatggagaagcaaaagccc	52	60
SYCP1Nterm_HindIII_ mouse_rev	aagctttatgctcactttccacttttttat	52	60
TEX12_BamHI_Mouse _5‘	ggatccatgatggcaaaccacctt	53	60
TEX12_HindIII_Mouse _3‘	aagcttcttgtgtagggtgttggtaattac	53	60
SYCE1_BamHI_Mouse_ 5‘	ggatccagcagcaaggagcagct	53	60
SYCE1_HindIII_Mouse_ 3‘	aagcttttaggtcctgcttgatggg	53	60
SYCP2_BamHI_Mouse _5‘	ggatccacagagaaaataacagaaagggat	54	60
SYCP2_HindIII_Mouse _3‘_Abs.1	aagcttggctgcatgattttcct	54	60
Foreward SYCP3 NT,rat, BamHI	ggatccgatgcttcgaggctg	52	57
Reverse SYCP3 NT, rat, XhoI	ctcgagagctttggtatacatttcta	52	57
SYCP3_NdeI_rat_for	catatgcttcgaggctgcg	52	52
SYCP3_XhoI_rat_rev	ctcgaggaataacatggattgaagagacttt	52	52
SYCE3 neu neo 5’	ctacccggtagaattgacctgcag	-	58
SYCE3 neu wt 5’	gggtaaatcaggttgaaggtcaggc	-	60
SYCE3 neu neo,wt 3’	gtcattctgggactcttgctatcctg	-	58

2.2.6 Genetic material

Table 5: List of genetic material. aa: amino acids.

Label	Bacterial strain	Vector	Insert
E.coli XL1-blue pSC B amp +SYCP3	E.coli XL1-blue	pSC B amp/kan	SYCP3 with N-terminal NdeI and C-terminal XhoI cutting point, no stopcodon
E.coli XL1-blue pET21a +SYCP3	E.coli XL1-blue	pET21a	SYCP3 with N-terminal NdeI and C-terminal XhoI cutting point, no stopcodon
E.coli XL1-blue pSC B amp SYCP1 N-Term Bam/Hind	E.coli XL1-blue	pSC B amp/kan	SYCP1 N-terminus, N-terminal BamHI and C-terminal HindIII cutting point
E.coli XL1-blue pQE30 SYCP1 N-Term PstI/HindIII	E.coli XL1-blue	pQE30	SYCP1 N-terminus, N-terminal PstI and C-terminal HindIII cutting point
SYCE1 in E. coli XL1-blue	E.coli XL1-blue	pSC B amp/kan	SYCE1 aa 190-329, N-terminal BamHI and C-terminal HindIII cutting points, with stopcodon
SYCE1 XL1-blue pQE30 BamHI/HindIII	E.coli XL1-blue	pQE30	SYCE1 aa 190-329, N-terminal BamHI and C-terminal HindIII cutting points, with stopcodon
TEX12 XL1 in E. coli XL1-blue	E.coli XL1-blue	pSC B amp/kan	TEX12 full length, N-terminal BamHI and C-terminal HindIII cutting points, no stopcodon
TEX12 Rosetta in E. coli XL1-blue	E.coli XL1-blue	pSC B amp/kan	TEX12 full length, N-terminal BamHI and C-terminal HindIII cutting points, no stopcodon
TEX12 XL1-blue pQE30 BamHI/HindIII	E.coli XL1-blue	pQE30	TEX12 full length, N-terminal BamHI and C-terminal HindIII cutting points, no stopcodon
SYCP2 Abs.1 XL1 pSC HindIII/ BamHI	E.coli XL1-blue	pSC B amp/kan	SYCP2 aa 1095-1230, N-terminal BamHI and C-terminal HindIII cutting points, with stopcodon

SYCP2 Abs.1 pQE30 XL1 HindIII/BamHI	E.coli XL1-blue	pQE30	SYCP2 aa 1095-1230, N-terminal BamHI and C-terminal HindIII cutting points, with stopcodon
SYCP2 Abs.1 pQE30 Rosetta blue HindIII/BamHI	Rosetta blue	pQE30	SYCP2 aa 1095-1230, N-terminal BamHI and C-terminal HindIII cutting points, with stopcodon
XL1blue pSC amp SYCP3 NT rat	E.coli XL1-blue	pSC B amp/kan	SYCP3 aa 1-357, N-terminal SalI and C-terminal XhoI cutting points
XL1blue pet21a SYCP3 NT rat	E.coli XL1-blue	pET21a	SYCP3 aa 1-357, N-terminal SalI and C-terminal XhoI cutting points

3. Methods

3.1 Microbiological methods

3.1.1 Bacterial cultures

LB-medium (pH 7.4):

10g/l Bacto-Trypton

5 g/l Yeastextract

10g/l NaCl

→ autoclaved, stored at 4°C

Table 6: List of antibiotics.

Antibiotic	[Stock]	[Working]
Ampicillin	50 mg/ml in H_2O	100 µg/ml
Chloramphenicol	34 mg/ml in 100% ethanol	34 µg/ml
Tetracyclin	15 mg/ml in 70% ethanol	15 µg/ml
Kanamycin	50 mg/ml in H_2O	50 µg/ml

For all bacterial cultures that were used during this dissertation the medium lysogeny broth (LB) was used and depending on the vector and bacteria combination, the respective antibiotic was added (Table 6). For dissolving ampicillin in water a few drops of 1M NaOH were needed.

3.1.1.1 Agar plate cultures

To cultivate bacteria and screen for clones 1.5% LB medium agar plates (w/v) including respective antibiotics were used. Cultures were usually incubated at 37 °C overnight or at least for 8 hours and stored at 4°C. If growth of colonies was needed to be prolonged lower temperatures were chosen.

3.1.1.2 Liquid cultures

Liquid bacterial cultures are daytime and overnight cultures that were used for protein or peptide overexpression and the cultivation of bacteria.

For daytime cultures 800 ml LB-medium, including the necessary antibiotic (Table 6), was inoculated with 40 ml overnight culture and incubated at 37°C until reaching an OD_{600} of 0.5-0.9. Then isopropyl-β-D-thiogalactopyranoside (IPTG) was added to a concentration of 1mM in total for starting protein overexpression. Incubation was continued for 4 hours (see "3.3 Proteinbiological Methods" for further information on protein purification).

For overnight cultures 50 ml LB medium was inoculated with a colony picked from an agar plate or from a glycerin culture and incubated at 37°C overnight.

3.1.1.3 Glycerine cultures

To store bacterial cultures for a longer time glycerine cultures were made of overnight cultures. Therefore, 800 µl overnight culture was carefully mixed with 200 µl glycerine and frozen at -80°C.

3.1.2 Photometric determination of cell density

For measuring the density of bacterial cultures, which is needed e.g. for daytime cultures, the optical density (OD) of the cultures was determined using a photometer. The photometer was first calibrated using LB medium and then the extinction of the sample was measured at a wavelength of 600 nm. An OD_{600} of 1 refers to $8x10^8$ bacteria per ml.

3.1.3 Generation of competent bacterial cells

<u>Transforming and Storage Solution (TSS) (pH6.5):</u>

LB medium

10% PEG 3350, 4000 or 8000

5% DMSO

50 mM $MgSO_4$ or $MgCl_2$

→ sterile filtrated, stored at -20°C

LB medium: (see 3.1.1.)

For transformation assays, competent cells were made by preparing 10 ml overnight cultures of the *E.coli* strain of interest (XL1-blue, Rosetta™ or Rosetta blue™).
On the next day 250 ml daytime culture was inoculated with 5 ml overnight culture and incubated at 37°C until reaching an OD_{600} of 0.6-0.8. The culture was centrifuged at 900xg for 10 minutes at 4°C and the bacterial sediment was dissolved in 6.25 ml cold TSS. Aliquots of 100 µl were made and shock frozen using fluid nitrogen and afterwards stored at -80°C.
The transformation efficiency was tested via a test transformation of the newly competent cells using 1, 10 and 100 pg pUC-vector-DNA and then counting the resulting colonies.

3.1.4 Transformation of DNA into bacteria

Plasmids were transformed into bacteria either for amplification or expression purposes. One aliquot of competent cells (100 µl) was thawed on ice and then carefully mixed with 50-150 ng purified plasmid DNA or a complete ligation mix. After an incubation time of 45 minutes on ice, the bacteria were heat-shocked at 42 °C for one minute and then put on ice for another minute. Then 900 µl of LB medium was added and the transformation-mix was agitated for one hour at 37°C. Afterwards 15 and 35 µl of the transformation-mix were transferred onto adequat selection plates (LB agar-plates including antibiotics) and incubated over night at 37 °C.

3.1.5 StrataBluntCloning

For cloning of blunt-ended PCR products, the StrataClone Blunt PCR Cloning Kit was used. Its instruction manual (catalog # 240207, Revision B.02) was followed with the following exceptions: 15 and 35 µl transformation mixture was plated onto the colorscreening plates.

3.2 Molecular Methods

3.2.1 Isolation of plasmids from bacteria (Miniprep)

For the isolation and purification of plasmid DNA from bacteria cells the Nucleospin® Plasmid (Machery-Nagel) miniprep kit was used, following the instruction manual. The isolated plasmids are of high purity and can be sequenced or used for cloning experiments.

3.2.2 DNA extraction from tissue

Sodium dodecyl sulfate (SDS)- mix (pH 7.5):
17 mM tris(hydroxymethyl)amino methane (Tris/HCL)
17 mM ethylenediaminetetraacetic acid (EDTA)
170 mM NaCl
0.85% (w/v) SDS
→ stored at room temperature

Proteinase K-Stock (Serva):
20 mg/ml in 10 mM $CaCl_2$
→ stored at -20°C in 100 or 200 µl aliquots

Saturated NaCl- solution:
6 M NaCl
→ stored at room temperature

For the genotyping of each mouse that was bred in our care, DNA had to be extracted from their tail or ear tissue. Therefore, a piece of tail or ear was removed from the mice, mixed with 500 µl SDS-mixture and 50 µl proteinase-K and rotated in a drying stove for laboratories over night at 56 °C. Then 250 µl saturated NaCl solution was added and the mixture was again rotated for 10 minutes at room temperature and subsequently incubated for 15 minutes on ice. Cell debris was precipitated by centrifugation at 4°C and 9000 rpm for 8 minutes and 500 µl of the lysate was transferred into another reaction tube and carefully inverted after adding 1 ml pre-cooled 100% ethanol (p.a.).

The DNA was precipitated by centrifugation and washed twice with 1 ml 80% ethanol (p.a., room temperature). The centrifugation steps were executed at room temperature and 14 000 rpm for 10 minutes. The supernatant was removed and the DNA pellet dried either at room temperature or on a heating plate (40°C), before resuspension with 15-30 µl ddH_2O, depending on the pellet size. DNA concentration and purity were measured using the Infinite M200 (Tecan). The extracts were stored at 4°C.

3.2.3 Polymerase chain reaction (PCR)

Phusion-PCR:

10 µl 5x Phusion™ HF Buffer (NEB)
1 µl Forward primer (Stock solution 10 pmol/µl)
1 µl Reverse primer (Stock solution 10 pmol/µl)
1 µl dNTPs (Mix, 10 mM/nucleotide, Fermentas)
1.5 µl DMSO (100%)
0.5 µl Phusion™ DNA Polymerase (2 Units/µl, NEB)
~ 300 ng genomic DNA
add ddH_2O to reach a total volume of 50 µl

Phusion PCR program:

Initial denaturation 2 min 98°C
Denaturation 15-20 sec 98°C
Annealing 15 sec ~52-62°C depending on primer
Elongation 15 sec/1 kb 72°C
Final elongation 5-7 min 72°C
Storage ∞ 4-8°C
Denaturation, annealing and elongation was repeated 35 times

Taq-PCR:

2.5 µl Taq-DNA-Polymerase 10x Reaction-Buffer

0.5 µl Forward primer (Stock solution 10 pmol/µl)

0.5 µl Reverse primer (Stock solution 10 pmol/µl)

0.5 µl dNTPs (Mix, 10 mM/nucleotide, Fermentas)

1.5 µl $MgCl_2$ (25 mM)

0.5 µl Tag-DNA-Polymerase (5 Units/µl)

~ 20-100 ng DNA or picked clone from agar plate

add ddH_2O to reach a total volume of 25 µl

Taq PCR program:

Initial denaturation 2 min 95°C

Denaturation 30 sec 95°C

Annealing 30 sec ~52-57°C depending on primer

Elongation 1 min/1 kb 72°C

Final elongation 10 min 72°C

Storage ∞ 4-8°C

Denaturation, annealing and elongation was repeated 25- 35 times

For genotyping and cloning experiments DNA templates have to be multiplied in vitro using polymerase chain reaction (PCR), which functionally resembles DNA replication. In principle PCR is the cyclic amplification of DNA, starting off with an activation step at 95-98°C for 2 minutes to activate the polymerase, followed by a denaturation step of 95-98°C for 15-30 seconds during which the DNA helix is broken down into single strands so that specifically designed primer pairs can bind their complementary sequences, forming the starting points of amplification. To ensure high amplification efficiencies several aspects have to be taken into account for primer design: Primer sequences have to be chosen in respect to high specificity and no formation of secondary products, like primer dimers or amplification side products. The GC amount should be between 40% and 60% and primers should have a length of 15-25 nucleotides. During the subsequent elongation step, deoxyribonucleoside triphosphates (dATP, dGTP, dCTP and dTTP) are added to the 5' ends of the prolonging primer sequences by a thermostable polymerase enzyme. The elongation temperature is adapted to the polymerase in use and the

elongation time is chosen based on the template size and the used polymerase as well. Denaturation, annealing and elongation were repeated for 25-35 times, a final elongation step at 72°C for 5-10 minutes allows the polymerase to finish off the end-adenylation.

For cDNA and genomic DNA amplification, especially for genotyping, the Phusion™ High-Fidelity DNA Polymerase was used. It is a fast and sensitive polymerase and has a proof-reading activity.

For the amplification of recombinant DNA in vectors and screening for positive clones from an agar plate during colony PCRs the Taq-Polymerase from the organism *Thermophilus aquaticus* was used. The polymerase was self-manufactured by Silke Braun and Elisabeth Meyer-Natus, Zoology I, University of Würzburg.

3.2.4 Restriction analyses

In order to transfer linear DNA between vectors during cloning experiments and also for screening for positive clones on an agar plate, the Thermo Scientific DoubleDigest reaction system was used. It uses restriction nucleases that recognize palindrome sequences and by cutting them, lead to sticky or blunt ends. During this thesis sticky ends were preferred. Restriction products can be separated using agarose gel electrophoresis and then can be extracted again.

Reaction mixture:

1 µg DNA

1 µl restriction enzyme 1

1-2 µl restriction enzyme 2

2 µl 10x buffer

add 20 µl ddH_2O

→ Incubation for 1-2 hours at 37°C and inactivation of enzymes at 60-80°C for 15-20 minutes depending on the enzyme in use.

For better results incubation of both enzymes could be separated. This was of use if the enzymes sterically interfered, thus lowering restriction efficiency or inhibiting it completely.

3.2.5 Ligation of DNA fragments

When vectors and inserts were cut with the same DoubleDigest system, their ends could be reconnected using the T4-DNA-Ligase (Fermentas). Beforehand, restriction products were separated using agarose gel electrophoresis, DNA bands of interest were extracted and subsequently used for the ligation mixture. During the ligation reaction, the T4-DNA-ligase forms a phosphodiester connection between the 3'-Hydroxyl- and the 5'-Phosphategroup.

Ligation mixture:

13 µl linear insert-DNA

+ 3 µl lineated vector-DNA

→ 65°C for 10 minutes, then:

+ 2 µl 10x T4-DNA-ligase-buffer

+ 2 µl 10 mM rATP (Fermentas)

+ 2 µl T4-DNA-ligase (5Units/µl)

→ 4°C overnight - for two days

3.2.6 DNA gel electrophoresis

6x DNA loading dye:

60% (v/v) glycerin

20% (v/v) 0.2 M EDTA

10% (v/v) ddH_2O

+ 4% orange G or 1% bromophenol blue or 2% xylene cyanol

50x Tris-acetat-EDTA- buffer (pH 8):

40 mM Tris-HCL

40 mM acetic acid

→ pH 8.0

+ 1 mM EDTA

PCR products and restriction products were visualized using 0.8-1% agarose gels (Sigma Aldrich) in 1xTAE (Tris-acetat-EDTA), which was covered with 1xTAE buffer. The gel

pockets were loaded with a ratio of 1:5 DNA loading dye and PCR product. Electrophoresis took place at approximately 120 V for 15-30 minutes, depending on the product size. During this time the negatively charged DNA fragments are pulled towards the anode of the electric field with speed according to their size. Subsequently, the gel was incubated in an ethidium bromide bath (150 ml ddH_2O + 50 µl 1% ethidium bromide stock solution) for 15-30 minutes, washed in ddH_2O and photographed if necessary using the intas® UV-transluminator. As a reference the GeneRuler™DNA Ladder Mix by Fermentas was used.

3.2.7 Gel extraction

DNA was extracted from agarose gels using the NucleoSpin® Gel and PCR Clean-up Kit (Macherey-Nagel) following its instruction manual with one variance: 680 µl and not 700 µl NT3 buffer was used for the washing steps.
The eluted DNA was dissolved in 30 µl ddH_2O and stored at -20°C.

3.2.8 DNA sequencing

DNA was sequenced either by GATC Biotech AG (https://www.gatc-biotech.com/de/home.html) or by Eurofins Genomics (http://www.eurofinsgenomics.eu/de.aspx). Sequences were analysed using NCBI (National Center for Biotechnology Information; https://www.ncbi.nlm.nih.gov/) and CLC Main Workbench (http://www.clcbio.com/).

3.3 Proteinbiological methods

3.3.1 His_6-tag purification of proteins

Buffer A-D:

100 mM NaH_2PO_4 x $2H_2O$

10 mM Tris/HCL

8 M Urea (buffer A pH 8, buffer B pH 6.3, buffer C pH 5.9, buffer D pH 4.5)

→ stored at room temperature

Neutralisation buffer (pH 9.5):

1 M Tris/HCL

→ stored at 4°C

His_6-Fusionproteins were produced using 600-800 ml day culture of the bacterial strains Rosetta™ or RosettaBlue™, depending on the used expression vector (see 2.1.2). The day culture was inoculated with 10 ml overnight culture per 200 ml day culture and incubated shaking at 37°C, until reaching an OD_{600} of 0.5-0.9. Then protein expression was induced by adding IPTG (isopropyl ß-D-1-thiogalactopyranoside) to a final concentration of 1 mM and the culture was again incubated for 4 hours (37°C, shaking). Afterwards, the bacterial culture was centrifuged at 3000 rpm and 4°C for 10 minutes, the supernatant was discarded and the cell pellets stored at -20 °C or directly affinity purified.

Before and after inducing protein expression 1 ml bacterial culture was sampled. The samples were centrifuged at 14 000 rpm and 4°C for 10 minutes, the supernatant was discarded and the cell pellets stored at -20 °C or directly run in a SDS-PAGE for expression control.

His_6-Fusionproteins were affinity purified based on the Ni-NTA Spin Kit Handbook 01/2008 by Qiagen (Hilden, Germany), using gravity-flow chromatography. For this the cell pellets were resuspended in buffer A (30-40 ml), sonificated 3 times for 15 seconds on ice (5 Mikro/Mini-Tip) and incubated for 1 hour at room temperature, to break down the cells and release the proteins within. Cellular parts were sedimented by centrifuging

at 10 000 rpm and 4°C for 15 minutes. The supernatant contains the proteins and was stored at 4°C or affinity purified.

Next a polypropylene column (Qiagen, Cat.no. 34964) was filled with 2 ml of a 1:1 suspension of nickel nitrilotriacetic acid (Ni-NTA) agarose (Qiagen, Cat.no. 30310) and 30% ethanol. Inside the column the metal is firmly held onto by NTA, which is a chelator and is strongly connected to the agarose, therefore immobilizing the metal in the column.

After the agarose sedimented to the bottom of the column, the matrix was equilibrated to pH 8 using 20 ml buffer A. The positively charged histidine side chain of the tagged proteins were now able to bind the Ni^{2+} of the Ni-NTA agarose matrix by replacing two water molecules of the metal with histidines. Unspecifically bound proteins were removed during several washing steps with 20 ml buffer A, 15 ml buffer B and 10 ml buffer C respectively. Elution of His_6-tagged proteins was achieved by reducing the pH of the matrix with 10 ml buffer D. Generally, monomeres are eluted at pH 5.9 and multimeres at pH 4.5. The flow-through was collected in 1.5 ml Eppendorf tubes (1 ml flow-through per tube). To avoid acid hydrolysis 50 µl neutralization buffer was added per tube. The affinity purified proteins were stored at 4°C.

3.3.2 Methanol-chloroform precipitation of protein samples

For precipitation of affinity purified proteins 4 volumes of pre-cooled methanol (-20°C) and 1 volume of chloroform (RT) were added to 1 volume of protein suspension and vortexed for 10 seconds. Then 3 volumes of ddH_2O (4°C) were added and incubated for 10 minutes on ice. After centrifuging the sample at 13000xg and room temperature for 10 minutes, three phases are visible with an organic phase on the bottom and an aqueous phase on the top. In between is a protein membrane. After the aqueous phase is discarded 4 volumes of methanol (-20°C) are added. After centrifuging the sample again at 13000xg and room temperature for 10 minutes, the supernatant is discarded and the protein pellet is dried at room temperature.

3.3.3 Antibody purification using HiTrap columns

Binding buffer (pH 8.3):
200 mM $NaHCO_3$
500 mM NaCl
→ stored at 4°C

Washing buffer 1 (4°C):
1 mM HCl
→ stored at 4°C

Buffer A (pH 8.3):
500 mM C_2H_7NO
500 mM NaCl
→ stored at 4°C

Buffer B (pH 4.0):
100 mM acetic acid
500 mM NaCl
→ stored at 4°C

Washing buffer 2:
3.5 M $MgCl_2$
→ stored at 4°C

PBS (pH 7.4):
140 mM NaCl
2.6 mM KCl
6.4 mM Na_2HPO_4
1.4 mM KH_2PO_4
→ stored at RT

PBS + 350 mM NaCl (pH 7.4):
→ stored at 4°C

Elution buffer (pH 2.5):
100 mM Glycerine
→ stored at 4°C

Neutralisation buffer (pH 9.5):
1 M Tris/HCl
→ stored at 4°C

Storage buffer (pH 7.0):
50 mM Na_2HPO_4
0.1% (w/v) NaN_3
→ stored at 4°C

All buffers were sterile filtered using 0.45 µm filters.

Antibodies were purified from blood serum using HiTrap™ NHS-activated High Performance columns (GE Healthcare Life Sciences). The columns were packed with NHS (N-hydroxysuccinimide)-activated Sepharose 4 Fast-Flow, which is a pre-activated agarose matrix that covalently binds amino-containing proteins and peptides by forming

amide bonds with primary amino groups. The affinity purified antigen of interest was dissolved in binding buffer with a concentration of 2-10 mg/ml and a maximum of 0.2% SDS. SDS was only added if there were problems with precipitation. Heating the sample to 95°C also helped to dissolve the antigen. Before putting it on the column the mixture was centrifuged for 5 minutes at 3000xg and room temperature to sediment undissolved particles, like antibody aggregates.

All solutions were put on the column with a flow rate of 1 ml/minute using an adapter, a laboratory pump and tubes of different diameter.

First, the matrix was equilibrated with 6 ml pre-cooled washing buffer 1. Then the column was loaded with 1 ml of the antigen solution and incubated for 1 hour at room temperature so that the antigen had enough time to saturate all binding sites of the columns matrix. Afterwards, redundant protein was washed of the matrix using 6 ml buffer A, 6 ml buffer B and again 6 ml buffer A. The first ml of the first washing step was collected, so that the binding efficiency could be tested using SDS-PAGE (see 3.3.4). The column was incubated in buffer A for 1 hour at room temperature, so that ethanolamine could saturate all free binding sites of the matrix, which had not bound any antigen beforehand. Again the column was washed with 6 ml buffer B, 6 ml buffer A, 6 ml buffer B and 20 ml PBS respectively.

After binding the antigen, the HiTrap™ column could be used for affinity purifying antibodies from serum. Therefore, the column was again washed with 10 ml washing buffer 2 to remove excessive antigen and protein fragments. A washing step with 30 ml PBS followed. The serum (5 ml guinea pig or 10 ml rabbit serum) was centrifuged at 3000xg and 4°C for 10 minutes and the supernatant mixed with 10-folds PBS before loading it onto the columns four times in a row. The column was washed with PBS (30 ml for guinea pig and 50 ml for rabbit), PBS + NaCl (30 ml for guinea pig and 50 ml for rabbit) and 10 ml PBS, respectively. The antibody was eluted using 15 ml elution buffer and to avoid acid hydrolysis 50 µl neutralisation buffer was added to each milliliter. The used HiTrap™ column was washed with 20 ml PBS and stored, loaded with storage buffer, at 4°C. The column could be used several times.

For further usage of the eluate, the buffer was exchanged during a dialysis with PBS at 4°C overnight. For this, 4 liter PBS was cooled down to 4°C and the eluate was pipetted into a dialysistube (Visking Type 20/32), which was cooked beforehand for 30 minutes to 1 hour in 2 mM EDTA (pH 8) and rinsed in ddH_2O, afterwards. The dialysistube is impermeable for molecules above 14 kDa.

The antibody was concentrated using Centriplus YM 50K centrifugal filter devices by Millipore. Centrifugation took place at 3000xg and 4°C. The Ultracel-YM membrane of the amicon tube is impermeable for molecules above 50 kDa, leaving intact antibodies above the filter. The antibody concentration was determined using a photometer and a wavelength of 280 nm, where an extinction of 1.48 represents 1.0 $^{mg}/_{ml}$. In the end an OD_{280} of 1.48-2.8 is preferred. If that was not possible, the dialysate was centrifuged down to 250 µl and stabilized to 1 mg/ml using BSA (p.a).
Aliquots of the purified and concentrated antibody were stored in two ways: most of them were shock-frozen using liquid nitrogen and afterwards stored at -70°C but if needed some were lyophilized in aliquots and stored at room temperature.

3.3.4 SDS-PAGE

Solution A:
29.22 % acrylamide
0.8 % bis-acrylamide
→ stored at RT

Solution B (pH 8.7):
1 M Tris/HCl
→ stored at RT

Solution C (pH 6.8):
1 M Tris/HCl
→ stored at RT

2xProteinsampling buffer (PPP) (pH 6.8):
120 mM Tris/HCl (pH 6.8)
10% (w/v) SDS
20% (v/v) glycerol

20% SDS (in ddH_2O):
→ stored at RT

→ adjust pH value and add 20 % ß-mercaptoethanol, stored at -20°C

Running buffer (pH 8.5):
25 mM Tris/HCl
112 mM glycerol
0.1 % (w/v) SDS
→ stored at RT

10% APS (in ddH_2O):
→ stored at 4°C

Coomassie:	Discolouration:
0.25% (w/v) Coomassie R250	10% (v/v) isopropanol
10% (v/v) isopropanol	5% (v/v) acetic acid
5% (v/v) acetic acid	

Table 7: Pipetting scheme for one separation-gel.

Chemical	10%	15%
Solution A	2.5 ml	3.75 ml
Solution B	2.8 ml	2.8 ml
20% SDS	37.5 µl	37.5 µl
ddH_2O	2.12 ml	0.86 ml
Temed	5 µl	5 µl
10% APS	50 µl	50 µl

Table 8: Pipetting scheme for one sampling-gel.

Chemical	5%
Solution A	0.84 ml
Solution C	0.63 ml
20% SDS	25 µl
ddH_2O	3,46 ml
Temed	5 µl
10% APS	75 µl

For separating proteins of different molecular mass, sodium dodecyl sulfate polyacrylamide gel electrophoresis (SDS-PAGE) according to Laemmli (Laemmli, 1970) was used. The proteins were chemically and physically denaturated before being loaded onto the gel using heat, SDS and ß-mercaptoethanol. The pore width of the gel matrix is determined by the acrylamide/bisacrylamide ration and has to be chosen according to the protein masses that are going to be separated. One fold protein sample were mixed with one fold 2xPPP and incubated at 95°C and loaded onto the gel. The gel is charged with 60 V while the samples run through the sampling-gel (5%) to form a compact front, ensuring an even run through the separation gel (10-15%). After reaching the separation-gel the voltage can be increased up to 100 V. The negatively charged SDS-protein complexes run towards the anode and proteins of higher mass run slower

through the gel in comparison to lighter proteins. As a reference the PageRuler Prestained protein ladder by Fermentas was used.
Afterwards the gel was either used in a WESTERN-Blot or stained in coomassie for at least three hours and stripped for at least 8 hours until protein bands are clearly visible. For preservation purposes the gel was dried using regenerated cellulose films.

3.3.5 WESTERN blot analyses

CAPS-buffer (pH 10):
50 mM CAPS
10% (v/v) methanol
→stored at RT

TBST (pH 7.4):
150 mM NaCl
10 mM Tris/HCl
0.1% (v/v) Tween®20
→ stored at RT

Saturation solution (pH 7.4-7.6):
10% (w/v) skimmed milk powder in TBST
→ stored at 4°C for one day

After proteins were electrophoretic separated using SDS-PAGE, they can be transferred onto a nitrocellulose membrane to be detected by indirect labelling them with peroxidase. This method can be used for separating and detecting proteins or protein parts or for testing antibodies.
First, the separation acrylamide-gel is removed from the electrophoretic chamber and washed in CAPS buffer for 5-10 minutes. A Whatman® Nitrocellulosemembrane (9x5 cm) and 18 Whatman® Gel Blotting-Papers (each 9x5 cm) are drained in CAPS buffer likewise. In a graphite blotting chamber nine blotting papers are put on the anode, afterwards the nitrocellulosemembrane, the gel and nine blotting papers are stacked on top, respectively, followed by the cathode. Proteins are transferred onto the membrane with a steady electric current of 1mA/cm^2 until the electric tension increases from 4V to 20V. Afterwards, the membrane was incubated in Ponceau S for 3 minutes and 5 minutes in ddH_2O to check if the transformation was successful. For complete discolouration the membrane was then incubated in TBST for 5 minutes.

Next, the membrane was incubated in 10% milk in TBST to saturate unspecific binding sites. First for one hour at RT and subsequently over night at 4°C. An incubation step of 2 hours at RT followed the next day. Then the membrane was incubated for 1-2 hours with the primary antibody, which was diluted in saturation solution, followed by three washing steps: Each for 10 minutes in TBST, to remove unbound antibodies. The secondary antibody was diluted in 10% milk likewise and put onto the membrane for a maximum of one hour before washing the membrane again three times for 10 minutes each.

In a dark room the ECL solutions A and B were mixed in a ratio of 1:1, poured onto the membrane and incubated for at least one minute. During this time the peroxidase of the secondary antibody splits peroxide, catalysing a redox-reaction between the two ECL solutions, which produces a light signal. This light signal can be used for X-ray film exposure, leading to the visualisation of the protein bands, which were transferred from the acrylamide-gel onto the nitrocellulose membrane. The developing time of the films depended on the degree of coupled peroxidase, which corresponds to the quantity of protein on the membrane.

3.4 Microscopic methods

3.4.1 Spermatocyte cell spread preparation

PBS (pH 7.4):
140 mM NaCL
2.6 mM KCl
6.4 mM Na_2HPO_4
1.4 mM KH_2PO_4
→ stored at RT

Hypotonic buffer (8.2):
30 mM Tris/HCl
17 mM Trisodium citrate
5 mM EDT
50 mM sucrose
5 mM DTT (Dithiothreitol)
→ stored at 4 °C

1% Paraformaldehyde (pH 7-9):

For dissolving 1% PFA in ddH_2O, the solution had to be heated to 60°C and mixed with a few drops of 1M NaOH. After the mixture cooled down, 0.15% Triton X-100 in ddH_2O was added and the pH value adjusted. → stored at 4°C

100 mM Sucrose:

→ stored at -20 °C

→ All chemicals were sterile filtrated.

For analysing the architecture of the synaptonemal complex (SC) regardless of the cell morphology, murine spermatocyte spreadings were prepared following the protocol of de Boer et al. 2009 (de Boer et al., 2009). Tubuli seminiferi were dissected from testes of wildtype mice and transferred into hypotonic buffer. Cells were allowed to swell for 30-60 minutes. Afterwards the tubuli were sheared and suspended in sucrose and transferred into a drop of 1% paraformaldehyde with 0.15 % Triton X-100 on a coverslide/-slip and distributed over the glass surface. Coverslides/-slips were incubated for 1-2 hours in a closed moist chamber and left to dry overnight in a semi-open moist chamber.

Cell spreads were prepared on cover slides (SuperFrost®Plus, Thermo Scientific) for Confocal Laser Scanning Microscopy (CLSM) and Structure Illumination Microscopy (SIM). For *direct* stochastic optical reconstruction microscopy (*d*STORM) cell spreads were prepared on cover slips (24 x 60 mm) to increase resolution. Cover slips were coated with 0.01% Poly-L-lysine for five minutes, washed with ddH_2O three times for 2 minutes and dried at RT. Coverslides and coverslips were drained in 1% paraformaldehyde directly before use.

3.4.2 Immunofluorescence on cell spread preparation

PBS (pH 7.4):

140 mM NaCL

2.6 mM KCl

6.4 mM Na_2HPO_4

1.4 mM KH_2PO_4

→ stored at RT

Blocking solution (pH 7.4) in PBS:

5% milk

5% FCS

→ stored at -20 °C

Cell spreads were used for immunofluorescence labelling, which was carried out as described in de Boer et al. 2009 (de Boer et al., 2009). First coverslides/slips were washed three times in PBS. Afterwards unspecific binding sites were saturated by covering the glas surface with blocking solution for 30-60 minutes. An incubation step with 150 µl per slide/slip of the primary antibody in the appropriate dilution in blocking solution followed for at least 1 hour. After washing again three times in PBS, another blocking step for 30-60 minutes followed, before incubating the sample with the secondary antibody for 20-30 minutes. If samples were going to be used for CLSM 30-50 µl Hoechst 33258 (1:333 in PBS) were pipetted onto the cell spreads and incubated for 10 minutes, before washing again with PBS.

Cell spreads for CLSM and SIM were embedded in 50 µl glycerol/PBS (1:1) using 24 x 60 mm cover slips (A. Hartenstein GmbH) for CLSM and 24 x 60 mm high precision cover slips (A. Hartenstein GmbH) for SIM. Samples were stored at 4°C. *d*STORM samples were stored in a cuvette at 4°C.

Coverslides/slips were covered with coverslips when incubating with antibodies to ensure covering of the whole surface and a minimum input of antibody. All incubation steps were executed in a closed moist chamber.

3.4.3 Testis suspension preparation and immunofluorescence

<u>PBS (pH 7.4):</u>
140 mM NaCL
2.6 mM KCl
6.4 mM Na_2HPO_4
1.4 mM KH_2PO_4
→ stored at RT

<u>Blocking solution (pH 7.4) in PBS:</u>
5% milk
5% FCS
→ stored at -20 °C

<u>1% Paraformaldehyde (pH 7-9):</u>
For dissolving 1% PFA in ddH_2O, the solution had to be heated to 60°C and mixed with a few drops of 1M NaOH. After the mixture cooled down, the pH value adjusted.
→ stored at 4°C

<u>0,1% Triton X-100 in ddH_2O: </u>→ stored at 4°C

Testis suspensions were prepared for analysing chromatin associated structures like the SC without destructing the cell. The cellular morphology is kept intact and results can be compared to in vivo circumstances. Testis suspensions were prepared in 8-Well-Lab-Tek II coverslip-chambers, which were covered in 0.01% Poly-L-Lysine. For this they were filled with 0.01% Poly-L-Lysine for at least 30 minutes. Afterwards they were washed two times with ddH_2O for 5-10 minutes each, before drying over night at RT.

Tubuli seminiferi were dissected from testes of wildtype mice and transferred into PBS, where they were minced using razor blades. Cells were flushed out by pipetting the suspension and separated from the remaining tissue by filtration through a nylonmesh (meshsize 30 µm). The filtrate was centrifuged at 500g and 4°C for 10 minutes. The supernatant was discarded and the remaining pellet resuspended in 1 ml PBS. Wells of the coverslip-chambers were filled with 200 µl cell suspension and cells were allowed to sink to the bottom for at least 10 minutes, before fixation with 350 µl 1% PFA for 5 minutes. Then 100 µl 0.1 % Triton X-100, which promotes permeability of cell membranes, was applied and incubated for 10 minutes. The supernatant in the wells was discarded and they were washed three times for 5 minutes in PBS. Immunofluorescence followed immediately by blocking for 30 minutes and carried out as described in **3.4.2**.

3.4.4 CLSM imaging and analysis

Confocal laser scanning microscopy (CLSM) is an optical imaging technique which was used for analysing immunofluorescence on cell spreads and testis suspensions with high contrast and depth selectivity. Imaging was performed using a Leica TCS-SP2 AOBS confocal laser scanning microscope (Leica, Bensheim, Germany) and a 63x/1.40 HCX PL APO Ibd.BL oil-immersion objective. Images were scanned at 800 Hz and 1024x1024 pixels and analysed using the Leica LCS Lite Software.

3.4.5 SIM imaging and analysis

Structured illumination microscopy (SIM) was used for analysing chromatin associated structures labelled on cell spreads with a resolution up to 100 nm.

SIM was performed using an Elyra S1 microscope with a Pln Apo 63x/1.4 Oil DICII objective. Images were scanned at 1280x1280 pixels with 5 rotations. For recordings

and further processing of images, the Zen 2012 Black Edition software as well as the Zen lite 2012 software from Zeiss were used.

3.4.6 *d*STORM imaging and analysis

Direct stochastic optical reconstruction microscopy (*d*STORM) was performed partly in cooperation with Thorge Holm (Department of Biotechnology and Biophysics, University of Würzburg) using the IX-71 inverted wide-field fluorescence microscope by Olympus (IX71; Olympus, Tokyo, Japan). A detailed description of the set-up can be found in van de Linde et al. 2011 (van de Linde et al., 2011). The microscope was set-up on a vibration-isolated optical table. For excitation of Alexa 647 (Al647), a 639 nm OPS Laser-Diode System (Genesis MX639-1000 STM, Coherent, Santa Clara, USA) was used. For the excitation of Al532 and Al488 a 514 nm OPS Laser-Diode System (Genesis MX514 STM; Coherent, Santa Clara, USA) and a 488 nm OPS Laser-Diode System (Sapphire 488 LP, Coherent, Santa Clara, USA) have been used respectively. Laser beams were spectrally cleaned either by the 642/10 nm BrightLine® single-band bandpass filter (FF01-642/10-25; Semrock, Rochester, USA), the Laser Clean-up filter (ZET 514/10; Chroma, Bellow Falls, USA) or by the 488/10 nm BrightLine® single-band bandpass filter (FF01-488/10-25; Semrock, Rochester, USA) and overlaid by a LaserMUX filter (LM01-552; Semrock, Rochester, USA). A system of lenses and dielectric mirrors was mounted on a custom made linear translation stage to switch between EPI, HILO and TIRF illumination. To focus and widen the laser beam onto the back focal plane (BFP) of a 60x PlanApo microscope objective with NA 1.45/ NA 1.49 by Olympus (APON 60XOTIRF; Olympus, Tokyo, Japan), achromatic lenses with focal lengths of 25 mm and 120 mm respectively (G322284000 and G322303000; Qioptiq, Göttingen, Germany) were used. The objective was mounted into a nosepiece stage (IX2-NPS; Olympus, Tokyo, Japan) to minimize sample drift. The broad band dielectric mirror BB2-E02 by Thorlabs (KCB2 and BB2-E02, Thorlabs, New Jersey, USA) was used to direct the laser beam into the back port of the microscope. It was reflected into the objective by the FF425/532/656-Di01 triplet band dichroic beam splitter by Semrock (FF425/532/656-Di01; Semrock, Rochester, USA). The emission light of the fluorophores is collected by the same objective and then, again, transmitted by the dichroic beam splitter FF425/532/656-Di01 by Semrock and a triplet band detection filter of Semrock (Em01-R442/514/647; Semrock, Rochester, USA). The emission light of the different Alexa

fluorophores is separated and spectrally filtered by a dichroic beam splitter (630dcxr; Chroma, Bellow Falls, USA), followed by BrightLine® single-band bandpass filters, with FF01-582/75-25 for Al532, FF01-697/75 for Al647 and FF01-480/17-25 for Al488 by Semrock. The filters are mounted inside a dual camera adaptor (TuCam; Andor, Belfast, UK) connecting two EMCCD cameras (iXon Ultra 897; Andor, Belfast, UK).

For 3D *d*STORM imaging (was performed in cooperation with Dr. Sven Proppert, Department of Biotechnology and Biophysics, University of Würzburg) a cylindrical lens is used for separating signals below and above the focal point due to an astigmatic refraction of the spherical light signal.

For super-resolution imaging data stacks consisted of 15000- 30000 images with frame rates of 50-100 frames per second and were recorded with exposure times between 10-20 ms and laser intensities of 1-3 kW cm-2. Conventional fluorescence images had been taken beforehand at exposure times between 10 - 1000 ms and low laser intensities to prevent photoswitching and bleaching.

For photoswitching a 100 mM β-mercaptoethylaminebuffer (MEA; Sigma) in PBS was used. For one-color measurements with Al647 an oxygen scavenger system containing 5-10% (w/v) glucose and 0.5 mg/ml glucose oxidase was used and the pH value was adjusted using KOH (4-5 M) to 7.4-7.7 (Schafer et al., 2013). For two-color experiments with either Al647 and Al532 or Al647 and Al488 no oxygen scavenger system was added and the pH value was adjusted to 8.2-8.5. Al647 was always recorded first, to prevent excitation of Al647 with the emission light of Al532 and Al488 and thereby reducing its quality and even cause photobleaching of the fluorophore.

3.4.7 Editing *d*STORM images

Images were reconstructed using rapidSTORM 3.2. (Wolter et al., 2010) with a pixel size of 10 nm, if not stated otherwise. The software uses an algorithm which fits a two-dimensional Gaussian function over the images and thereby detects the localizations of single fluorescence signals. Both cameras were aligned using multifluorescent beads called TetraSpecks (Life Technologies). For two-colour imaging, images of the two different cameras were transformed onto each other by marking them with landmarks in bUnwapJ, Fiji (Arganda-Carreras et al., 2006). Chromatic aberrations were corrected using a non-linear elastic transformation matrix (Fiji, Plugin bUnwarpJ) (Arganda-Carreras et al., 2006).

3.4.8 Quantitative evaluation of distances and diameters of chromosome axes proteins

Average distance measurements for the determination of distances and diameters of chromosome axes proteins were calculated by Christian Franke, Department of Biotechnology and Biophysics, University of Würzburg. Calculations were made from frontal and lateral views with lateral views being areas of helical cross-overs of the SC. For each calculation an in-house written python routine was used to separate single SCs and cohesins with a canny edge filter. This way a mask was generated, which was used on the output image data given by the software rapi*d*STORM 3.2 to find localizations of potential SCs and cohesins. In this connection complexes showing crossed regions or extreme curving were discarded from the analyses. Next, a high-order polynominal was fitted onto the data and used as a guideline for the application of a sliding window algorithm. The sliding window algorithm moved in 25 nm steps leading to overlapping segments, for all of which the localization distances were determined. These distances were perpendicularly projected to the current slope of the polynominal and then histogrammed. The resulting histogram was the basis for the protein strand diameter calculations. To determine the SD of the localizations, bi-gaussian and mono-gaussian models were used. All obtained values for each segment along the protein strand are then again histogrammed. The mean value for each measurement can be determined by again using bi- and mono-gaussian fits. Overall, for each protein of interest 5-54 SCs were processed in the described way. To detect only the cohesins that localize to the SC region a mask-filter based on the properties of SYCP3 was applied. For a more detailed description on the used methods please see Schücker et al., 2015 and Schücker et al., 2016 (under review).

4. Results

4.1 Super-resolution imaging

We were able to image chromosome axis proteins with super-resolution microscopy using standard immunofluorescence protocols, which are also used for CLSM. Sample preparation for cell spreads did not have to be altered, likewise. In the end the highest resolution was obtained using *d*STORM with 20 nm. Whereat the increase in structural information has proven to be substantial (Figure 15).

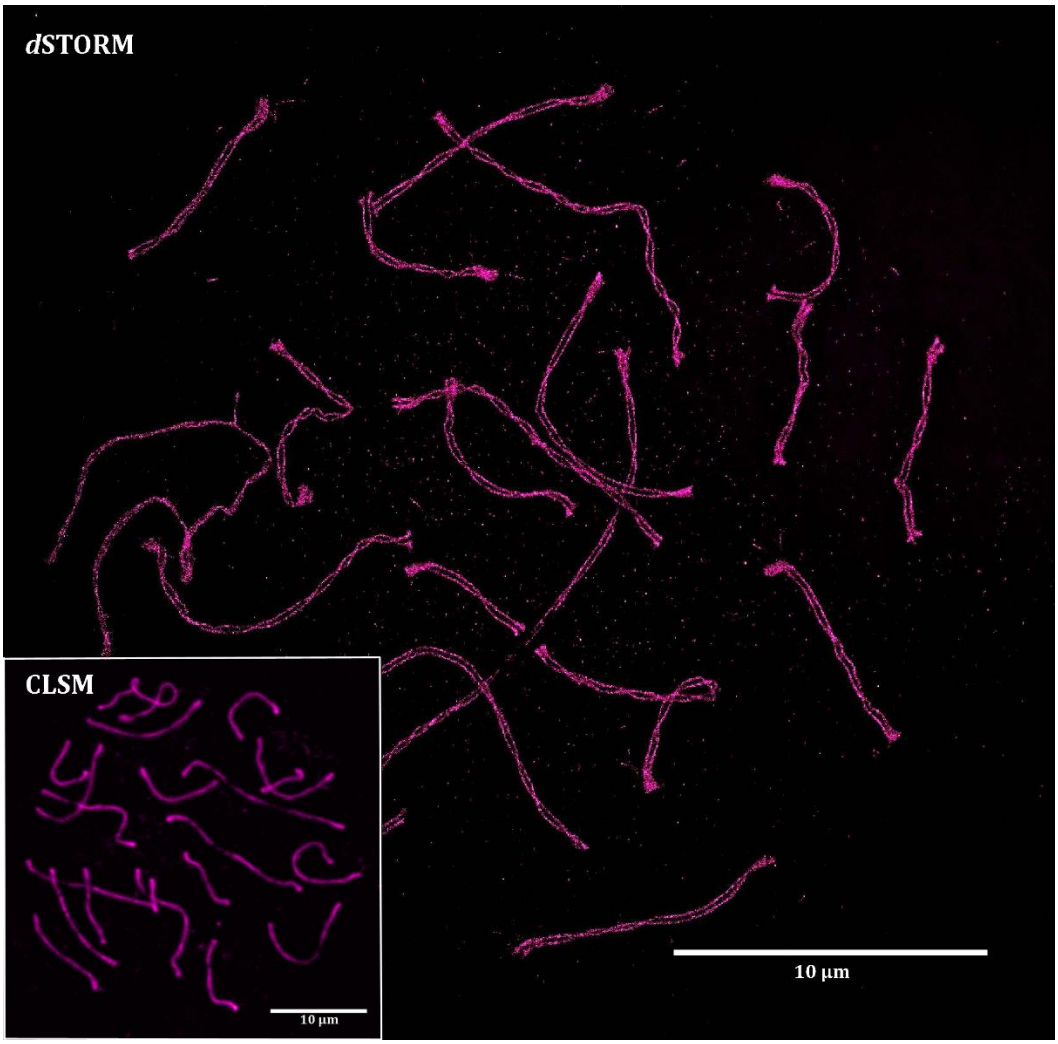

Figure 15: Imaging of SYCP3 with CLSM and *d*STORM.
Big image: *d*STORM image of SYCP3 labelled with Al647. Smaller image: CLSM image of SYCP3 labelled with TexasRed.

Additionally, protocols for the preparation of testis suspensions in Lab-Tek chambers for 3D imaging were successfully adapted for super-resolution microscopy. 3D imaging

was conducted with SIM and *d*STORM, with *d*STORM, again, providing the highest resolution with 40 nm and the greatest gain in information (Figure 16).

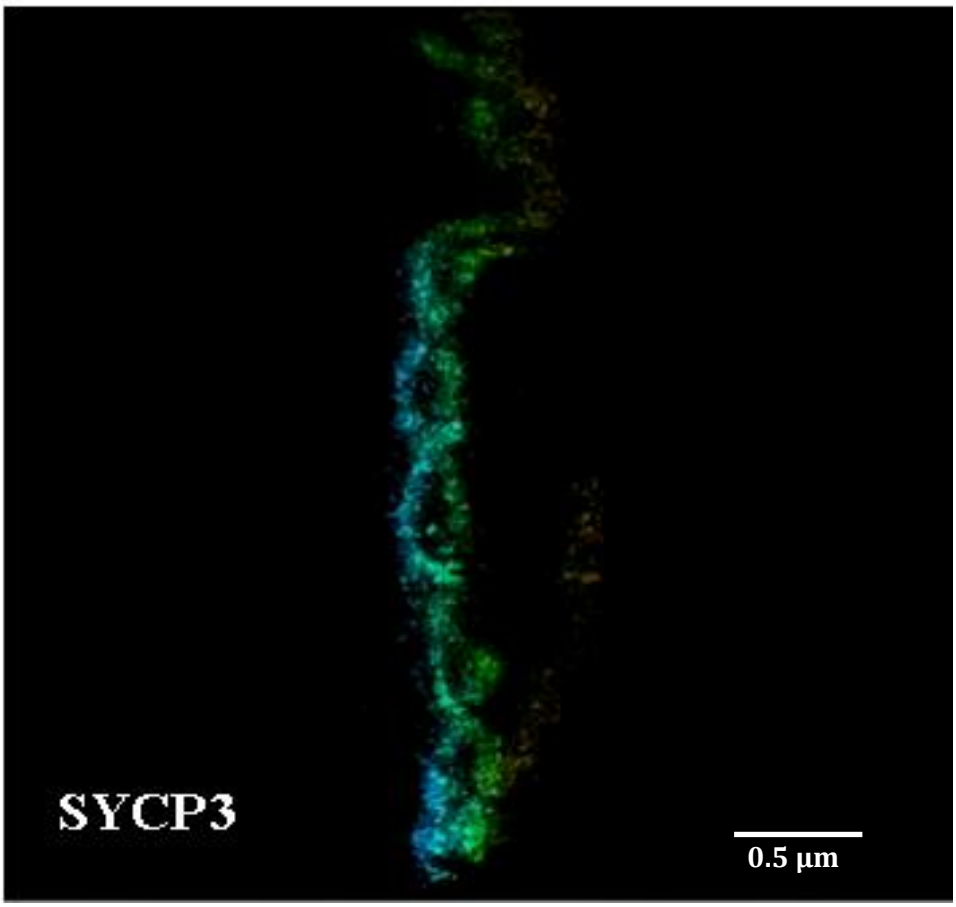

Figure 16: 3D imaging of SYCP3 using *d*STORM.
SYCP3 was labelled with Al647. The image was taken in cooperation with Dr. Sven Proppert (Department of Biotechnology and Biophysics, University of Würzburg).

4.2 Super-resolution imaging of synaptonemal complex proteins

As demonstrated in previous studies, SC substructures (LEs and CR) cannot be resolved as individual structures in CLSM images. Different SC proteins co-localize on one single strand, making it impossible to further analyse their nanomolecular structure (Figure 17 a-d). In clear contrast, the LEs and the CE are easily resolved as strands that are separated from each other using *d*STORM, which also depicts a gap in between them (Figure 17 e-h).

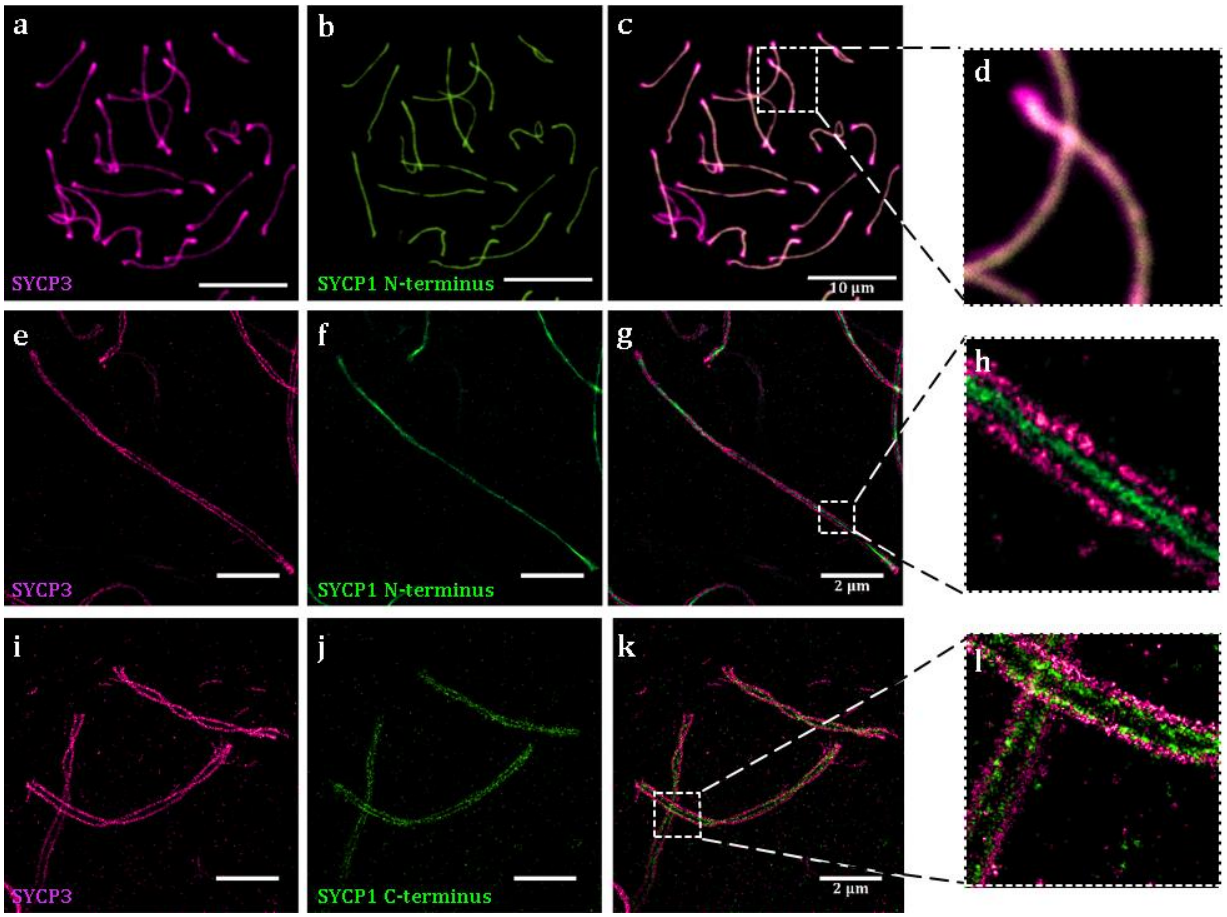

Figure 17: Fluorescence imaging of SYCP3 and SYCP1.
(a-c) CLSM imaging of SYCP3, labelled with TexasRed, and SYCP1 N-terminus labelled with Al488. Scale bars: 10 µm. **(d)** Magnified view of **(c)**. **(e-g)** *d*STORM imaging of SYCP3, labelled with Al647, and SYP1 C-terminus labelled with Al532. **(h)** Magnified view of **(g)**. **(i-l)** *d*STORM imaging of SYCP3, labelled with Al647, and SYP1 C-terminus labelled with Al532. Figure adapted from Schücker et al. 2015.

Notably, *d*STORM can resolve the different spatial positions of the N- and C-terminus of the TF protein SYCP1 (Figure 18 a-d). For that we labelled them with different photostable fluorophors in two-colour experiments. We were able to localize the N-termini in the CE as a continuous monomodal signal. The C-terminus depicts a discontinuous signal adjacent to the LEs of the SC (Figure 17 i-l and 18 b).

Labelling SYCP3 and SYCP2 with different fluorophores in two-colour experiments shows that both proteins co-localize homogeneously on the LE axis (Figure 18 e-h).

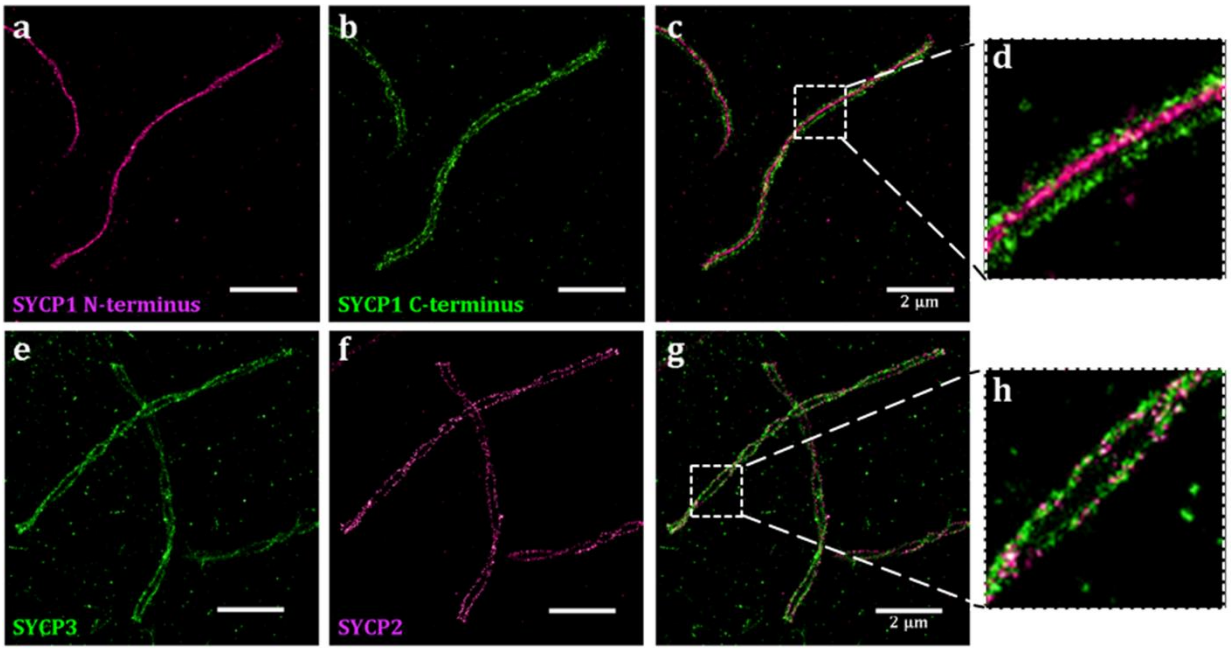

Figure 18: *d*STORM imaging of SYCP1, SYCP2 and SYCP3.
(a-c) *d*STORM imaging of SYCP1 N- and C-terminus. The N-terminus was labelled with Al647 and the C-terminus was labelled with Al532. **(d)** Magnified view of SYCP1 N- and C-terminus Overlay. **(e-g)** *d*STORM imaging of SYCP3, labelled with Al532, and SYCP2, labelled with Al647. **(h)** Magnified view of SYCP3 and SYCP2 Overlay. Figure adapted from Schücker et al. 2015.

4.2.1 The molecular organization of the SYCP1 C-terminus

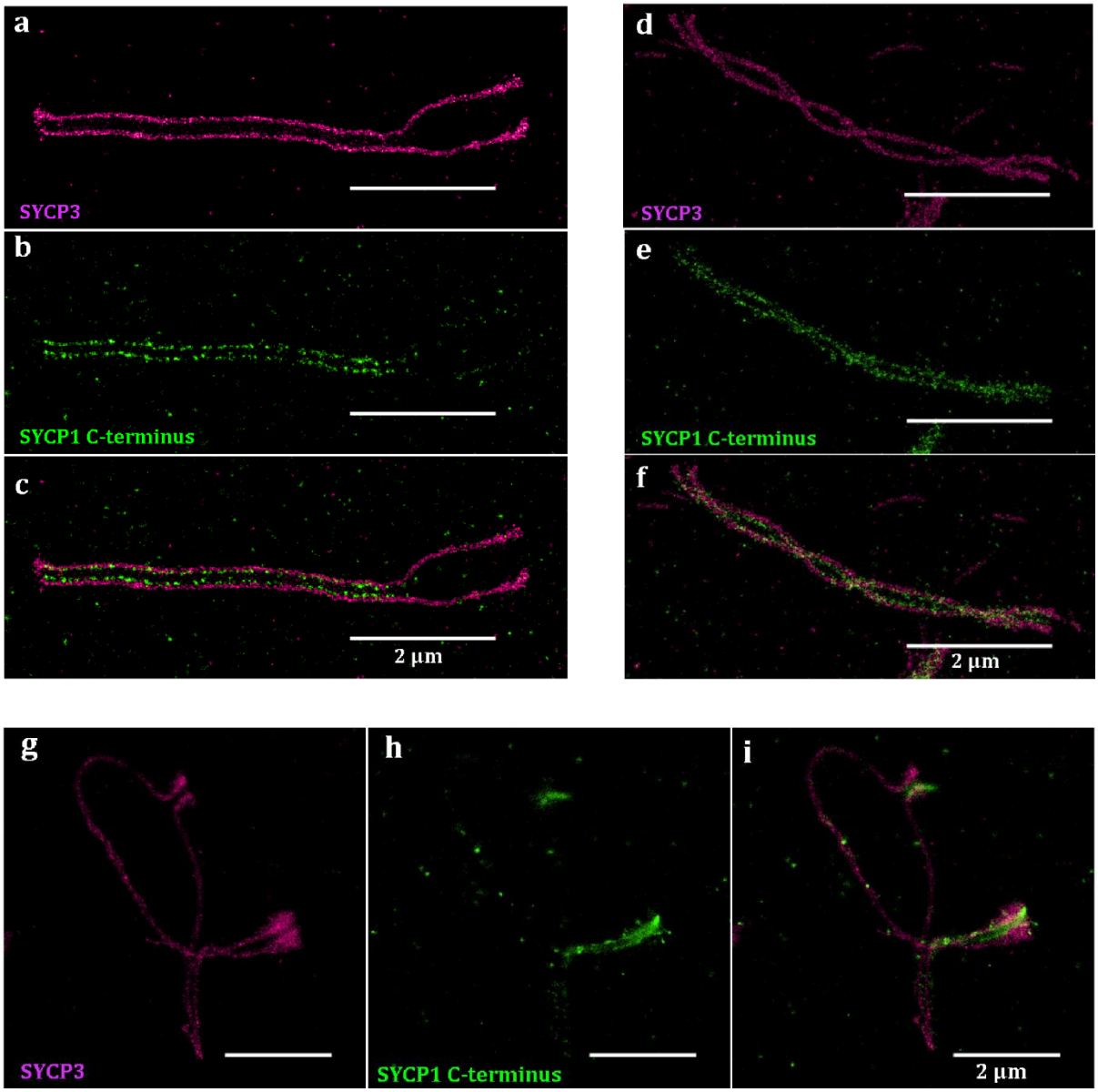

Figure 19: SYCP1 C-terminus during prophase I.
(a-b) *d*STORM images of SYCP3 (a) and SYCP1 C-terminus (b) during zygotene. **(c)** Overlay of (a) and (b). **(d-e)** *d*STORM images of SYCP3 (d) and SYCP1 C-terminus (e) during pachytene. **(f)** Overlay of image (d) and (e). **(g-h)** *d*STORM images of SYCP3 (g) and SYCP1 C-terminus (h) during diplotene. **(i)** Overlay of (g) and (h). In all images SYCP3 was labelled with Al647 and SYCP1 was labelled with Al532.

The C-terminus of SYCP1 was analysed during different prophase I stages of meiosis I using *d*STORM to gain further information about its dynamics and distribution. You can see that during zygotene the C-terminus of SYCP1 assembles alongside the LEs (marked here with SYCP3) in form of two parallel discontinuous signals (Figure 19 a-c). During the following pachytene stage more SYCP1 proteins seem to be recruited to the LEs, leading to an increase in SYCP1 signal detection. Nonetheless, SYCP1 C-terminal

signalling stays bimodal and discontinuous (Figure 19 d-f). During diplotene SYCP1 starts to disappear from the LEs (Figure 19 g-i). This disassembling mostly begins in the middle parts of the SC and continuous until late diplotene until SYCP1 is completely absent from the axis.

4.2.2 The molecular organization of CE proteins

Super-resolution images of the lateral views of the CE proteins SYCE1, SYCE2, SYCE3, TEX12 and SYCP1 N-termini show bimodal distributions, which from now on are going to be addressed as "bubbles". At these sites, the signals split into two parallel lines separated by a small interspace (Figure 20 and figure 21). These bubbles are already faintly visible in SIM images (Figure 20). Whereat *d*STORM images provide a more detailed look and offer the opportunity for more sensitive follow-up investigations, like distance measurements (Figure 21). These bubbles could also be detected in two-colour assays and always appeared at sites of helical turn of the SC (Figure 18 a-c).

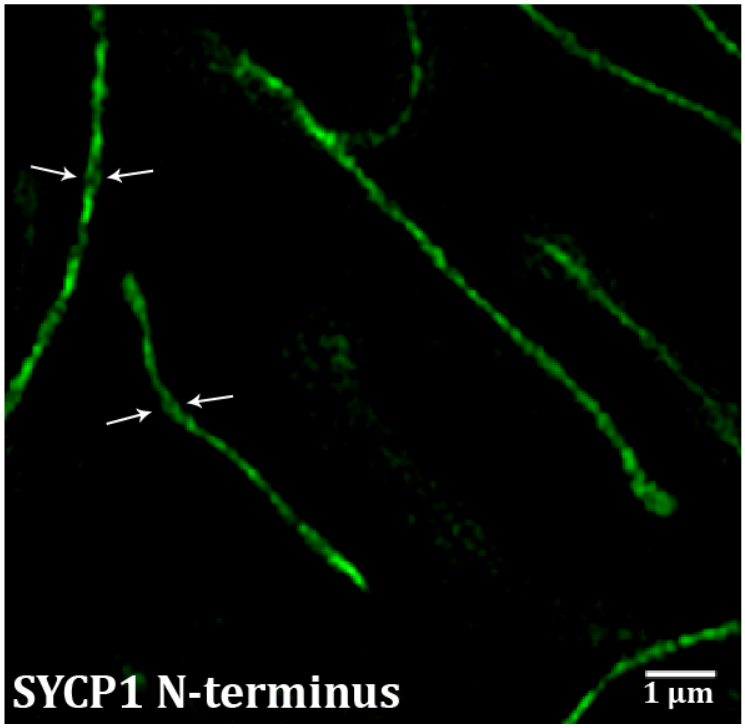

Figure 20: SIM imaging of the SYCP1 N-terminus.
SIM image of SYCP1 N-terminus labelled with Al488.

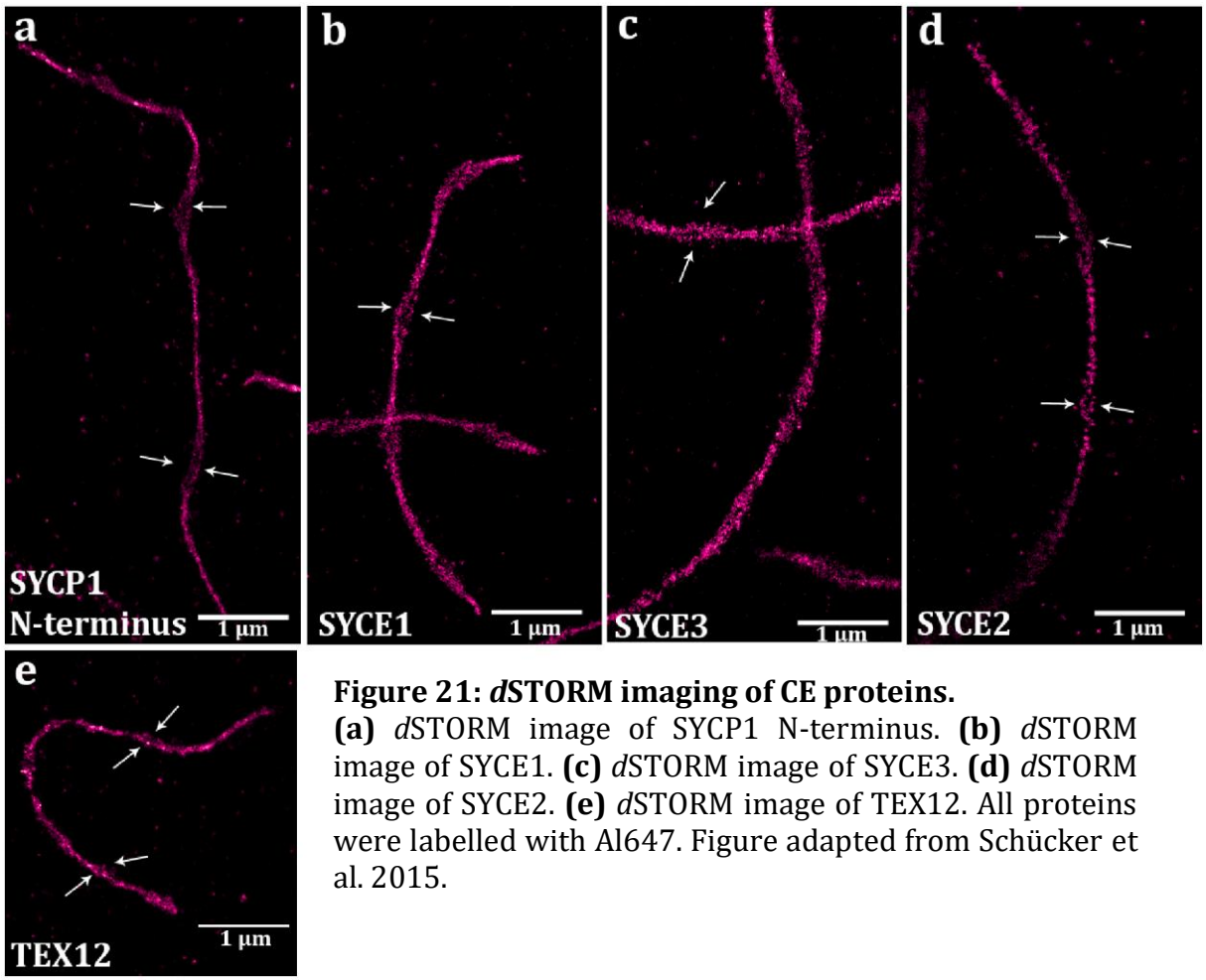

Figure 21: *d*STORM imaging of CE proteins.
(a) *d*STORM image of SYCP1 N-terminus. **(b)** *d*STORM image of SYCE1. **(c)** *d*STORM image of SYCE3. **(d)** *d*STORM image of SYCE2. **(e)** *d*STORM image of TEX12. All proteins were labelled with Al647. Figure adapted from Schücker et al. 2015.

4.3 Average protein distributions of SC proteins

To reconstruct 3D molecular protein maps of SC proteins, the average position of fluorescent probes was determined. To achieve this, frontal and lateral views of one-colour *d*STORM experiments were imaged, taking advantage of the fact that the experimental conditions for one fluorophore can be optimized (Heilemann et al., 2008; van de Linde et al., 2011). This way, an average of 2200 photons per frame were detected and a localization precision of 20 nm in xy dimension was obtained. With a typical data size of 5-54 SC investigated per prepared cell nucleus, the standard error of localization determination lies between 0.6 to 2.4 nm. A single cell preparation compiles enough photons to reconstruct a 3D model of SC proteins with nanometer precision.

The results state that SYCP3 and SYCP2 are arranged as two cables separated by 221.6 ± 6.1 nm (s.d.) and 218.5 ± 6.4 nm (s.d.) respectively and show distribution widths of 55.8 ± 2.3 nm (s.d.) and 51.2 ± 1.2 nm (s.d.) respectively (Figure 22 a). In conclusion, both proteins mainly co-localize on the LEs with little variations. The helical LE structure surrounds the CR, which is composed of the proteins SYCP1, TEX12, SYCE3, SYCE2 and

SYCE1. Overall the CR exhibits a width of 148.2 ± 2.6 nm (s.d.) defined by the average positions of the SYCP1 C-termini signals (Figure 22 a). The C-terminal SYCP1 signal has a width of 45.2 ± 1.5 nm (s.d.).

Of the analysed proteins in the CR the N-terminus of SYCP1 shows the tightest monomodal distribution with 39.8 ± 1.1 nm (s.d) in frontal view (Figure 22 a). SYCE2 partially overlaps with the SYCP1 signal (63.3 ± 2.1 nm, s.d.) (Figure 22 a). SYCE3 shows a wider but also monomodal signal of 67.8 ± 2.1 nm (s.d.) (Figure 22 a). The signal of SYCE1 is 54.8 ± 2.8 nm (s.d.) wide (Figure 22 a).

The distribution of SYCP1 N-terminus, SYCE3, SYCE2 and SYCE1 localizations in lateral view depicts two helical cables separated by 99.1 ± 4.8 nm (s.d.), 105.5 ± 5.3 nm (s.d.), 107.0 ± 4.6 nm (s.d) and 96.7 ± 8.8 nm (s.d.), respectively (Figure 22 b).

Data on the average protein distribution of TEX12 is still missing.

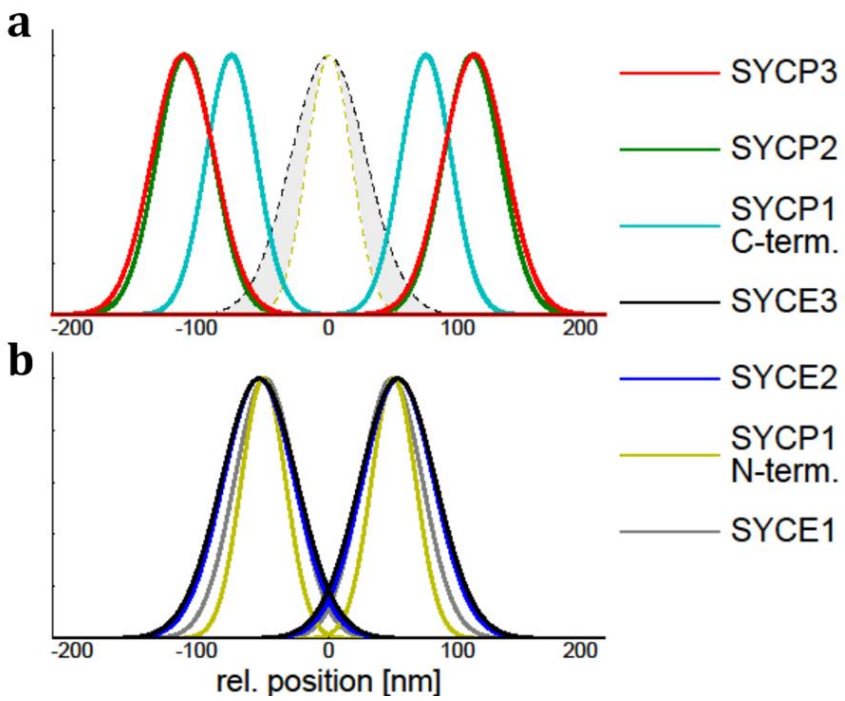

Figure 22: Average protein distributions of synaptonemal complex proteins.
(a) Frontal and **(b)** lateral average protein position determination of SC proteins. Figure taken from Schücker et al. 2015 and generated by Thorge Holm (Department of Biotechnology and Biophysics, University of Würzburg).

4.4 Super-resolution imaging of cohesins

During this work the cohesins SMC3, STAG3 and STAG2 were analysed. To determine where the cohesins localize on the chromosome axis, one and two-colour immunofluorescence assays on spermatocyte spreads where applied. In two-colour assays a LE protein (SYCP3 or SYCP2) of the SC was labelled as a reference. Signal distributions were measured during pachytene of prophase I using line profiles in Zen lite 2012 for SIM images or average distance measurements for *d*STORM images (see 3.4.8). In the end all cohesins showed different signal distributions.

4.4.1 SMC3 forms continuous bimodal structures

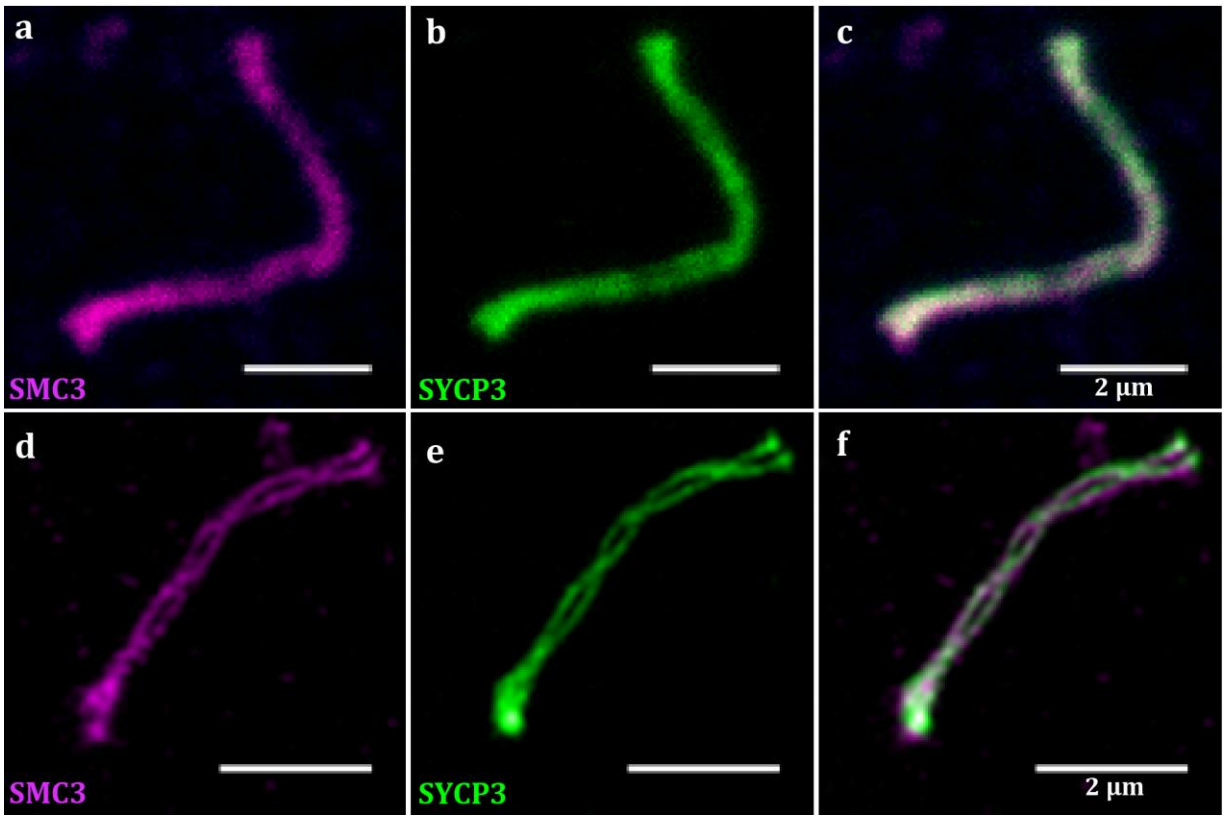

Figure 23: Fluorescence imaging of SMC3 and SYCP3.
(a-b) CLSM image of SMC3 and SYCP3. **(c)** Overlay of CLSM images. **(d-e)** SIM images of SMC3 and SYCP3. **(f)** Overlay of SIM images. SMC3 labelled with Al647 and SYCP3 labelled with Al488. Figure taken from Schücker et al. 2016 (under review).

SMC3 was labelled at its C-terminal domain, which is located at its head domain. SIM imaging revealed that SMC3 forms two continuous signalling strands that overlap with the LEs (Figure 23). In order to further investigate the dynamics of SMC3, it was labelled

together with the N-terminus of SYCP1 and imaged using SIM. It can be shown that during early diplotene SYCP1 locates between the unfused SMC3 strands and disassembles during further progression of this stage, remaining only between fused SMC3 strands, which typically represent nascent chiasmatas and centromeric regions (Figure 24).

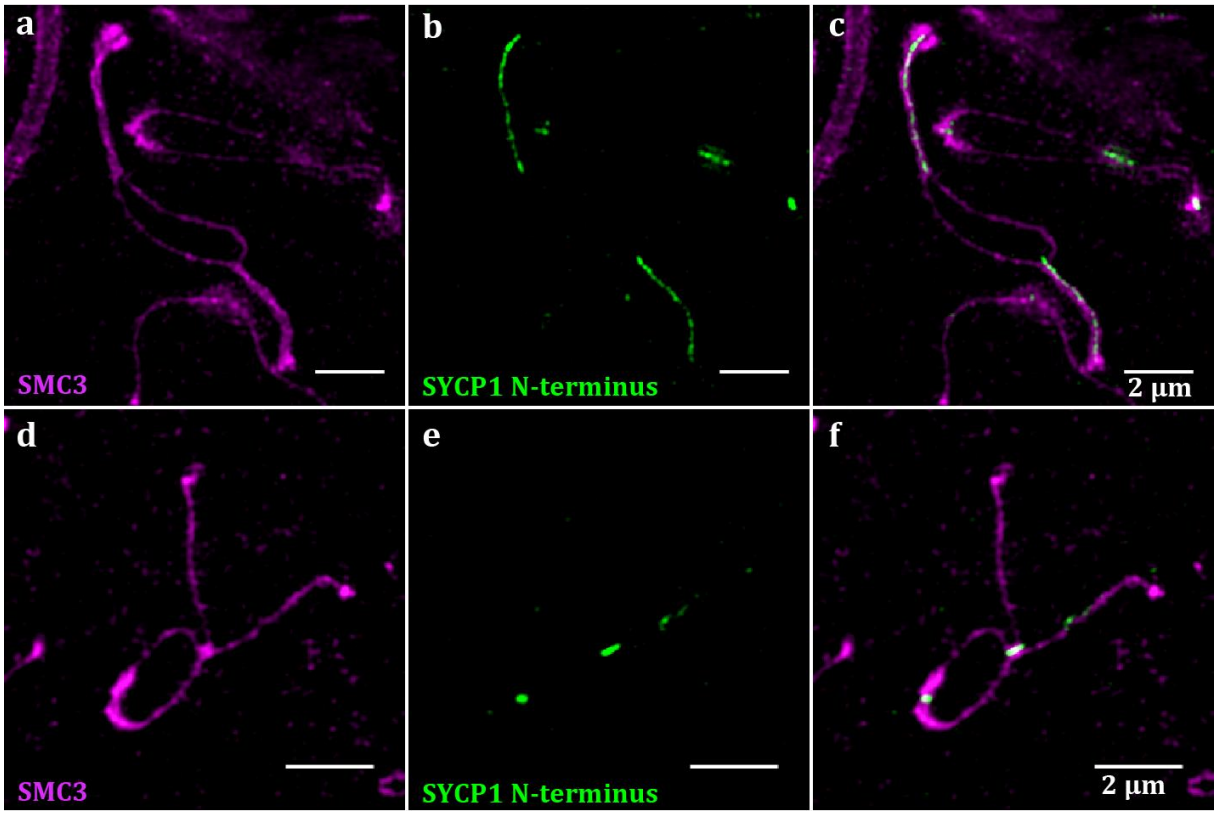

Figure 24: SIM imaging of SMC3 and SYCP1 during diplotene.
(a-c) SMC3 and SYCP1 N-terminus during early diplotene. **(d-f)** SMC3 and SYCP1 N-terminus during late diplotene. SMC3 labelled with Al647 and SYCP1 N-terminus labelled with Al488.

4.4.2 STAG3 forms aggregates localized on the lateral elements

In CLSM images STAG3 shows a continuous signal overlapping with the LEs of the SC (Figure 25 a-c). Using SIM imaging it became clear that STAG3 does not form continuous strands as the LEs or SMC3 but instead forms aggregates on the chromosome axes (Figure 25 d-f).

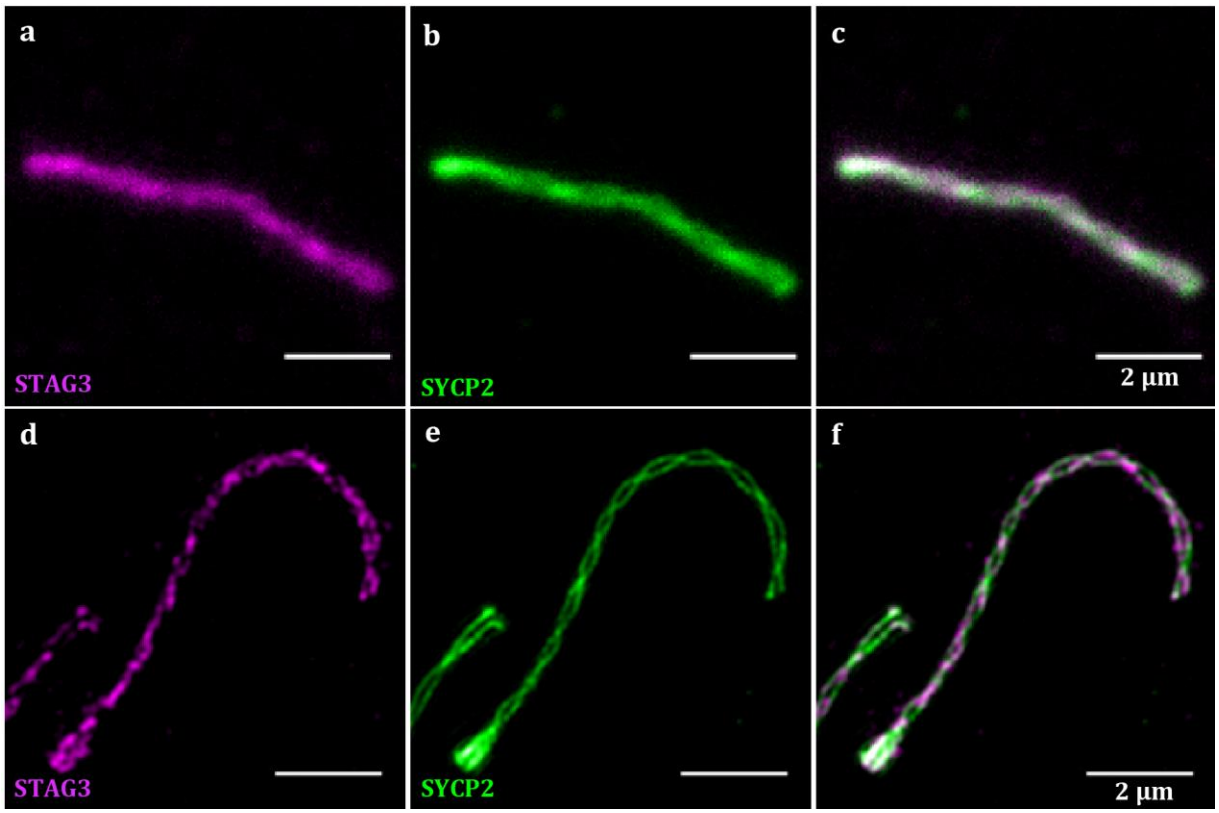

Figure 25: Fluorescence imaging of STAG3 and SYCP2.
(a) CLSM image of STAG3 labelled with Texas Red. **(b)** CLSM image of SYCP2 labelled with Al488. **(c)** Overlay of CLSM images. **(d)** SIM image of STAG3 labelled with Al647. **(e)** SIM image of SYCP2 labelled with Al488. **(f)** Overlay of SIM images. Figure taken from Schücker et al. 2016 (under review).

4.4.3 STAG3 and SMC3 distance measurements

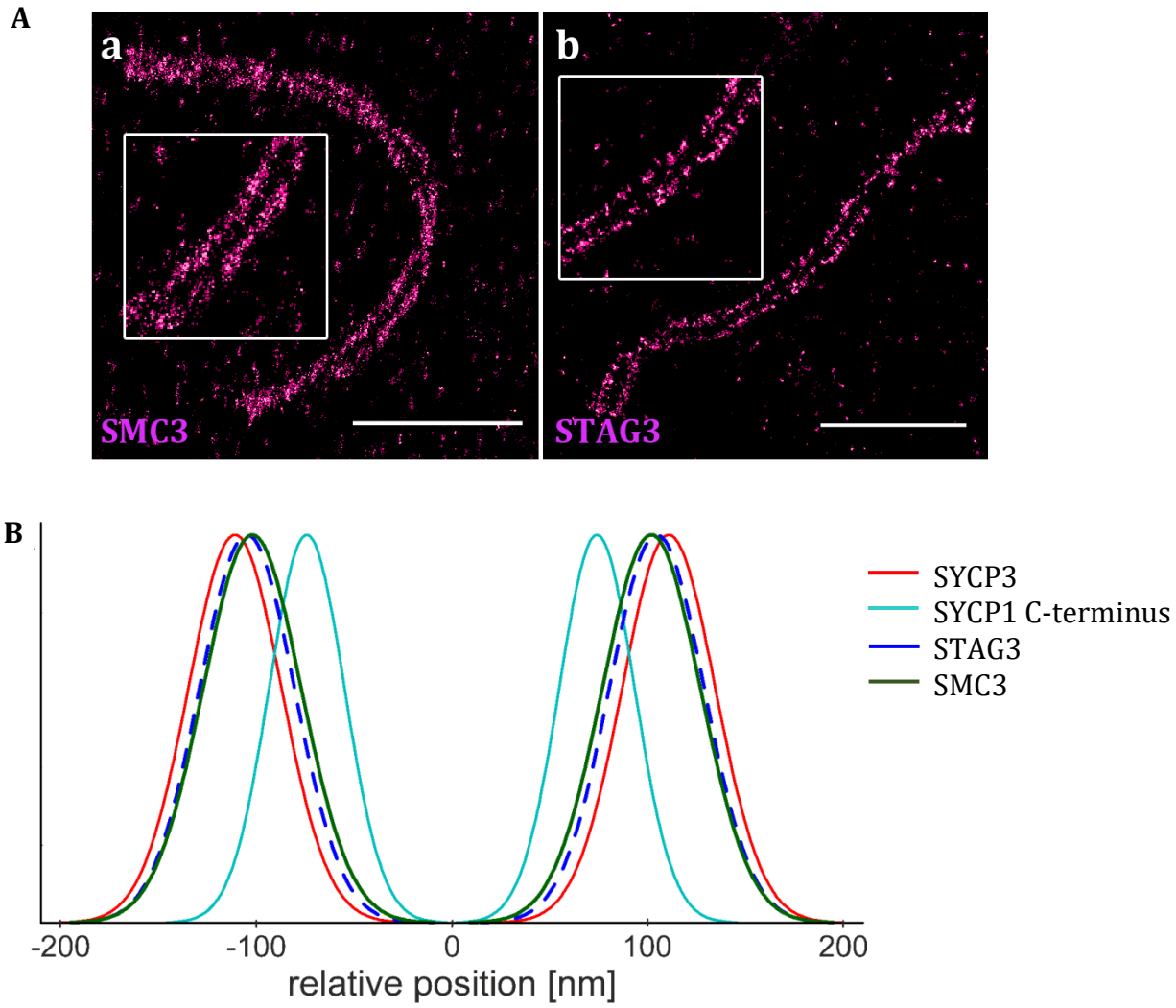

Figure 26: *d*STORM analysis of SMC3 and STAG3.
(A) *d*STORM imaging of SMC3 and STAG3 labelled with Al647. Scale bar= 2 µm **(B)** Average protein distributions of SMC3 (distance = 203.9 nm ± 27.95 nm (s.d.), width = 50 nm ± 9.9 nm (s.d.)) and STAG3 (distance = 209.3 nm ± 29.95 nm (s.d.), width = 56.8 nm ± 19.1 nm (s.d.)) in correspondence to SYCP3 (distance = 221.6 nm ± 6.1 nm (s.d.), width = 55.8 nm ± 2.3 nm (s.d.)) and SYCP1 C-terminus (distance = 148.2 nm ± 2.6 nm (s.d.), width = 45.2 nm ± 1.5 nm (s.d.)). Figure taken from Schücker et al. 2016 (under review). Part (B) was generated by Christian Franke (Department of Biotechnology and Biophysics, University of Würzburg).

*d*STORM images of SMC3 verify the results obtained by SIM imaging and in combination with average distance measurement declare that the SMC3 axes have a width of 50.0 nm

± 9.9 nm (s.d.) and have a distance of 203.9 nm ± 27.95 (s.d.) nm to each other (Figure 26 A and B).

The same applies for STAG3. *d*STORM images of also verify the results obtained by SIM imaging and together with average distance measurement declare that the signal axes have a width of 56.8 nm ± 19.1 nm (s.d.) and are about 209.3 nm ± 29.95 nm (s.d.) apart from each other (Figure 26 A and B).

4.4.4 STAG2 localizes to the lateral elements and the central region

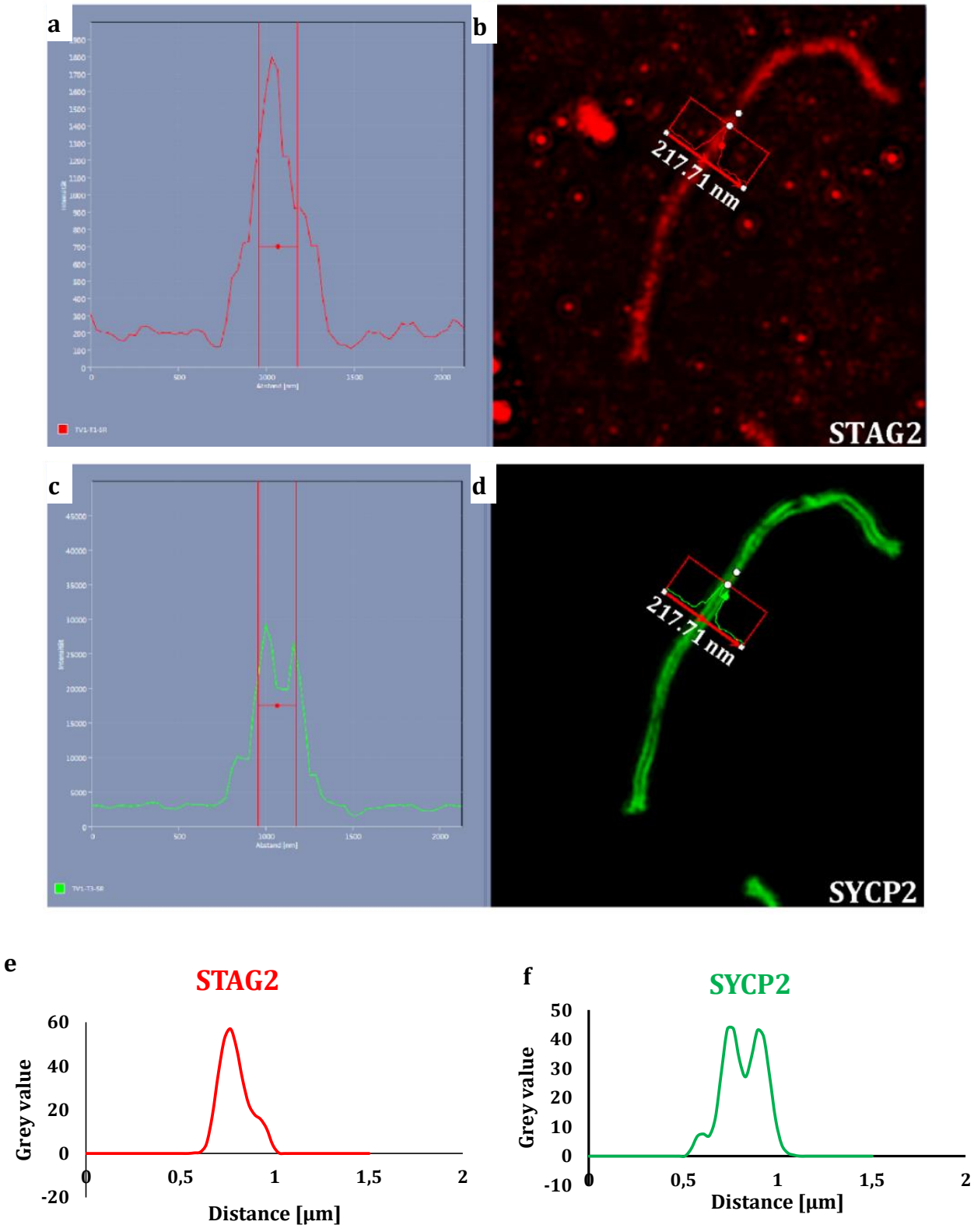

Figure 27: SIM imaging of STAG2 and SYCP2 including line profiles.
(a-b) SIM image of STAG2 labelled with Al647 and corresponding line profile produced with the Zen software. **(c-d)** SIM image of SYCP2 labelled with Al488 and corresponding line profile produced with the Zen software. **(e)** Plotting the grey values of STAG2 localizations of image (b) against their corresponding distance. **(f)** Plotting the grey values of SYCP2 localizations of image (d) against their corresponding distance.

In SIM images LE proteins showed two signal maxima with a distance of 217.71 nm (Figure 27 c, d and f). In contrast, STAG2 did not depict two maxima, but one single signal with 217.71 nm in overall diameter, likewise (Figure 27 a, b and e).

Conclusively, STAG2 can not only be detected along the LEs of SCs but in their CR, too. This data is in consistence with recently obtained immunogold EM data. Data on *d*STORM imaging is still missing at this point.

5. Discussion

For this work three different optical imaging techniques were used in combination with different immunofluorescence assays for analysing chromatin associated structures during meiosis. The main focus of this work was to resolve the structure of the synaptonemal complex (SC) throughout meiosis I with isotropic resolution. For this, all seven SC proteins were immunolabelled with different Alexa fluorophores and imaged using *d*STORM. To ensure valid results, primary antibodies were tested in CLSM and Westernblot beforehand, as well as in one and two colour experiments, meaning that for a positive control some samples were labelled with a functional antibody for a specific SC protein and the antibody to be tested. In addition, some samples were only labelled with the antibody of interest to preclude false positive results. Secondary antibodies were tested in immunofluorescence assays for cross-reactions with other species or false positive results due to unspecific binding (e.g. background signal). To achieve this, wrong antibody combinations were used, e.g. a guinea pig primary antibody was tried to be labelled with a secondary antibody directed against rabbit proteins. To test for false positive results no primary antibody was applied. Instead, the sample was only tried to be labelled with a secondary antibody. These controls had to be done for all batches of antibodies to ensure the validity of this work.

Another focus of this work was to locate cohesin complexes (CCs) along the chromosome axis. Determining the composition and spatiotemporal localization of individual CCs and thereby evaluating their function throughout meiosis remains challenging. For this thesis three different cohesins, namely STAG2, STAG3 and SMC3, were analysed. The focus was put on cohesins on the chromosome axis, because of their interplay with the SC and their combined influence on the chromosome architecture and possible collaboration in the events of recombination during meiosis. The mechanism of which is still elusive. Cohesins on the chromatin loops were neglected for this study. The validity of results was ensured as described above for SC proteins.

This thesis also provides protocols with new technical advantages for the analyses of proteins associated with chromatin during meiosis. So far, meiotic proteins were analysed using CLSM and TEM, providing essential information about their organization during the process of meiosis. Nonetheless, these approaches are limited by different factors. CLSM uses either direct or, more commonly, indirect immunofluorescence

labelling. This means that either the primary antibody is directly bound to a fluorophore or that a secondary antibody, which is bound to a fluorophore, binds to your primary antibody, enhancing the signal. In conclusion, you get lots of signal and the sample preparation is fast and easy. The drawback is that a resolution better than 200 nm cannot be achieved due to the Abbe diffraction limit of light, as described above. In contrast, TEM provides an astonishing resolution of approximately 0.2-2 nm, because it uses extremely short wavelengths of accelerated electrons instead of light for imaging of objects. This can be explained again by the diffraction limit determined by the equation $d= \lambda/NA$, which illustrates that the diffraction limit and the resolution are inversely proportional to each other. Conclusively, in order to increase your resolution you have to use either shorter wavelengths or media and optics with larger refraction indices, or both. The drawback of TEM is that sample preparation is time-consuming and quantitative analysis of the signal is tedious because of the low binding efficiency of gold-labelled antibodies and the problem of pinpointing their localization with high accuracy. Furthermore, the low binding efficiency prevents high labelling densities of any structure, reducing the structural resolution as stated by the Nyguist Shannon Theorem (Shannon, 1949).

The generation of localization maps of different proteins along the chromosome axis by immunogold EM and CLSM remains challenging. Conclusively, new approaches were needed, which can overcome these technical limitations and reach molecular resolution. This was achieved by the recent breakthrough of Eric Betzig, Stefan W. Hell and William E. Moerner, who were able to bypass the Abbe diffraction limit by using microscopic systems, the resolution of which is not limited by diffraction any more. They did neither change the wavelength nor the numerical aperture of the optical system and the Abbe diffraction limit of light is still present but they bypassed it by either separating the fluorescence signals in time and space or physically reduced the fluorescent area. During this work *d*STORM and SIM were used. They combine easy and fast sample preparation with high labelling densities and resolutions between ~ 20-100 nm in xy-dimension and ~40-300 nm in z dimension. Sample preparation stays the same as for CLSM (immunofluorescence assays), but photostable fluorophores have to be used in order to avoid instant bleaching of the sample. In combination with particle averaging methods, different protein localization maps of chromosome axis proteins were delivered with high precision (Loschberger et al., 2012; Schücker et al., 2015; Szymborska et al., 2013).

5.1 Super-resolution imaging reveals new information on the organization of chromosome axis proteins

SIM and *d*STORM images of chromosome axes proteins show a tremendous increase in resolution compared to CLSM (Figure 15). Whereas CLSM depicts all cohesins and all SC proteins as co-localizing single-stranded continuous proteins (Figure 17 a-d, Figure 23 a-c, Figure 25 a-c), SIM and *d*STORM now reveal bimodal distributions and aggregates, where none were seen before. Starting with the TFs of the SC, which consist of SYCP1 homodimers, previous experiments indicated that their C-termini are anchoring in the LEs, while their N-termini meet in the CE, where they interact (Liu et al., 1996; Meuwissen et al., 1992; Schmekel et al., 1996). We were able to confirm the localization of N-termini in the CE and verify that they overlap (Figure 18 a and d). This is in accordance with previous immunogold EM and biochemical data (Liu et al., 1996; Schmekel et al., 1996). In addition, we were now able to distinguish between the N- and C-terminus of SYCP1 in one assay by labelling them with different fluorophores and imaging them with *d*STORM (Figure 18 a-d). The C-terminus depicts a discontinuous signal adjacent to the LEs of the SC (Figure 19). This spotty signalling might correlate to the anchoring sites of the C-terminus to the LEs. Nevertheless, it cannot be excluded that it is caused by a steric disability of the antibody to bind epitopes that are not exposed to the outer periphery of the LEs but lie hidden inside the LEs and cannot be accessed by the antibodies.

Previous immunogold EM data suggested that SYCP3 is homogeneously distributed in the LEs and that SYCP2 is enriched towards the inner edge of the LEs (Tarsounas et al., 1997; Winkel et al., 2009). However, with the resolution provided by *d*STORM, the two proteins SYCP2 and SYCP3 appear to co-localize along the axial LE structures (Figure 18 h). Average position determination reveals that both proteins are arranged as two cables separated by 221.6 ± 6.1 nm (s.d.) and 218.5 ± 6.4 nm (s.d.) respectively and thereby do not show any preferential arrangement of SYCP2 towards the inner LE periphery (Figure 22 a).

5.2 Generation of 3D protein maps from *d*STORM imaging

3D maps of chromosome axis proteins were reconstructed using *d*STORM images of frontal and lateral SC positions (sites of helical turnovers of the SC) and average position determination, whereas a single cell preparation generated enough photons for reconstruction.

It was shown that in frontal view the N-termini of SYCP1 lie directly in the centre of the CE (39.8 ± 1.1 nm s.d.) and that SYCE2 (63.3 ± 2.1 nm, s.d.) overlaps with the N-termini (Figure 22 a). This is in agreement with previous co-immunoprecipitation results (Fraune et al., 2012; Hamer et al., 2006). It is suggested that SYCP1 binds SYCE3 directly but the binding sites remain elusive (Fraune et al., 2012; Schramm et al., 2011). SYCE3 shows a monomodal but wider signal distribution with 67.8 nm ± 2.1 nm (s.d.) in comparison to SYCP1 N-terminus and SYCE2 (Figure 22 a). This states that its binding is not restricted to the SYCP1 N-terminus.

Imaging of the lateral view of the CE proteins have shown a bimodal distribution for all of them (Figure 20), meaning that their signals split up into two parallel lines separated by a small interspace. It has to be pointed out that the degree of this interspace can be affected by the size of the antibodies and the corresponding restricted accessibility of protein epitopes. Nonetheless, previous immunogold EM studies have shown no indication for sucha bimodal distribution for neither of these proteins. However, our results are in agreement with previous TEM data showing that TFs are organized into more than one layer (Costa et al., 2005; Hamer et al., 2006; Liu et al., 1996; Ollinger et al., 2005; Schmekel et al., 1996; Schramm et al., 2011).

The model depicted in figure 28 represents all average distances of the aforementioned proteins in one 3 D model (Figure 28). Unfortunately, 3D imaging of SC proteins could not be used so far for the creation of a 3D model, because only one colour imaging was successfully realised up to this point. It can also be concluded that there is no benefit for the creation of a refined SC model using 3D *d*STORM since we have a decline in resolution in comparison to 2D *d*STORM and as just mentioned can not image more than one protein at a time.,

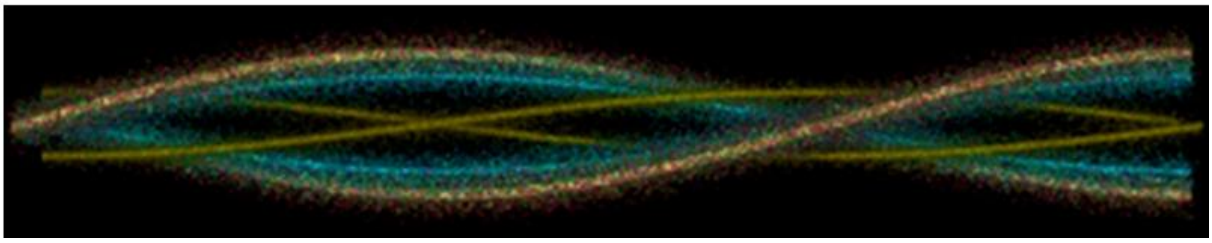

Figure 28: 3D model of synaptonemal complex proteins.
The depicted 3D-model was generated by using average protein position determination and ImageJ. Depicted in red are SYCP2 and SYCP3, in blue the C-terminus of SYCP1 and in yellow the CE proteins. Figure taken from Schücker et al. 2015 and generated by Thorge Holm (Department of Biotechnology and Biophysics, University of Würzburg).

5.3 Cohesin complexes are organized orderly on the chromosome axis

Murine RAD21L and REC8 were imaged with 3D-SIM in 2016 by Rong et al. . They found out that both cohesins localise between the LEs and the TFs during pachytene (Rong et al., 2016). The presented results further expand our knowledge of cohesin organization in mammalian meiotic chromosome axes by adding information about the topography of the murine SMC3, STAG3 and STAG2.

Previous studies state that cohesin complex cores, represented by REC8 and RAD21L, are located to the most inner part of the LEs (Ishiguro et al., 2014). Additionally it was shown that the RAD21 cohesin axes co-localise with the LEs of the SC (Gomez et al., 2007). During this work STAG3, which is the predominant STAG protein of CCs (Gutierrez-Caballero et al., 2011; Ishiguro et al., 2011; Lee and Hirano, 2011), was imaged using CLSM, SIM and *d*STORM (Figure 25 a and d and Figure 26 (A)b).

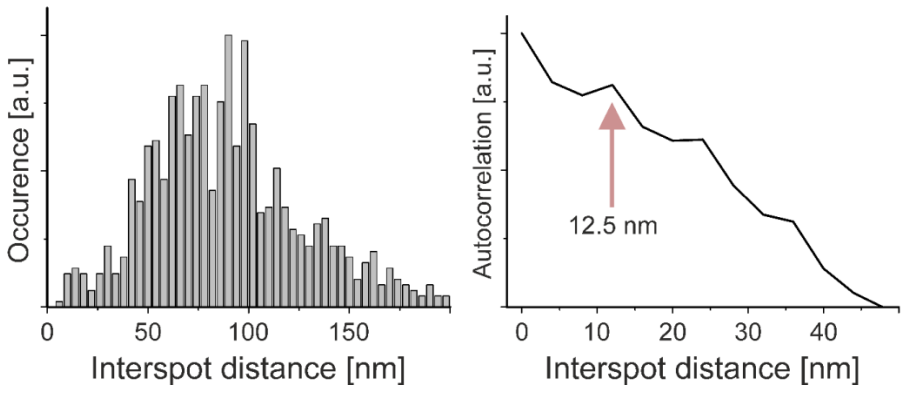

Figure 29: Statistic analysis of STAG3 interspot distances.
Left: Interspot distance distribution of STAG3. Right: Autocorrelation of the interspot distance distribution. Figure taken from Schücker et al. 2016 (under review) and generated by Christian Franke (Department of Biotechnology and Biophysics, University of Würzburg).

Apart from REC8, STAG3 is known to be part of the main CCs that are required for centromeric cohesion between sister chromatids (Ward et al., 2016). STAG3 is also required for stabilizing cohesins onto the chromosome axe (Ward et al., 2016). The results show that the STAG3 signal is spotty, which indicates that in regions where no STAG3 was detected CCs with other STAG proteins might be present. STAG3 forms a bimodal signal with strand distances of 209.3 nm ± 29.95 nm and a signal width of 56.8 nm ± 19.1 nm (Figure 26 B). In conclusion, STAG3 also co-localizes with the LEs with a tendency towards the inner edge of the LEs. The distribution of the interspot distances of STAG3 was analysed by Christian Franke of the University of Würzburg. He used autocorrelation to analyse the interspot distance distribution, which resulted in significant peak distances of 12.5 nm (Figure 29). This indicates a sub-resolution organization of STAG3. This might seem surprising since the ring diameter of CCs is about 50 nm (Haering et al., 2002). To gain more insight into the localization of CC arms in comparison to CC cores, SMC3 was imaged as well. Our results clearly show that SMC3, which is known to be part of every meiotic CCs, is forming two continuous protein strands within a distance of 203.9 nm ± 27.95 nm and SMC3 does not form aggregates (Figure 23 d and f). Conclusively, CCs might overlap alongside the chromosome axes and have an orderly organization with the hinge region pointing towards the outer edges of the LEs and the STAG and α-kleisin subunits, as well as the SMC head domains pointing towards the TFs (Figure 30). Thereby it seems that most of the CCs containing STAG3 and SMC3 are located to the inner edge of the LEs. From this CC organization and the fact that CCs play crucial roles in the formation of the SC and the fixation and formation of chromatin loops on the chromosome axis, the conclusion to be drawn is that the SMC head domains and the STAG subunits might play a role in the partner search of homologous chromosomes and their subsequent synapsis. The question remains whether or not CCs recruit SYCP1 to the CR and/or interact with SYCP1 to stabilize the SC.

It has to be pointed out that the spotty signal of STAG3 makes it difficult for the used algorithm to accurately pinpoint solely true STAG3 signals and distinguish it from the background signal leading to a high standard deviation of the average protein distribution.

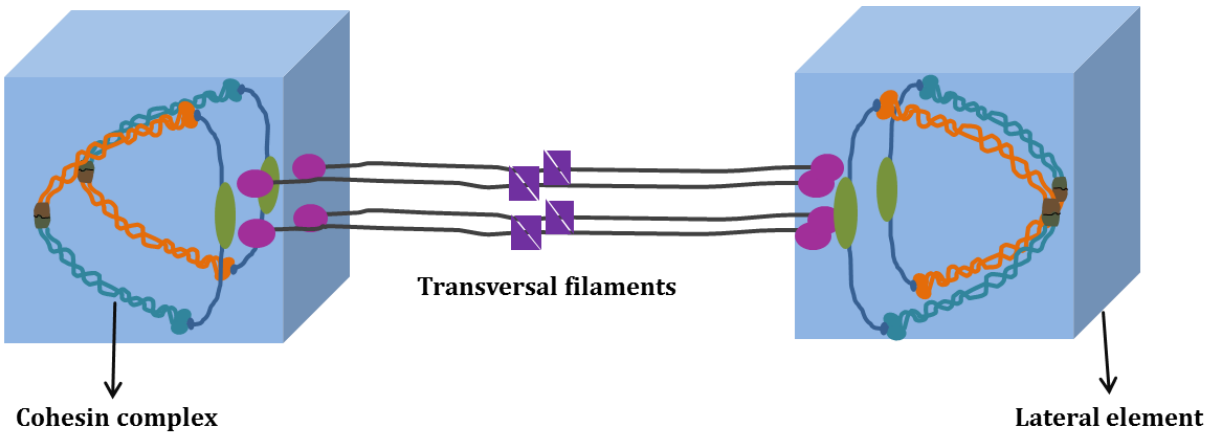

Figure 30: Organization of cohesin complexes on the chromosome axis.
Orientation of cohesin complexes on the murine meiotic chromosome axis as derived from the analysis of STAG3 and SMC3.

STAG2 as another, not so abundant component of CCs, was also imaged. STAG2 is known to be the main STAG protein in somatic cells, where it is required for cohesion along chromosome arms and centromeres. Nonetheless, the role of STAG2 during meiosis is still not unravelled and there is contradictory data on its localization (Fukuda et al., 2014; Llano et al., 2014; Prieto et al., 2002; Ward et al., 2016). Surprisingly, STAG2, which also localizes to CC cores but is not as abundant as STAG3, shows a monomodal distribution of about 218 nm in diameter (Figure 27). Therefore, STAG2 does not only co-localize with the LEs of the SC but also with the CR and therefor with the regulatory factor sororin, which was just recently declared to load to the CR, where it has a regulatory function in centromeric cohesion. It is known that beside SMC3 acetylation, sororin is essential for chromatin cohesion during the S-phase of somatic cells, where it binds the regulatory factor Pds5 and thereby prevents the activity of WAPL as a CCs releasing factor (Nishiyama et al., 2010). Sororin is also known to interact with the SGO2-PP2A complex, which protects sororin from phosphorylation and thus sustaining centromeric cohesion (Liu et al., 2013; Gómez et al., 2016). STAG2 has also been proven to be protected by the SGO2-PP2A complex and to also bind PDS5 in somatic cells (Losada et al., 2005). These facts point towards an indirect interaction between sororin and STAG2 in somatic cells. Such an indirect interaction is still unknown for meiotic cells. So far Gómez et al. and Llano et al. discovered that SGO2-PP2A protects centromeric cohesins from cleavage by separase during meiosis I (Gomez et al., 2007;

Llano et al., 2008). Additionally, Gómez et al. found out just recently that sororin seems to play a role in centromeric cohesion in collaboration with SGO2-PP2A in mammalian meiotic cells as well. Our results reinforce a possible direct or indirect interaction between sororin and STAG2, because they clearly show that STAG2 does not only locate to the LEs but to the CR, likewise. There it could interact with sororin and possibly with the SGO2-PP2A complex as well, like in somatic cells, and possibly have a function in maintaining centromeric cohesion. Further our results on SMC3 reinforce this point of view, since they clearly show that SMC3, which is part of every known CCs, does not locate to the CR. Conclusively, STAG2 on the LEs are part of CCs but STAG2 in the CR must have different functions, like centromeric cohesion, as described above. Our results also confirm in extend the findings of Vázquez Nin et al. in 1993 who discovered that only little DNA is located in the CR, mostly in regions of recombination nodules, whereas in the LEs the DNA density is much higher (Vázquez Nin et al., 1993). This reinforces the hypothesis that STAG2 in the CR must have a function separate from CCs.
Further analyses of SMC3, SMC1α, shugosin2 and sororin knock-out mice might provide useful information on the dependency of STAG2 loading to the CR on CCs.

In summary, these results verify that CCs have an orderly organization alongside the chromosome axis and that cohesins in the CR have a function independent of CCs (Gomez et al., 2016; Gyuricza et al., 2016).

It has to be pointed out that the high divergence in standard deviation of SMC3 are caused by a high background of the samples, which seem to be caused by the primary antibody. To exclude or verify this conclusion and confirm the measurements, repeating the immunofluorescence with another SMC3 antibody is advisable. For STAG3 the high divergence in standard deviation is caused by a high background as well as by the spottiness of the signal, which makes it difficult to scan the axes continuously.

5.4 Future prospects

This work was just the beginning of unravelling the structure of the mammalian meiotic chromosome axis. There are still many more questions that need to be answered in order to gain more knowledge about the interplay between the processes of synapsis, cohesion and recombination. Especially their role in shaping and monitoring the chromatin structure during meiosis and the events of recombination. Additionally, the exact kinetics and localisation of distinct CCs throughout meiosis as well as their composition during different phases are still elusive. Therefore multi-colour approaches analysing two to three cohesins at a time during different meiotic phases using super-resolution microscopy should be conducted. This way the localisations and dynamics of nearly distinct CCs might be observable. Also analysing one cohesin with various antibodies that are directed against different epitopes of the protein might give more insight into its orientation on the chromosome axis. The same applies for CCs as a whole, which should also be labelled at their hinge region and, at best, simultaneously at their SMC head domain or another associated protein, to further improve our knowledge on their organization on the chromosome axis. In more detail, *d*STORM imaging of STAG2 and two-colour imaging of SMC3 in combination with STAG2 and SMC3 in combination with STAG3 might be useful. Also, SMC1α and SMC1β should be analysed using SIM and *d*STORM in one- and two-colour approaches in combination with stromal antigen proteins and SMC3 to see if they might or might not partially be located in the CR and if they have an orderly organization that confirms the results presented here. Furthermore, antibodies against the hinge region of CCs should be prepared to get a closer look onto their location on the chromosome axis and see whether or not our presented model on CCs organisation can be verified and/or modified.

As mentioned before, only CCs on the chromosome axis were under observation during this thesis. Up to date the analysis of CCs on chromatin loops remains methodological challenging but in order to fully understand CCs, their analysis is crucial. In consequence suitable protocols or maybe even different techniques need to be developed and/or tested. Also, super-resolution analyses of other cohesion associated proteins, e.g sororin or shugoshin, together with cohesins in one and two-colour assays should be conducted to gain more insight into the spatiotemporal regulation of CCs during meiosis.

To further verify the presented results and maybe even gain more structural information a recently established method, called Expansion microscopy (ExM), might be an interesting tool (Chen et al., 2015). To take a step forward, expanded and labelled

gels should not only be analysed using CLSM but also *d*STORM. This might further increase the achievable resolution and give us more information about the chromosome axis.

Since meiotic germ cells can be prepared for microscopic analysis and highly specific antibodies are available, proteins of the chromosome axis are predestined for super-resolution microscopy. The SC, as prepared in this thesis, has proven to be a superb probe for super-resolution microscopy, providing the ability to be used for establishing new protocols and also improving sophisticated microscopic techniques. It can be recommended to use the SC as a model protein complex for developing protocols for the analysis of protein complexes and maybe other biological samples with newly emerging microscopic techniques, like 3D *d*STORM and ExM.

6. References

Adelfalk, C., Janschek, J., Revenkova, E., Blei, C., Liebe, B., Gob, E., Alsheimer, M., Benavente, R., de Boer, E., Novak, I. et al. (2009). Cohesin SMC1beta protects telomeres in meiocytes. *J Cell Biol* **187**, 185-99.

Alsheimer, M., Baier, A., Schramm, S., Schutz, W. and Benavente, R. (2010). Synaptonemal complex protein SYCP3 exists in two isoforms showing different conservation in mammalian evolution. *Cytogenet Genome Res* **128**, 162-8.

Arganda-Carreras, I., Sorzano, C. O. S., Marabini, R., Carazo, J. M., Ortiz-De-Solorzano, C. and Kybic, J. (2006). Consistent and elastic registration of histological sections using vector-spline regularization. *Computer Vision Approaches to Medical Image Analysis* **4241**, 85-95.

Baarends, W. M. and Grootegoed, J. A. (2003). Chromatin dynamics in the male meiotic prophase. *Cytogenet Genome Res* **103**, 225-34.

Beckouet, F., Hu, B., Roig, M. B., Sutani, T., Komata, M., Uluocak, P., Katis, V. L., Shirahige, K. and Nasmyth, K. (2010). An Smc3 acetylation cycle is essential for establishment of sister chromatid cohesion. *Mol Cell* **39**, 689-99.

Betzig, E., Patterson, G. H., Sougrat, R., Lindwasser, O. W., Olenych, S., Bonifacino, J. S., Davidson, M. W., Lippincott-Schwartz, J. and Hess, H. F. (2006). Imaging intracellular fluorescent proteins at nanometer resolution. *Science* **313**, 1642-5.

Biswas, U., Hempel, K., Llano, E., Pendas, A., Jessberger, R. (2016). Distinct roles of meiosis-specific cohesin complexes in mammalian spermatogenesis. *PLOS Genetics* **12(10)**, e1006389.

Bolcun-Filas, E., Costa, Y., Speed, R., Taggart, M., Benavente, R., De Rooij, D. G. and Cooke, H. J. (2007). SYCE2 is required for synaptonemal complex assembly, double strand break repair, and homologous recombination. *J Cell Biol* **176**, 741-7.

Bolcun-Filas, E., Hall, E., Speed, R., Taggart, M., Grey, C., de Massy, B., Benavente, R. and Cooke, H. J. (2009). Mutation of the mouse Syce1 gene disrupts synapsis and suggests a link between synaptonemal complex structural components and DNA repair. *PLoS Genet* **5**, e1000393.

Botelho, R. J., DiNicolo, L., Tsao, N., Karaiskakis, A., Tarsounas, M., Moens, P. B. and Pearlman, R. E. (2001). The genomic structure of SYCP3, a meiosis-specific gene encoding a protein of the chromosome core. *Biochim Biophys Acta* **1518**, 294-9.

Buonomo, S. B., Clyne, R. K., Fuchs, J., Loidl, J., Uhlmann, F. and Nasmyth, K. (2000). Disjunction of homologous chromosomes in meiosis I depends on proteolytic cleavage of the meiotic cohesin Rec8 by separin. *Cell* **103**, 387-98.

Carpenter, A. T. (1975). Electron microscopy of meiosis in Drosophila melanogaster females: II. The recombination nodule--a recombination-associated structure at pachytene? *Proc Natl Acad Sci U S A* **72**, 3186-9.

Carpenter, A. T. (2003). Normal synaptonemal complex and abnormal recombination nodules in two alleles of the Drosophila meiotic mutant mei-W68. *Genetics* **163**, 1337-56.

Chen, F., Tillberg, P. W. and Boyden, E. S. (2015). Optical imaging. Expansion microscopy. *Science* **347**, 543-8.

Cohen, P. E., Pollack, S. E. and Pollard, J. W. (2006). Genetic analysis of chromosome pairing, recombination, and cell cycle control during first meiotic prophase in mammals. *Endocr Rev* **27**, 398-426.

Costa, Y., Speed, R., Ollinger, R., Alsheimer, M., Semple, C. A., Gautier, P., Maratou, K., Novak, I., Hoog, C., Benavente, R. et al. (2005). Two novel proteins recruited by synaptonemal complex protein 1 (SYCP1) are at the centre of meiosis. *J Cell Sci* **118**, 2755-62.

Creighton, H. B. and McClintock, B. (1931). A Correlation of Cytological and Genetical Crossing-Over in Zea Mays. *Proc Natl Acad Sci U S A* **17**, 492-7.

de Boer, E., Lhuissier, F. G. and Heyting, C. (2009). Cytological analysis of interference in mouse meiosis. *Methods Mol Biol* **558**, 355-82.

de Rooij, D. G. and Grootegoed, J. A. (1998). Spermatogonial stem cells. *Curr Opin Cell Biol* **10**, 694-701.

Dobson, M. J., Pearlman, R. E., Karaiskakis, A., Spyropoulos, B. and Moens, P. B. (1994). Synaptonemal complex proteins: occurrence, epitope mapping and chromosome disjunction. *J Cell Sci* **107 (Pt 10)**, 2749-60.

Eijpe, M., Offenberg, H., Jessberger, R., Revenkova, E. and Heyting, C. (2003). Meiotic cohesin REC8 marks the axial elements of rat synaptonemal complexes before cohesins SMC1beta and SMC3. *J Cell Biol* **160**, 657-70.

Fawcett, D. W. (1956). The fine structure of chromosomes in the meiotic prophase of vertebrate spermatocytes. *J Biophys Biochem Cytol* **2**, 403-6.

Feramisco, J. R., Glass, D. B. and Krebs, E. G. (1980). Optimal spatial requirements for the location of basic residues in peptide substrates for the cyclic AMP-dependent protein kinase. *J Biol Chem* **255**, 4240-5.

Fraune, J., Brochier-Armanet, C., Alsheimer, M., Volff, J. N., Schucker, K. and Benavente, R. (2016). Evolutionary history of the mammalian synaptonemal complex. *Chromosoma* **125**, 355-60.

Fraune, J., Schramm, S., Alsheimer, M. and Benavente, R. (2012). The mammalian synaptonemal complex: protein components, assembly and role in meiotic recombination. *Exp Cell Res* **318**, 1340-6.

Fukuda, T., Fukuda, N., Agostinho, A., Hernandez-Hernandez, A., Kouznetsova, A. and Hoog, C. (2014). STAG3-mediated stabilization of REC8 cohesin complexes promotes chromosome synapsis during meiosis. *EMBO J* **33**, 1243-55.

Gomez, R., Felipe-Medina, N., Ruiz-Torres, M., Berenguer, I., Viera, A., Perez, S., Barbero, J. L., Llano, E., Fukuda, T., Alsheimer, M. et al. (2016). Sororin loads to the synaptonemal complex central region independently of meiotic cohesin complexes. *EMBO Rep* **17**, 695-707.

Gomez, R., Valdeolmillos, A., Parra, M. T., Viera, A., Carreiro, C., Roncal, F., Rufas, J. S., Barbero, J. L. and Suja, J. A. (2007). Mammalian SGO2 appears at the inner centromere domain and redistributes depending on tension across centromeres during meiosis II and mitosis. *EMBO Rep* **8**, 173-80.

Gruber, S., Haering, C. H. and Nasmyth, K. (2003). Chromosomal cohesin forms a ring. *Cell* **112**, 765-77.

Gustafsson, M. G. (2000). Surpassing the lateral resolution limit by a factor of two using structured illumination microscopy. *J Microsc* **198**, 82-7.

Gutierrez-Caballero, C., Herran, Y., Sanchez-Martin, M., Suja, J. A., Barbero, J. L., Llano, E. and Pendas, A. M. (2011). Identification and molecular characterization of the mammalian alpha-kleisin RAD21L. *Cell Cycle* **10**, 1477-87.

Gyuricza, M. R., Manheimer, K. B., Apte, V., Krishnan, B., Joyce, E. F., McKee, B. D. and McKim, K. S. (2016). Dynamic and Stable Cohesins Regulate Synaptonemal Complex Assembly and Chromosome Segregation. *Curr Biol* **26**, 1688-98.

Haering, C. H., Lowe, J., Hochwagen, A. and Nasmyth, K. (2002). Molecular architecture of SMC proteins and the yeast cohesin complex. *Mol Cell* **9**, 773-88.

Haering, C. H. and Nasmyth, K. (2003). Building and breaking bridges between sister chromatids. *Bioessays* **25**, 1178-91.

Hamer, G., Gell, K., Kouznetsova, A., Novak, I., Benavente, R. and Hoog, C. (2006). Characterization of a novel meiosis-specific protein within the central element of the synaptonemal complex. *J Cell Sci* **119**, 4025-32.

Hamer, G., Wang, H., Bolcun-Filas, E., Cooke, H. J., Benavente, R. and Hoog, C. (2008). Progression of meiotic recombination requires structural maturation of the central element of the synaptonemal complex. *J Cell Sci* **121**, 2445-51.

Handel, M. A. (2004). The XY body: a specialized meiotic chromatin domain. *Exp Cell Res* **296**, 57-63.

Hauf, S., Roitinger, E., Koch, B., Dittrich, C. M., Mechtler, K. and Peters, J. M. (2005). Dissociation of cohesin from chromosome arms and loss of arm cohesion during early mitosis depends on phosphorylation of SA2. *PLoS Biol* **3**, e69.

Hauf, S., Waizenegger, I. C. and Peters, J. M. (2001). Cohesin cleavage by separase required for anaphase and cytokinesis in human cells. *Science* **293**, 1320-3.

Heilemann, M., van de Linde, S., Schuttpelz, M., Kasper, R., Seefeldt, B., Mukherjee, A., Tinnefeld, P. and Sauer, M. (2008). Subdiffraction-resolution fluorescence imaging with conventional fluorescent probes. *Angew Chem Int Ed Engl* **47**, 6172-6.

Hell, S. W. and Wichmann, J. (1994). Breaking the diffraction resolution limit by stimulated emission: stimulated-emission-depletion fluorescence microscopy. *Opt Lett* **19**, 780-2.

Henderson, S. A. (1970). The time and place of meiotic crossing-over. *Annu Rev Genet* **4**, 295-324.

Heyting, C., Dietrich, A. J., Moens, P. B., Dettmers, R. J., Offenberg, H. H., Redeker, E. J. and Vink, A. C. (1989). Synaptonemal complex proteins. *Genome* **31**, 81-7.

Heyting, C., Moens, P. B., van Raamsdonk, W., Dietrich, A. J., Vink, A. C. and Redeker, E. J. (1987). Identification of two major components of the lateral elements of synaptonemal complexes of the rat. *Eur J Cell Biol* **43**, 148-54.

Hirano, T. (2002). The ABCs of SMC proteins: two-armed ATPases for chromosome condensation, cohesion, and repair. *Genes Dev* **16**, 399-414.

Hodges, C. A., Revenkova, E., Jessberger, R., Hassold, T. J. and Hunt, P. A. (2005). SMC1beta-deficient female mice provide evidence that cohesins are a missing link in age-related nondisjunction. *Nat Genet* **37**, 1351-5.

Hopkins, J., Hwang, G., Jacob, J., Sapp, N., Bedigian, R., Oka, K., Overbeek, P., Murray, S. and Jordan, P. W. (2014). Meiosis-specific cohesin component, Stag3 is essential for maintaining centromere chromatid cohesion, and required for DNA repair and synapsis between homologous chromosomes. *PLoS Genet* **10**, e1004413.

Huckins, C. (1971 a). The spermatogonial stem cell population in adult rats. I. Their morphology, proliferation and maturation. *Anat Rec* **169**, 533-57.

Huckins, C. (1971 b). The spermatogonial stem cell population in adult rats. 3. Evidence for a long-cycling population. *Cell Tissue Kinet* **4**, 335-49.

Huckins, C. and Oakberg, E. F. (1978). Morphological and quantitative analysis of spermatogonia in mouse testes using whole mounted seminiferous tubules, I. The normal testes. *Anat Rec* **192**, 519-28.

Ishiguro, K., Kim, J., Fujiyama-Nakamura, S., Kato, S. and Watanabe, Y. (2011). A new meiosis-specific cohesin complex implicated in the cohesin code for homologous pairing. *EMBO Rep* **12**, 267-75.

Ishiguro, K., Kim, J., Shibuya, H., Hernandez-Hernandez, A., Suzuki, A., Fukagawa, T., Shioi, G., Kiyonari, H., Li, X. C., Schimenti, J. et al. (2014). Meiosis-specific cohesin mediates homolog recognition in mouse spermatocytes. *Genes Dev* **28**, 594-607.

Jessberger, R. (2011). Cohesin complexes get more complex: the novel kleisin RAD21L. *Cell Cycle* **10**, 2053-4.

Jordan, P. W., Karppinen, J. and Handel, M. A. (2012). Polo-like kinase is required for synaptonemal complex disassembly and phosphorylation in mouse spermatocytes. *J Cell Sci* **125**, 5061-72.

Keeney, S., Giroux, C. N. and Kleckner, N. (1997). Meiosis-specific DNA double-strand breaks are catalyzed by Spo11, a member of a widely conserved protein family. *Cell* **88**, 375-84.

Kishimoto, A., Nishiyama, K., Nakanishi, H., Uratsuji, Y., Nomura, H., Takeyama, Y. and Nishizuka, Y. (1985). Studies on the phosphorylation of myelin basic protein by protein kinase C and adenosine 3':5'-monophosphate-dependent protein kinase. *J Biol Chem* **260**, 12492-9.

Kitajima, T. S., Kawashima, S. A. and Watanabe, Y. (2004). The conserved kinetochore protein shugoshin protects centromeric cohesion during meiosis. *Nature* **427**, 510-7.

Klar, T. A., Jakobs, S., Dyba, M., Egner, A. and Hell, S. W. (2000). Fluorescence microscopy with diffraction resolution barrier broken by stimulated emission. *Proc Natl Acad Sci U S A* **97**, 8206-10.

Klink, A., Lee, M. and Cooke, H. J. (1997). The mouse synaptosomal complex protein gene Sycp3 maps to band C of chromosome 10. *Mamm Genome* **8**, 376-7.

Kuroda, M., Oikawa, K., Ohbayashi, T., Yoshida, K., Yamada, K., Mimura, J., Matsuda, Y., Fujii-Kuriyama, Y. and Mukai, K. (2005). A dioxin sensitive gene, mammalian WAPL, is implicated in spermatogenesis. *FEBS Lett* **579**, 167-72.

Laemmli, U. K. (1970). Cleavage of structural proteins during the assembly of the head of bacteriophage T4. *Nature* **227**, 680-5.

Lafont, A. L., Song, J. and Rankin, S. (2010). Sororin cooperates with the acetyltransferase Eco2 to ensure DNA replication-dependent sister chromatid cohesion. *Proc Natl Acad Sci U S A* **107**, 20364-9.

Lammers, J. H., Offenberg, H. H., van Aalderen, M., Vink, A. C., Dietrich, A. J. and Heyting, C. (1994). The gene encoding a major component of the lateral elements of synaptonemal complexes of the rat is related to X-linked lymphocyte-regulated genes. *Mol Cell Biol* **14**, 1137-46.

Lee, J. and Hirano, T. (2011). RAD21L, a novel cohesin subunit implicated in linking homologous chromosomes in mammalian meiosis. *J Cell Biol* **192**, 263-76.

Lee, J., Iwai, T., Yokota, T. and Yamashita, M. (2003). Temporally and spatially selective loss of Rec8 protein from meiotic chromosomes during mammalian meiosis. *J Cell Sci* **116**, 2781-90.

Liebe, B., Alsheimer, M., Hoog, C., Benavente, R. and Scherthan, H. (2004). Telomere attachment, meiotic chromosome condensation, pairing, and bouquet stage duration are modified in spermatocytes lacking axial elements. *Molecular Biology of the Cell* **15**, 827-837.

Liu, H., Rankin, S. and Yu, H. (2013). Phosphorylation-enabled binding of SGO1-PP2a to cophesin protects sororn and centromeric cohesion during mitosis. *Nat Cell Biol* **15**, 40-49.

Liu, J. G., Yuan, L., Brundell, E., Bjorkroth, B., Daneholt, B. and Hoog, C. (1996). Localization of the N-terminus of SCP1 to the central element of the synaptonemal complex and evidence for direct interactions between the N-termini of SCP1 molecules organized head-to-head. *Exp Cell Res* **226**, 11-9.

Llano, E., Gomez, H. L., Garcia-Tunon, I., Sanchez-Martin, M., Caburet, S., Barbero, J. L., Schimenti, J. C., Veitia, R. A. and Pendas, A. M. (2014). STAG3 is a strong candidate gene for male infertility. *Hum Mol Genet* **23**, 3421-31.

Llano, E., Gomez, R., Gutierrez-Caballero, C., Herran, Y., Sanchez-Martin, M., Vazquez-Quinones, L., Hernandez, T., de Alava, E., Cuadrado, A., Barbero, J. L. et al. (2008). Shugoshin-2 is essential for the completion of meiosis but not for mitotic cell division in mice. *Genes Dev* **22**, 2400-13.

Losada, A., Yokochi, T. and Hirano, T. (2005). Functional contribution of Pds5 to cohesin-mediated cohesion in human cells and Xenopus egg extracts. *J Cell Sci* **118**, 2133-2141.

Loschberger, A., van de Linde, S., Dabauvalle, M. C., Rieger, B., Heilemann, M., Krohne, G. and Sauer, M. (2012). Super-resolution imaging visualizes the eightfold symmetry of gp210 proteins around the nuclear pore complex and resolves the central channel with nanometer resolution. *J Cell Sci* **125**, 570-5.

Lupas, A., Van Dyke, M. and Stock, J. (1991). Predicting coiled coils from protein sequences. *Science* **252**, 1162-4.

Mark Petronczki, M. F. S., Kim Nasmyth. (2003). Un Ménage à Quatre: The Molecular Biology of Chromosome Segregation in Meiosis. *Cell* **112**, 423-440.

McDougall, A., Elliott, D. J. and Hunter, N. (2005). Pairing, connecting, exchanging, pausing and pulling chromosomes. *EMBO Rep* **6**, 120-5.

McGuinness, B. E., Hirota, T., Kudo, N. R., Peters, J. M. and Nasmyth, K. (2005). Shugoshin prevents dissociation of cohesin from centromeres during mitosis in vertebrate cells. *PLoS Biol* **3**, e86.

McNicoll, F., Stevense, M. and Jessberger, R. (2013). Cohesin in gametogenesis. *Curr Top Dev Biol* **102**, 1-34.

Meuwissen, R. L., Meerts, I., Hoovers, J. M., Leschot, N. J. and Heyting, C. (1997). Human synaptonemal complex protein 1 (SCP1): isolation and characterization of the cDNA and chromosomal localization of the gene. *Genomics* **39**, 377-84.

Meuwissen, R. L., Offenberg, H. H., Dietrich, A. J., Riesewijk, A., van Iersel, M. and Heyting, C. (1992). A coiled-coil related protein specific for synapsed regions of meiotic prophase chromosomes. *EMBO J* **11**, 5091-100.

Michaelis, C., Ciosk, R. and Nasmyth, K. (1997). Cohesins: chromosomal proteins that prevent premature separation of sister chromatids. *Cell* **91**, 35-45.

Miyamoto, T., Hasuike, S., Yogev, L., Maduro, M. R., Ishikawa, M., Westphal, H. and Lamb, D. J. (2003). Azoospermia in patients heterozygous for a mutation in SYCP3. *Lancet* **362**, 1714-9.

Moens, P. B., Kolas, N. K., Tarsounas, M., Marcon, E., Cohen, P. E. and Spyropoulos, B. (2002). The time course and chromosomal localization of recombination-related proteins at meiosis in the mouse are compatible with models that can resolve the early DNA-DNA interactions without reciprocal recombination. *J Cell Sci* **115**, 1611-22.

Morelli, M. A. and Cohen, P. E. (2005). Not all germ cells are created equal: aspects of sexual dimorphism in mammalian meiosis. *Reproduction* **130**, 761-81.

Moses, M. J. (1956). Chromosomal structures in crayfish spermatocytes. *J Biophys Biochem Cytol* **2**, 215-8.

Nasmyth, K. (2001). Disseminating the genome: joining, resolving, and separating sister chromatids during mitosis and meiosis. *Annu Rev Genet* **35**, 673-745.

Nasmyth, K. (2011). Cohesin: a catenase with separate entry and exit gates? *Nat Cell Biol* **13**, 1170-7.

Nishiyama, T., Ladurner, R., Schmitz, J., Kreidl, E., Schleiffer, A., Bhaskara, V., Bando, M., Shirahige, K., Hyman, A. A., Mechtler, K. et al. (2010). Sororin mediates sister chromatid cohesion by antagonizing Wapl. *Cell* **143**, 737-49.

Oakberg, E. F. (1956 a). A description of spermiogenesis in the mouse and its use in analysis of the cycle of the seminiferous epithelium and germ cell renewal. *Am J Anat* **99**, 391-413.

Oakberg, E. F. (1956 b). Duration of spermatogenesis in the mouse and timing of stages of the cycle of the seminiferous epithelium. *Am J Anat* **99**, 507-16.

Oakberg, E. F. (1971). Spermatogonial stem-cell renewal in the mouse. *Anat Rec* **169**, 515-31.

Offenberg, H. H., Schalk, J. A., Meuwissen, R. L., van Aalderen, M., Kester, H. A., Dietrich, A. J. and Heyting, C. (1998). SCP2: a major protein component of the axial elements of synaptonemal complexes of the rat. *Nucleic Acids Res* **26**, 2572-9.

Ollinger, R., Alsheimer, M. and Benavente, R. (2005). Mammalian protein SCP1 forms synaptonemal complex-like structures in the absence of meiotic chromosomes. *Mol Biol Cell* **16**, 212-7.

Ortiz, R., Kouznetsova, A., Echeverria-Martinez, O. M., Vazquez-Nin, G. H. and Hernandez-Hernandez, A. (2016). The width of the lateral element of the synaptonemal complex is determined by a multilayered organization of its components. *Exp Cell Res* **344**, 22-9.

Page, S. L. and Hawley, R. S. (2003). Chromosome choreography: the meiotic ballet. *Science* **301**, 785-9.

Page, S. L. and Hawley, R. S. (2004). The genetics and molecular biology of the synaptonemal complex. *Annu Rev Cell Dev Biol* **20**, 525-58.

Parra, M. T., Viera, A., Gomez, R., Page, J., Carmena, M., Earnshaw, W. C., Rufas, J. S. and Suja, J. A. (2003). Dynamic relocalization of the chromosomal passenger complex proteins inner centromere protein (INCENP) and aurora-B kinase during male mouse meiosis. *J Cell Sci* **116**, 961-74.

Patterson, G., Davidson, M., Manley, S. and Lippincott-Schwartz, J. (2010). Superresolution Imaging using Single-Molecule Localization. *Annual Review of Physical Chemistry, Vol 61* **61**, 345-367.

Pelttari, J., Hoja, M. R., Yuan, L., Liu, J. G., Brundell, E., Moens, P., Santucci-Darmanin, S., Jessberger, R., Barbero, J. L., Heyting, C. et al. (2001). A meiotic chromosomal core consisting of cohesin complex proteins recruits DNA recombination proteins and promotes synapsis in the absence of an axial element in mammalian meiotic cells. *Mol Cell Biol* **21**, 5667-77.

Petronczki, M., Siomos, M. F., Nasmyth, K. (2003). Un Ménage à Quatre: The Molecular Biology of Chromosome Segregation in Meiosis. *Cell,* **112**, 423-440.

Pinna, L. A. (1990). Casein kinase 2: an 'eminence grise' in cellular regulation? *Biochim Biophys Acta* **1054**, 267-84.

Prieto, I., Pezzi, N., Buesa, J. M., Kremer, L., Barthelemy, I., Carreiro, C., Roncal, F., Martinez, A., Gomez, L., Fernandez, R. et al. (2002). STAG2 and Rad21 mammalian mitotic cohesins are implicated in meiosis. *EMBO Rep* **3**, 543-50.

Prieto, I., Suja, J. A., Pezzi, N., Kremer, L., Martinez, A. C., Rufas, J. S. and Barbero, J. L. (2001). Mammalian STAG3 is a cohesin specific to sister chromatid arms in meiosis I. *Nat Cell Biol* **3**, 761-6.

Rankin, S. (2005). Sororin, the cell cycle and sister chromatid cohesion. *Cell Cycle* **4**, 1039-42.

Rankin, S., Ayad, N. G. and Kirschner, M. W. (2005). Sororin, a substrate of the anaphase-promoting complex, is required for sister chromatid cohesion in vertebrates. *Mol Cell* **18**, 185-200.

Revenkova, E., Eijpe, M., Heyting, C., Gross, B. and Jessberger, R. (2001). Novel meiosis-specific isoform of mammalian SMC1. *Mol Cell Biol* **21**, 6984-98.

Revenkova, E. and Jessberger, R. (2006). Shaping meiotic prophase chromosomes: cohesins and synaptonemal complex proteins. *Chromosoma* **115**, 235-40.

Riedel, C. G., Katis, V. L., Katou, Y., Mori, S., Itoh, T., Helmhart, W., Galova, M., Petronczki, M., Gregan, J., Cetin, B. et al. (2006). Protein phosphatase 2A protects centromeric sister chromatid cohesion during meiosis I. *Nature* **441**, 53-61.

Rong, M., Matsuda, A., Hiraoka, Y. and Lee, J. (2016). Meiotic cohesin subunits RAD21L and REC8 are positioned at distinct regions between lateral elements and transverse filaments in the synaptonemal complex of mouse spermatocytes. *J Reprod Dev*.

Sage, J., Martin, L., Cuzin, F. and Rassoulzadegan, M. (1995). cDNA sequence of the murine synaptonemal complex protein 1 (SCP1). *Biochim Biophys Acta* **1263**, 258-60.

Salic, A., Waters, J. C. and Mitchison, T. J. (2004). Vertebrate shugoshin links sister centromere cohesion and kinetochore microtubule stability in mitosis. *Cell* **118**, 567-78.

Schafer, P., van de Linde, S., Lehmann, J., Sauer, M. and Doose, S. (2013). Methylene blue- and thiol-based oxygen depletion for super-resolution imaging. *Anal Chem* **85**, 3393-400.

Schalk, J. A., Dietrich, A. J., Vink, A. C., Offenberg, H. H., van Aalderen, M. and Heyting, C. (1998). Localization of SCP2 and SCP3 protein molecules within synaptonemal complexes of the rat. *Chromosoma* **107**, 540-8.

Scherthan, H., Weich, S., Schwegler, H., Heyting, C., Harle, M. and Cremer, T. (1996). Centromere and telomere movements during early meiotic prophase of mouse and man are associated with the onset of chromosome pairing. *J Cell Biol* **134**, 1109-25.

Schmekel, K., Meuwissen, R. L., Dietrich, A. J., Vink, A. C., van Marle, J., van Veen, H. and Heyting, C. (1996). Organization of SCP1 protein molecules within synaptonemal complexes of the rat. *Exp Cell Res* **226**, 20-30.

Schramm, S., Fraune, J., Naumann, R., Hernandez-Hernandez, A., Hoog, C., Cooke, H. J., Alsheimer, M. and Benavente, R. (2011). A novel mouse synaptonemal complex protein is essential for loading of central element proteins, recombination, and fertility. *PLoS Genet* **7**, e1002088.

Schücker, K., Holm, T., Franke, C., Sauer, M. and Benavente, R. (2015). Elucidation of synaptonemal complex organization by super-resolution imaging with isotropic resolution. *Proc Natl Acad Sci U S A* **112**, 2029-33.

Schücker, K., Franke, C., Jessberger, R., Sauer, M. and Benavente, R. (2016) Super-resolution imaging reveals polarized orientation of cohesin complexes in the meiotic chromosome axis, *J Cell Sci*, **under review**

Shannon, C. E. (1949). Communication in the Presence of Noise. *Proceedings of the Institute of Radio Engineers* **37**, 10-21.

Solari, A. J. (1974). The behavior of the XY pair in mammals. *Int Rev Cytol* **38**, 273-317.

Sumara, I., Vorlaufer, E., Gieffers, C., Peters, B. H. and Peters, J. M. (2000). Characterization of vertebrate cohesin complexes and their regulation in prophase. *J Cell Biol* **151**, 749-62.

Sumara, I., Vorlaufer, E., Stukenberg, P. T., Kelm, O., Redemann, N., Nigg, E. A. and Peters, J. M. (2002). The dissociation of cohesin from chromosomes in prophase is regulated by Polo-like kinase. *Mol Cell* **9**, 515-25.

Szymborska, A., de Marco, A., Daigle, N., Cordes, V. C., Briggs, J. A. and Ellenberg, J. (2013). Nuclear pore scaffold structure analyzed by super-resolution microscopy and particle averaging. *Science* **341**, 655-8.

Tarsounas, M., Pearlman, R. E., Gasser, P. J., Park, M. S. and Moens, P. B. (1997). Protein-protein interactions in the synaptonemal complex. *Mol Biol Cell* **8**, 1405-14.

Tarsounas, M., Pearlman, R. E. and Moens, P. B. (1999). Meiotic activation of rat pachytene spermatocytes with okadaic acid: the behaviour of synaptonemal complex components SYN1/SCP1 and COR1/SCP3. *J Cell Sci* **112 (Pt 4)**, 423-34.

Uhlmann, F. (2011). Cohesin subunit Rad21L, the new kid on the block has new ideas. *EMBO Rep* **12**, 183-4.

Uhlmann, F., Lottspeich, F. and Nasmyth, K. (1999). Sister-chromatid separation at anaphase onset is promoted by cleavage of the cohesin subunit Scc1. *Nature* **400**, 37-42.

Valdeolmillos, A. M., Viera, A., Page, J., Prieto, I., Santos, J. L., Parra, M. T., Heck, M. M., Martinez, A. C., Barbero, J. L., Suja, J. A. et al. (2007). Sequential loading of cohesin subunits during the first meiotic prophase of grasshoppers. *PLoS Genet* **3**, e28.

van de Linde, S., Loschberger, A., Klein, T., Heidbreder, M., Wolter, S., Heilemann, M. and Sauer, M. (2011). Direct stochastic optical reconstruction microscopy with standard fluorescent probes. *Nat Protoc* **6**, 991-1009.

Vázquez Nin, G. H., Flores, E., Echeverría, O. M., Merkert, H., Wettstein, R. and Benavente, R. (1993). Immunocytochemical localization of DNA in synaptonemal complexes of rat and mouse spermatocytes, and of chick oocytes. *Chromosoma* **102**, 457-463.

von Wettstein, D. (1984). The synaptonemal complex and genetic segregation. *Symp Soc Exp Biol* **38**, 195-231.

Waizenegger, I. C., Hauf, S., Meinke, A. and Peters, J. M. (2000). Two distinct pathways remove mammalian cohesin from chromosome arms in prophase and from centromeres in anaphase. *Cell* **103**, 399-410.

Wang, P. J., McCarrey, J. R., Yang, F. and Page, D. C. (2001). An abundance of X-linked genes expressed in spermatogonia. *Nat Genet* **27**, 422-6.

Ward, A., Hopkins, J., McKay, M., Murray, S. and Jordan, P. W. (2016). Genetic Interactions Between the Meiosis-Specific Cohesin Components, STAG3, REC8, and RAD21L. *G3 (Bethesda)* **6**, 1713-24.

Winkel, K., Alsheimer, M., Ollinger, R. and Benavente, R. (2009). Protein SYCP2 provides a link between transverse filaments and lateral elements of mammalian synaptonemal complexes. *Chromosoma* **118**, 259-67.

Wolter, S., Endesfelder, U., van de Linde, S., Heilemann, M. and Sauer, M. (2011). Measuring localization performance of super-resolution algorithms on very active samples. *Opt Express* **19**, 7020-33.

Wolter, S., Schuttpelz, M., Tscherepanow, M., S, V. D. L., Heilemann, M. and Sauer, M. (2010). Real-time computation of subdiffraction-resolution fluorescence images. *J Microsc* **237**, 12-22.

Xu, Z., Cetin, B., Anger, M., Cho, U. S., Helmhart, W., Nasmyth, K. and Xu, W. (2009). Structure and function of the PP2A-shugoshin interaction. *Mol Cell* **35**, 426-41.

Yang, F., De La Fuente, R., Leu, N. A., Baumann, C., McLaughlin, K. J. and Wang, P. J. (2006). Mouse SYCP2 is required for synaptonemal complex assembly and chromosomal synapsis during male meiosis. *J Cell Biol* **173**, 497-507.

Yuan, L., Pelttari, J., Brundell, E., Bjorkroth, B., Zhao, J., Liu, J. G., Brismar, H., Daneholt, B. and Hoog, C. (1998). The synaptonemal complex protein SCP3 can form multistranded, cross-striated fibers in vivo. *J Cell Biol* **142**, 331-9.

Zhang, B., Chang, J., Fu, M., Huang, J., Kashyap, R., Salavaggione, E., Jain, S., Kulkarni, S., Deardorff, M. A., Uzielli, M. L. et al. (2009). Dosage effects of cohesin regulatory factor PDS5 on mammalian development: implications for cohesinopathies. *PLoS One* **4**, e5232.

Zhang, B., Jain, S., Song, H., Fu, M., Heuckeroth, R. O., Erlich, J. M., Jay, P. Y. and Milbrandt, J. (2007). Mice lacking sister chromatid cohesion protein PDS5B exhibit developmental abnormalities reminiscent of Cornelia de Lange syndrome. *Development* **134**, 3191-201.

Zickler, D. and Kleckner, N. (1998). The leptotene-zygotene transition of meiosis. *Annu Rev Genet* **32**, 619-97.

Zickler, D. and Kleckner, N. (1999). Meiotic chromosomes: integrating structure and function. *Annu Rev Genet* **33**, 603-754.

Appendix 1 Abbreviations and units

%= Percent

Ø= Diameter

®= registered

™= Trademark

©= Copyright

°C= Degree of celcius

α= Alpha or anti

β= Beta

λ= Gamma

µg= Microgram

µl= Microliter

A= Ampere or adenine

aa= Amino acid(s)

AE= Axial element

Al= Alexa

Amp= Ampicillin

APC/C= Anaphase-promoting complex/cyclosome

APS= Ammonium persulfate

ATM=Ataxia telangiectasia mutated

ATP= Adenosintriphosphate

ATR= Ataxia telangiectasia and Rad3 related

BFP= Back focal plane

bp= Basepair

BSA= Bovineserum Albumin

C_2H_7NO= Ethanolamine

C= Cytosin

Cat.no.= Catalogue number

CDK= Cyclin-dependent kinase

cDNA= Complementary DNA

CE= Central element

cm^2= Square centimetre

CoAT= Cohesin acetyltransferase

CoDAC= Cohesin deacetyltransferase

CR= Central region

Da= Dalton

dHJ= Double Holiday Junction

dH_2O= destilled water

DMF= Dimethylformamide

DMSO= Dimethylsulfoxide

DNA= Desoxyribonucleic acid

DSBR= Double strand break repair

DTT= Dithiothreitol

dNTP= Deoxynucleoside triphosphate

DSB= Double strand break

*d*STORM= *direct* stochastic optical reconstruction microscopy

DTT= Dithiothreitol

ECL= Enhanced Chemiluminescence

E.coli= Escherichia coli

EDTA= Ethylenediaminetetraacetic acid

e.g.= For example

EN= Early recombination nodules

FCS= Fetal calf serum

Fig.= Figure

G= Guanosine

g= gram or gravity acceleration

Gp= Guinea pig

G-phase= Growth phase

GST= Glutathione-S-Transferase

GTP= Guanosine Guanosinetriphosphate triphosphate

h= Hour

H_2O= Water

HRP= Horseradish peroxidase

HILO= Highly inclined lamination optical sheet microscopy

HJ= Holiday Junction

IPTG= Isopropyl ß-D-1thiogalactopyranoside

ISC= Intersystem crossing

KH_2PO_4= Monopotassium phosphate

kan= Kanamycin

kb= Kilobases

kDa= Kilodalton

kg= Kilogram

KOH= Potassium hydroxide

L= Liter

LB= Lysogeny broth

LE= Lateral element

M= Molar

mA= Milliamper

mcs= Multiple cloning site

MEA= β-mercaptoethylaminebuffer

mg= Milligram

MgCl= Magnesium chloride

min= Minute

Ml= Milliliter

mM= Millimolar

M= Mol

NaCl= sodium chloride

$NaHCO_3$= Sodium bicarbonate

Na_2HPO_4= Disodium phosphate

NaN_3= Sodium azide

NaOH= Sodium hydroxide

NBD= Nucleotide binding site

NCBI= National Center of Biotechnology Information

NIPBL= Nipped-B-like protein

NLS= Nulcear localization signal

nm= Nanometer

NTP= Nucleoside triphosphate

OD= Optical density

o/n= over night

PAGE= Polyacrylamide gel electrophoresis

PBS= Phosphate-buffered saline

PCR= Polymerase chain reaction

PEG= Polyethylene glycol

PFA= Paraformaldehyde

PLK= Polo-like kinase

Rb= Rabbit

RN= Recombination nodule

RNA= Ribonucleic acid

rpm= Rounds per minute

RAM= Random-access memory

RT= room temperature

S= Svedberg

SAC= Spindle assembly checkpoint

SC= Synaptonemal complex

SCC= sister chromatid cohesion

SDSA= synthesis dependent strand annealing

sec= seconds

SGO= Shugosin

SL= Stock solution

SDS= Sodium dodecyl sulfate

SMC= structural maintenance of chromosomes

S-phase= Synthesis phase

SYCE= Synaptonemal complex central element protein

SYCP= Synaptonemal complex protein

PALM= Photoinduced

PP2A= Phosphatase 2 A

TBST= Tris buffered Saline with Tween

TEX12= testis expressed sequence 12

TF= Transversal filaments

TN= Transformed recombination nodules

Tris/HCL= Tris hydrochloride

TSS= Transformation and storage solution

Tween 20= Polysorbate 20

U= Units

UV= Ultraviolet

V= Volt

v/v= Volume per volume

WAPL= wings apart-like protein homologue

w/v= mass per volume

Appendix 2 Chemicals and kits

5xPhusion™ HF buffer, NEB

Agarose, Sigma-Aldrich

Acrylamide, Applichem

APS, Sigma-Aldrich

Bacto-Trypton, BD

BamHI unique buffer, Fermentas

B-mercaptoethanol, Applichem

β-mercaptoethylaminebuffer (MEA), Sigma-Aldrich

BSA, Sigma-Aldrich

BSA receptor grade, lyophil., Serva

Buffer 10x tango, Fermentas

Buffer R, Fermentas

CAPS= N-cyclohexyl-3-aminopropanesulfonic acid, Sigma-Aldrich

Chloroform, Roth

Coomassie Brilliant Blue R-250, Applichem

D(+)-Sucrose, Applichem

Disodium phosphate, Applichem

DMSO, Applichem

dNTPs, Fermentas

DTT, Applichem

ECL™ Solutions A and B, Amersham Bioscience

EDTA = Ethylenediaminetetraacetic acid, Applichem

Ethanol, Roth

Ethanolamine, Sigma-Aldrich

Ethidium bromide, Applichem

FCS, Sigma-Aldrich

Glucose, Sigma-Aldrich

Glucose oxidase, Sigma-Aldrich

Glycerol, Applichem

Hoechst 33258, Roche

Hydrochloric acid, Applichem

IPTG, Applichem

Isopropanol, Roth

Potassium chloride, Applichem

Magnesium chloride, Roth

Methanol, Roth

Milk powder, Roth

Monopotassium phosphate, Applichem

(Ni-NTA) agarose, Qiagen, Cat.no. 30310

NulceoSpin® Gel and PCR Clean-up Kit, Macherey-Nagel

NulceoSpin® Plasmid, Macherey-Nagel

Paraformaldehyde, Applichem

PEG, Otto Nordwald GmbH

Ponceau S, Applichem

Poly-L-lysine, Sigma-Aldrich

Polypropylene columns, Qiagen, Cat.no. 34964

rATP, Fermentas

SDS, Biorad

Sodium azide, Sigma-Aldrich

Sodium bicarbonate, Applichem

Sodium chloride, Roth

Sodium hydroxide, Applichem

Strata Blunt PCR Cloning Kit, Agilent Technologies

T4 DNA ligase buffer, Fermentas

Temed, Applichem

Tris/HCL = Tris(hydroxymethyl)amino methane, Roth

Trisodium citrate, Roth

Triton X-100, Roth

Tween®20, Applichem

Urea, Applichem

Yeast extract, Roth

Appendix 3 Equipment

480/17 nm BrightLine® single-band bandpass filter FF01-480/17-25; Semrock

488/10 nm BrightLine® single-band bandpass filter FF01-488/10-25; Semrock

582/75 nm BrightLine® single-band bandpass filter FF01-582/75-25; Semrock

642/10 nm BrightLine® single-band bandpass filter, FF01-642/10-25, Semrock

697/75 nm BrightLine® single-band bandpass filter FF01-697/75-25-D; Semrock

8-Well-Lab-Tek II coverslide-chambers, Nunc, Thermo Fisher Scientific

Accuracy scale Mettler AC 100, Mettler

Achromatic lens, G322284000, Qioptiq

Achromatic lens, G322303000, Qioptiq

Amicon® Ultra-15, Centrifugal filter devices, 10K/3K, Merck Millipore

APON 60XOTIRF; Olympus

Biophotometer, Eppendorf

Broad band dielectric mirror BB2-E02, Thorlabs

Centrifuge 5415 C, Eppendorf

Centrifuge Minifuge T, Heraeus

Centrifuge Sorvall RC-5B, Du Pont Instruments

Cover slips (24 x 60 mm), A. Hartenstein

Cover slips (24 x 40 mm), A. Hartenstein

Dialysistube VISKING Typ 20/32, Carl Roth

Dichroic beam splitter 630dcxr; Chroma

Dual camera adaptor TuCam; Andor

EMCCD camera iXon Ultra 897; Andor

Eppendorf tubes, various volumes, Eppendorf Ag

Filtertissue made of polyamide, 30 µm, A. Hartenstein

Fluorescencemicroscope Axiophot Stereo HB050, Zeiss

Genesis MX639-1000 STM, Coherent

Genesis MX514 STM; Coherent

Graphite Blotchamber, LMS (Hartenstein)

Heating block, Liebisch (Hartenstein)

High precision cover slips (24x60 mm), A. Hartenstein

HiTrap™ column, GE Healthcare Life Sciences

KCB2- Right-Angle Kinematic Mirror Mount; Thorlabs

Latex gloves, diverse

Leica TCS-SP2 AOBS confocal laser scanning microscope, Leica

Magnetic stirrer M35, GLW

Multiply-Pro cups 0.2 ml, Sarstedt

Nitrile gloves, diverse

Nosepiece stage IX2-NPS; Olympus

Paper hand towel, diverse

Petri dishes, 35-92mm, Sarstedt

pH meter pH 523, WTW (Hartenstein)

Pipettes, various

Power supply 500 V 1 A, Heidelberg Steril GARD Hood Class III Müller Labortechnik

Protein gel chamber Mini V8, Gibco BRL

Razorblades, various

Sapphire 488 LP, Coherent, Santa Clara, USA

Scales Mettler PJ 3600 DeltaRange, Mettler

Shaker WS5, Laborgerätebau Edmund Bühler, Tübingen

Sonifier B12, Branson Sonic Power Company

SuperFrost®Plus cover slides, Thermo Fisher Scientific

Syringe filter 25 mm, 0.2 µm/ 0.45 µm Cellulose acetate membrane, VWR International

TetraSpecks, Life Technologies

Thermocycler TECHNE PROGENE, Thermo-Dux, Göttingen

Triplet band dichroic beam spitter FF425/532/656-Di01; Semrock

Tubes 15/50 ml, Sarstedt

Whatman® Gel-Blotting-Papers, A. Hartenstein

Whatman® Nitrocellulose, A. Hartenstein

Vortex L24, GLW, Würzburg

Intas® UV-transluminator

Appendix 4 Software

Adobe Acrobat XI Pro

Adobe Photoshop CS5

Andor Solis Imaging and Spectograph Software

CLC Main Wokbench 6

DYMO Label v.8

EndNote

Fiji Win64

Leica LCS Lite Software

Microsoft Office

OriginPro 9.1G 64Bit

rapidSTORM

Zen 2012 Black Edition

Zen lite 2012

Eidesstattliche Erklärung

Hiermit erkläre ich an Eides statt, die Dissertation: „The molecular architecture of the meiotic chromosome axis as revealed by super-resolution microscopy“, eigenständig, d. h. insbesondere selbständig und ohne Hilfe eines kommerziellen Promotionsberaters, angefertigt und keine anderen, als die von mir angegebenen Quellen und Hilfsmittel verwendet zu haben.

Ich erkläre außerdem, dass die Dissertation weder in gleicher noch in ähnlicher Form bereits in einem anderen Prüfungsverfahren vorgelegen hat und dass ich die Regeln der Julius-Maximilians-Universität Würzburg über gute wissenschaftliche Praxis eingehalten habe.

Hammelburg, den 09.02.2017

_____

Unterschrift

Danksagung

An dieser Stelle möchte ich mich bei all denen bedanken, die mich während meiner Zeit als Studentin und Doktorandin begleitet und unterstützt haben und zu all den schönen Erinnerungen, die ich aus der Zeit mitnehmen durfte, beigetragen haben. Es war eine ganz besondere Zeit!

Ganz besonders möchte ich mich bei Prof. Ricardo Benavente bedanken, der es mir ermöglicht hat in einer tollen Arbeitsgruppe und einem tollen Institut meine Zeit als Doktorandin verbringen zu können und Teil spannender Projekte und Kooperationen zu sein! Vielen Dank für deine Geduld, die vielen Zusprüche und Hilfen und den zahlreichen Diskussionen und Feedback! Ich habe so viel gelernt und kann mich glücklich schätzen in deiner Arbeitsgruppe gelandet zu sein! Mein Dank geht weiter an Prof. Manfred Alsheimer für die vielen interessanten und lehrreichen Gespräche.

Weiter möchte ich mich bei Prof. Markus Sauer für die Übernahme des Zweitgutachtens meiner Doktorarbeit bedanken und für die einmalige Möglichkeit in die spannende Welt der hochauflösenden Mikroskopie eintauchen zu können. Vielen Dank, dass ich so toll in deine Arbeitsgruppe mit aufgenommen worden bin und alle Räumlichkeiten und Set-ups nutzen durfte! An dieser Stelle möchte ich mich auch bei Thorge Holm bedanken, der mir mit unendlicher Geduld und biologenfreundlich alles über hochauflösende Mikroskopie, insbesondere über *d*STORM, gezeigt und erklärt hat, egal wie oft ich die gleichen banalen Fragen gestellt habe. Vielen Dank für den vielen Kaffee und die Schokolade und die Zeit, die du investiert hast mir alles beizubringen! Die vielen Stunden des Messens und Auswertens haben einfach nur Spaß gemacht! Mein Dankeschön geht auch an Christian Franke, der sich die Zeit genommen hat mir bei der Auswertung meiner Daten zu helfen und an Dr. Sven Proppert für die Hilfe bei den 3D *d*STORM Messungen.

Weiter möchte ich mich bei all meinen lieben Arbeitskollegen aus der Zoologie I, der EM und dem Lehrstuhl für Biotechnologie und Biophysik und ganz besonders dem Alsavente-Labor-Team für die super tolle Arbeitsatmosphäre, die vielen Diskussionen, der ehrlichen Kritik und für eure Hilfe und Freundschaft bedanken! Mit euch zu arbeiten war wundervoll und lehrreich zugleich!

Ein ganz besonderes Dankeschön geht an meine Schwiegereltern, Linda und Rainer, an Nora und der ganzen Oberhausener-Sippschaft. Ein Teil eurer Familie zu sein ist was

ganz Besonderes! Meinem Vater möchte ich für die Unterstützung danken, ohne die es mir nicht möglich gewesen wäre mein Studium zu absolvieren und meine Doktorarbeit fertigzustellen!
Zu guter Letzt möchte ich mich bei meinem besten Freund und der Liebe meines Lebens Basti bedanken. Du bist immer für mich da, unterstützt mich wo du nur kannst und erwartest von mir nichts. Ich liebe dich!

Publications and articles:

1. K. Schücker, T. Holm, C. Franke, M. Sauer and R. Benavente, Elucidation of synaptonemal complex organization by super-resolution imaging with isotropic resolution, *Proc Natl Acad Sci USA*, 2015, **112** (7), 2029-33.

2. K. Schücker, T. Holm, C. Franke, M. Sauer and R. Benavente, Tiefere Einblicke in die molekulare Architektur meiotischer Chromosomen, *GIT Spezial BIOforum*, 2015, **2/15**, 16-17.

3. J. Fraune, C. Brochier-Armanet, M. Alsheimer, JN. Volff, K. Schücker, R. Benavente, Evolutionary history of the mammalian synaptonemal complex, *Chromosoma*, 2016, **125** (3), 355-60.

4. K.Schücker, C. Franke, R. Jessberger, M. Sauer and R. Benavente, Super-resolution imaging reveals polarized orientation of cohesin complexes in the meiotic chromosome axis, *J Cell Sci*, under review.